The Thesis Committee for Emily Bradshaw Marino
Certifies that this is the approved version of the following thesis:

Isolating Lithologic Controls on Landscape Morphology in the Guadalupe Mountains, New Mexico and Texas

APPROVED BY
SUPERVISING COMMITTEE:

Supervisor:

Joel Johnson

Paola Passalacqua

David Mohrig

Isolating Lithologic Controls on Landscape Morphology in the Guadalupe Mountains, New Mexico and Texas

by

Emily Bradshaw Marino, B.S.

Thesis

Presented to the Faculty of the Graduate School of

The University of Texas at Austin

in Partial Fulfillment

of the Requirements

for the Degree of

Master of Science in Geological Sciences

The University of Texas at Austin

May 2017

Dedication

To my loving parents, Thomas and Lucy Bradshaw, who have always supported me and encouraged me to follow my dreams.

Acknowledgements

First, I would like to express my sincere gratitude and appreciation to my advisor, Joel Johnson, for his guidance, support, and patience throughout my time at the Jackson School. I would also like to thank my committee members, David Mohrig and Paola Passalacqua for their assistance with writing this thesis. I am grateful for the opportunities I have been given during my time at the University of Texas and I value the efforts of all the faculty and staff I have had the pleasure of working with. I am beholden to the Jackson School of Geosciences for providing support for my studies and fostering an environment of world class research and scientific study.

Though my time in the field was short, I am very appreciative of the funding I received to help with my field studies and would like to thank the Jackson School and the Surface and Hydrologic Processes committee for the seed grant award. A special thanks to Conrad Suen for agreeing to be my field assistant on such short notice and for braving the desert heat, thunderstorms, as well as the ants in your tent. I would also like to thank Nicole Gasparini for offering collaboration on my project, as well as Jordan Adams for her help in the field. Also, much appreciation to Brendan Murphy for helping me with field equipment and GIS-related questions, as well as Hima Hassenruck-Gudipati for help with MatLab. Greatest of thanks to my all friends and family, who have provided an ear to listen, a shoulder to cry on, and unlimited hugs when needed. I could not have done it without you.

Last, but certainly not least, I would like to my thank my dear husband, Anthony Marino, who enthusiastically embarked on this journey with me. His unwavering love and support helped me though the worst of times and the best of times alike.

Abstract

Isolating Lithologic Controls on Landscape Morphology in the Guadalupe Mountains, New Mexico and Texas

Emily Bradshaw Marino, M.S. Geo. Sci.

The University of Texas at Austin, 2017

Supervisor: Joel Johnson

In many geomorphic studies, lithologic contrasts are often acknowledged as important for landscape form, but are otherwise ignored in attempts to infer tectonic forcing or climatic control from topography. It remains difficult to separate the effects of tectonics, climate, and lithology due to the limitations of commonly used landscape evolution models. Tectonic inactivity and relatively little spatial variability in climate make the Guadalupe Mountains of Texas and New Mexico an ideal site to isolate and investigate the effects of lithology on topography.

To assess the control of lithology, I compared topographic metrics including channel steepness index, channel concavity, and topographic relief in different mapped lithologic units across the region. Topographic metrics were calculated using elevation data extracted from USGS 10m Digital Elevation Models. These metrics were grouped spatially based on 23 regionally mapped lithologic units, including abundant limestone and dolomite with some evaporites, sandstone, and shale. To better evaluate the different rock units, I used published unit descriptions to develop a simple, semi-quantitative system to estimate

the relative durability rating (RDR) of each rock unit. This rating system accounts for rock type and other rock properties such as relative bed thicknesses or spatial heterogeneity.

RDR values were found to be correlated with unit-averaged channel steepness for each of the 23 lithologies in the region. Channel steepness shows a moderate correlation with RDR ($R^2 = 0.44$; Kendall's $\tau = 0.52$), demonstrating quantifiable control on landscape form. However, concavity does not show a significant correlation ($R^2 = 0.016$; Kendall's $\tau = 0.13$). Stratigraphic relationships among units suggest that thick, resistant reef deposits exert the main lithologic control on overall channel forms in the region. Less resistant units stratigraphically below these reef deposits generally have higher than expected steepness given their RDR. Units at the bottom typically have high concavity values as well. The opposite is true for weaker units stratigraphically above the resistant reef formations, which have lower steepness and higher convexity. The contrasting influence of strong units above or below weaker units and their observed effects on channel form should improve our ability to infer rock properties from topography, and to predict the evolution of landscapes with lithologic variability.

Table of Contents

List of Tables

List of Figures

INTRODUCTION

Iconic landscapes of the American Southwest, with towering cliffs rising out of the surrounding desert, display clear examples of lithologic control. Horizontal layers of rocks are stacked atop one another in these arid and semi-arid settings, resulting in contrasting morphologies: steep cliffs as described above, as well as more gentle hillslopes, both influenced by bedrock strength and other rock properties (Figure 1). The various processes and controls that shape the landscape are often studied through the examination of rivers and streams and though channels only account for a small percentage of the land surface, they serve as a key boundary condition for hillslope erosion, setting the relief structure and ultimately controlling denudation rates through incision (Whipple and Tucker, 1999; Kirby et al., 2003; Whipple, 2004). The morphology of bedrock channels is especially important, as changes in the shape of longitudinal stream elevation profiles carry crucial information concerning climatic, tectonic, and lithologic variations (Whipple and Tucker 1999; Snyder et al., 2000; Perron and Royden, 2013). Streams in steady state are expected to demonstrate concave-up morphologies (Snyder et al. 2000; Whipple, 2004); however, changes in the long profile are often manifested as knickpoints, knickzones, or convex reaches (Pederson and Tressler, 2012). Generally, these deviations can represent adjustments from tectonic or climatic fluctuations, base-level drop, or contrasts in rock strength (Duvall et al., 2004; Hilley and Arrowsmith, 2008; Berlin and Anderson, 2009). However, it remains difficult to separate the effects of the various feedbacks due to the limitations of models most commonly used. Equations used to quantify these changes in channel form are most commonly derived from the Shear-stress/Stream power erosion model (Sklar and Dietrich, 1998; Whipple and Tucker, 1999; Lague, 2014), which serves to simplify complex relationships and feedbacks into a model that can be easily applied and tested.

a.

b.

c.

d.

Figure 1. Photographs from the Guadalupe Mountains showing the variety of cliff faces and hillslopes in the region. Photo (a) is more representative of the lower relief topography in the north, where the other photos (b, c, and d) are representative of the higher relief topography in the central and southern regions. Photo (b) shows El Capitan.

The stream power erosion model is a semi-empirical set of equations widely used to predict erosion rates and patterns along bedrock channels. With increasing access to digital topographic information, these equations have been used broadly for a variety of geomorphic studies. Examples of its applications include mapping river incision rates and inferring uplift patterns (Wobus et al, 2006; Kirby and Whipple, 2012), modeling knickpoint migration (Crosby and Whipple, 2006; Berlin and Anderson, 2009), and using it in landscape evolution studies and numerical models (Stock and Montgomery, 1999; Han et al., 2015; Forte et al, 2016). Though this model is widely applied, it is simplistic and lacks sensitivity to account for complex tectonic, climatic, and lithologic variability (Whipple and Tucker, 1999; Lague, 2014). It remains difficult to separate these effects and many studies have avoided addressing this issue by isolating variables of interest. For example, lithologic contrasts are often acknowledged as important, but by focusing on environments without variable lithologies, studies can better determine the effects of tectonic forcing (e.g. DiBiase et al., 2012) or climatic control (Moon et al., 2011; Chadwick et al., 2013; Murphy et al., 2016). Isolating variables in this way successfully removes complicating effects, but even in seemingly homogeneous lithologies, there can be variations in erodibility across the landscape (Snyder et al., 2000; Small et al., 2015). Ignoring lithology also overlooks the possible influence of stratigraphic lithologic contrasts, which could impact both channel and hillslope form.

The importance of lithologic control has been evident since early geomorphic studies (Gilbert, 1877). Hack's (1975) model of dynamic equilibrium balanced erosional and resistive forces over time and through this, he recognized that areas of resistant rock typically had steeper slopes and relief than softer, more erodible rock units. Transitioning across multiple rock types within channels has also been shown to significantly affect overall channel form in some landscapes, often resulting in convex reaches and again

with generally higher steepness values for stronger lithologic units (Duvall et al., 2004; Jansen et al., 2010; Pike et al., 2010; Goode et al., 2010). Bursztyn et al. (2015) found a correlation between measured rock tensile strength and river gradient ($R^2 = 0.51$), as well as a significant power-law correlation between reach-averaged unit strength and stream unit power ($R^2 = 0.60$). The effects of lithology and bedrock strength are not only limited to channels. For example, Hurst et al. (2013) show that increased incision rates due to uplift, result in varying hillslope morphologies for different lithologies in the Sierra Nevada range. The granodiorite hillslopes display a shape similar to model predictions of steady state hillslope morphology, suggesting rapid adjustment to incision. However, hillslopes underlain by metavolcanic rocks display high gradients with lower hilltop curvature, indicating slower adjustment to incision. Johnstone and Hilley (2014) showed that downslope transport rates of sediment vary due to varying soil thickness and slope, which are attributed to the varying weatherability of the different lithologic strata in the Gabilan Mesa of California. These studies show the importance of lithologic influences outside of channels. Despite the empirical evidence from these studies, there remains a surprising lack of understanding of how measurable lithologic properties, such as bedrock strength or jointing/fracturing, quantitatively control channel slope or concavity.

Selby (1980) developed an empirical, semi-quantitative system to evaluate geomorphic rock mass strength and the stability of bedrock slopes, including factors such as intact rock strength, weathering, groundwater flow, and the spacing, orientation, width and continuity of joints. Several other geomorphic studies have focused on bedrock slope stability, demonstrating that these properties can significantly influence morphology (Schmidt and Montgomery, 1995; Clarke and Burbank, 2011). Roy et al. (2016) explored the mechanical properties of rocks through landscape modeling, finding that mechanical heterogeneities can exert strong controls on both the rates and patterns of erosion.

Additional numerical modeling studies further explore variations in rock strength, but also investigate bedrock properties such bed thickness and bedding orientations, with results indicating that contrasts in these properties can generate changes in landscape form and can also impart significant spatial variations on erosion rates (Forte et al., 2016; Perne et al., 2016). The complex interactions of varying rock properties within these models suggest that real world interactions are likely even more complex, possibly resulting in misleading erosion rates and model results for studies discounting these factors. I hypothesize that topographic metrics can be used to predict or infer some bedrock properties, such as erodibility, which are imbedded within the morphology of the landscape. I also hypothesize that channel profile shape is heavily influenced by the most resistant units, whose position in relation to weaker units can significantly affect morphology, resulting in variability among predicted relationships with topographic metrics.

This thesis analyzes the relationship between channel morphology and bedrock lithology. First, I further consider the stream power erosion model and how the interplay of variables obfuscate the influence of lithology and bedrock properties. Then I discuss the regional setting for this study, exploring how the geologic history, climate, tectonics, and variations in lithology make the Guadalupe Mountains an appropriate setting to study the effect of lithology on topography. To evaluate the enigmatic relationship between bedrock properties and the stream power law, I compare calculated steepness and concavity indices to the relative durability of mapped lithologic units. I then determine if these topographic measurements can serve as a predictor of bedrock properties and discuss in detail the spatial distribution and patterns of these metrics across the Guadalupe Mountains region. I investigate specific areas in the region where these relationships appear variable and perhaps different, in order to better understand complicating factors affecting the

channel morphology. Confounding factors such as spatial lithologic variations within mapped units, as well as interactions between units of softer and harder rock, offer potential explanations for variability.

THEORETICAL BACKGROUND

As discussed above, the stream power erosion law is often used to model some of the feedbacks involved in bedrock incision, in order to predict erosional patterns. The stream power erosion law is shown in equation 1:

$$E = KA^m S^n \tag{1}$$

where (E) is the rate of erosion, (K) is bedrock erodibility, (A) is the contributing drainage area, and (S) is channel gradient or slope. Exponents m and n are often determined empirically. The contributing drainage area serves as a proxy for the discharge, which is assumed to scale with the size of the watershed (Sklar and Dietrich, 1998). It is important to note that many different properties are embedded within the erodibility term (K), including bedrock strength, which is considered a first-order control, but also weatherability and climate, channel-width scaling, and sediment load (Howard and Kerby, 1983; Whipple and Tucker, 1999). In some numerical models, the value of K is empirically fit based on topography (Howard et al., 1994; Stock and Montgomery, 1999). Despite the importance of rock strength, understanding the role of other properties within the erosion model remains a major task.

For quantitative analysis and the study of longitudinal river profiles (Figure 2a), equation 1 can be rearranged to solve for slope, where gradient is expressed as a power law function of contributing drainage area:

$$S = k_s A^{-m/n} \tag{2}$$

where $k_s = (E/K)^{1/n}$ and represents the steepness index, which is the channel gradient normalized to the contributing drainage area (Wobus, Crosby, and Whipple, 2006). The value m/n can be evaluated from the slope of a regression line in log-log space and can be

rewritten to represent the shape or concavity of the stream (Sklar and Dietrich, 1998) as shown in equation 3:

$$S = k_s A^{-\theta} \tag{3}$$

where θ is the concavity index (Flint, 1974; Wobus et al., 2006), which is the measure of how slope changes longitudinally with drainage area (Wobus, Crosby, and Whipple, 2006). In many eroding landscapes, equation 3 is most applicable to drainage areas larger than roughly 0.1 to 5 km^2, below which debris flows and landsliding may be more important than fluvial processes (Lague, 2014). Since the setting of this study has relatively little tectonic activity or climatic variance, equation 3 can be used to explore lithologic influences on overall longitudinal form of river profiles.

Normalized steepness indices (k_{sn}), along with a common reference concavity index (θ_{REF}), allows for meaningful comparisons among channels within a region. The reference concavity is a representation of the general shape of stream profiles across the entire region and equation 4 shows the normalized version of Flint's Law:

$$S = k_{sn} A^{-\theta_{REF}} \tag{4}$$

The normalized channel steepness index (k_{sn}) is very sensitive to the reference concavity value (θ_{REF}) and in order to compare k_{sn} values for different channels across the region, θ_{REF} must be fixed (Whipple and Tucker, 1999; Han et al., 2015). To find the most appropriate θ_{REF} value, the general shape of streams across the region were evaluated. For analysis, the logarithm of reach slope (S) and drainage area (A) are plotted against one another, creating what is commonly referred to as a slope-area plot (Figure 2b). To find concavity, we calculate the slope of the regression line fitted to the slope-area data in log-log space. By taking the logarithm of equation 3, the terms become linear as shown in equation 5:

$$Log(S) = \Theta Log(A) + Log(k_s) \tag{5}$$

This linear equation follows the typical structure of y = mx +b, where log of slope is y, log of drainage area is x, θ represents slope (m), and log (k_s) is the y-intercept (b) (Figure 2b). This analysis was completed for many streams across the region and the average regressed concavity (θ_{REF}) of approximately 0.34 was found. According to Whipple (2004), θ_{REF} values for bedrock channels often vary between roughly 0.3 – 1.2, with lower values often representing short, steep drainages or downstream increases in either incision rates or rock strength. With an appropriate θ_{REF} value, we can perform regression analysis on the slope-area data to find values of normalized steepness indices (k_{sn}) by taking the logarithm of equation 4 to make the terms linear:

$$Log(S) = \Theta_{REF} Log(A) + Log(k_{sn}) \tag{6}$$

where log of slope is y, log of drainage area is x, $\theta_{REF} = 0.34$, and log (k_{sn}) is the y-intercept (Figure 2b). Equation 6 can be used to fit distinct values of k_{sn} along the channel profile by setting regression bounds manually, allowing for different segments of the stream to be fitted independently. Equation 5 is used to fit the distinct values of concavity along the profile.

a.

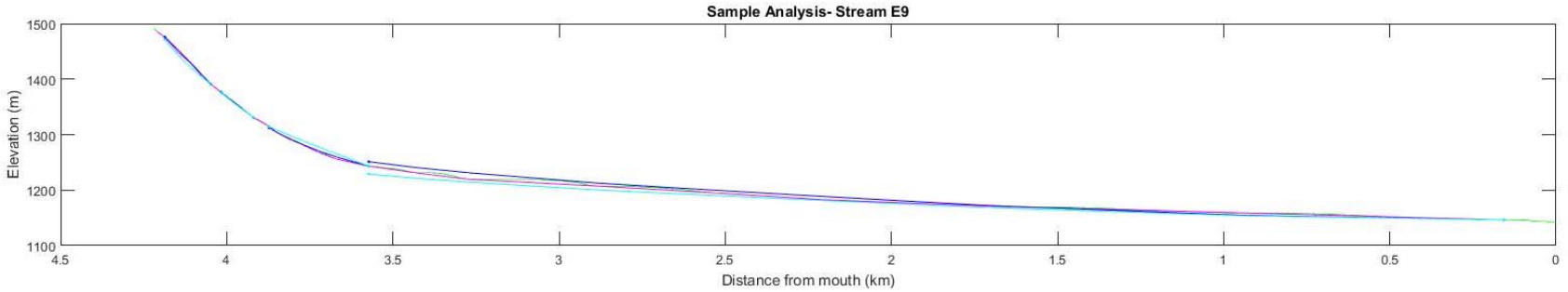

b.

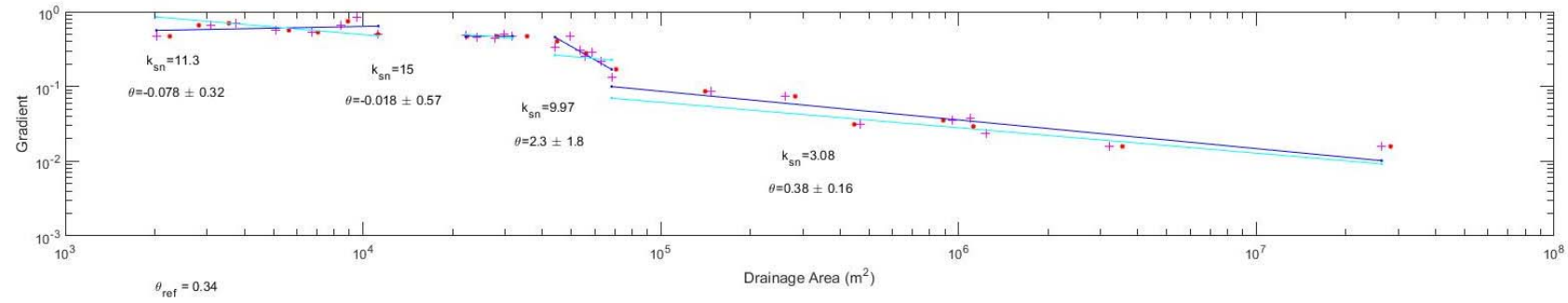

Figure 2. (a) Longitudinal Stream Profile (b) Slope Area Plot, used for fitting k_{sn} and concavity indices. Four distinct sections of the profile are fitted in this example, giving four different values of k_{sn} and concavity.

Normalized steepness is a useful metric for evaluating the role of lithology across the region because according to stream power relationships, we expect steeper channels to have higher shear stresses, thus faster erosion rates (Whipple and Tucker, 1999). Without other complicating factors, such as uplift or climate variability, we expect stronger lithologic units to be less erodible and to adjust to a steeper gradient than weaker units (Duvall et al., 2004; Jansen et al., 2010). This can be seen in figure 3a, which shows the expected form of the steady state hillslope in an environment with layered rocks of different erodibility. In this scenario, the channel slope of each unit is maintained according to strength and the more resistant unit has a higher k_{sn}. Additionally, streams in steady state are expected to generally have concave-up morphologies (Snyder et al. 2000; Whipple, 2004), but still maintain steeper slopes in the resistant units and lower slopes in the less resistant units above and below (Figure 3a). The changes in both steepness and concavity can be seen in the corresponding slope-area plot (Figure 3c). In this plot, the changes surrounding the resistant unit are obvious. The slope of this line represents the concavity and the concavity of the resistant unit is shown as lower than the weaker units for the steady state form. There could be a variety of options for the concavity of this unit, but given that convex reaches can represent a change in rock type when other factors are ruled out (Pike et al., 2010), a lower concavity seems more likely.

This study aims to examine the changes in the longitudinal profiles of streams across the region, in hopes of quantifying the effects of erodibility of upon steepness and concavity. However, since real landscapes are not likely follow the steady state model outlined above, there could be substantial deviations from the expected channel form. Complex interactions of softer and harder beds could result in significant variations in steepness and concavity, as illustrated in figure 3b. When examining steepness in particular, I hypothesize that the effects of the resistant bed may be to steepen the

underlying weak unit, while the weak unit above becomes less steep (Figure 3b). Both responses can be attributed to the influence of the resistant bed, which "pins' both upper and lower units in place as a consequence of geometry and reduced erosion rates of that resistant unit. This resistant unit provides a protective layer for underlying units, reducing their lateral retreat just below this contact. The mechanisms behind this steepening, likely due to sediment load, are discussed in detail in the discussion section. Alternatively, this resistant unit serves as a less erodible base level for the weaker upper units, limiting their downcutting.

When examining the response of concavity alone, again, the units below and above respond differently (Figure 3b). Units below, will steepen just below the "pinned" contact, resulting in a more concave profile, while units above may weather away just above the "pinned" contact, resulting in more convexity and signifying a change in lithologic resistance. The expression of these responses is evident in the slope-area plot (Figure 3d), where the lower unit has a steeper slope and higher y-intercept, indicating both higher k_{sn} and concavity. In contrast, the upper unit has a lower slope and y-intercept. This response, and many variations of it, was observed in many of the actual slope-area plots from the region (Figure 2b). These changes were quantified for across the region to discern if patterns exist and to what degree the deviations from steady state described above were present in this landscape.

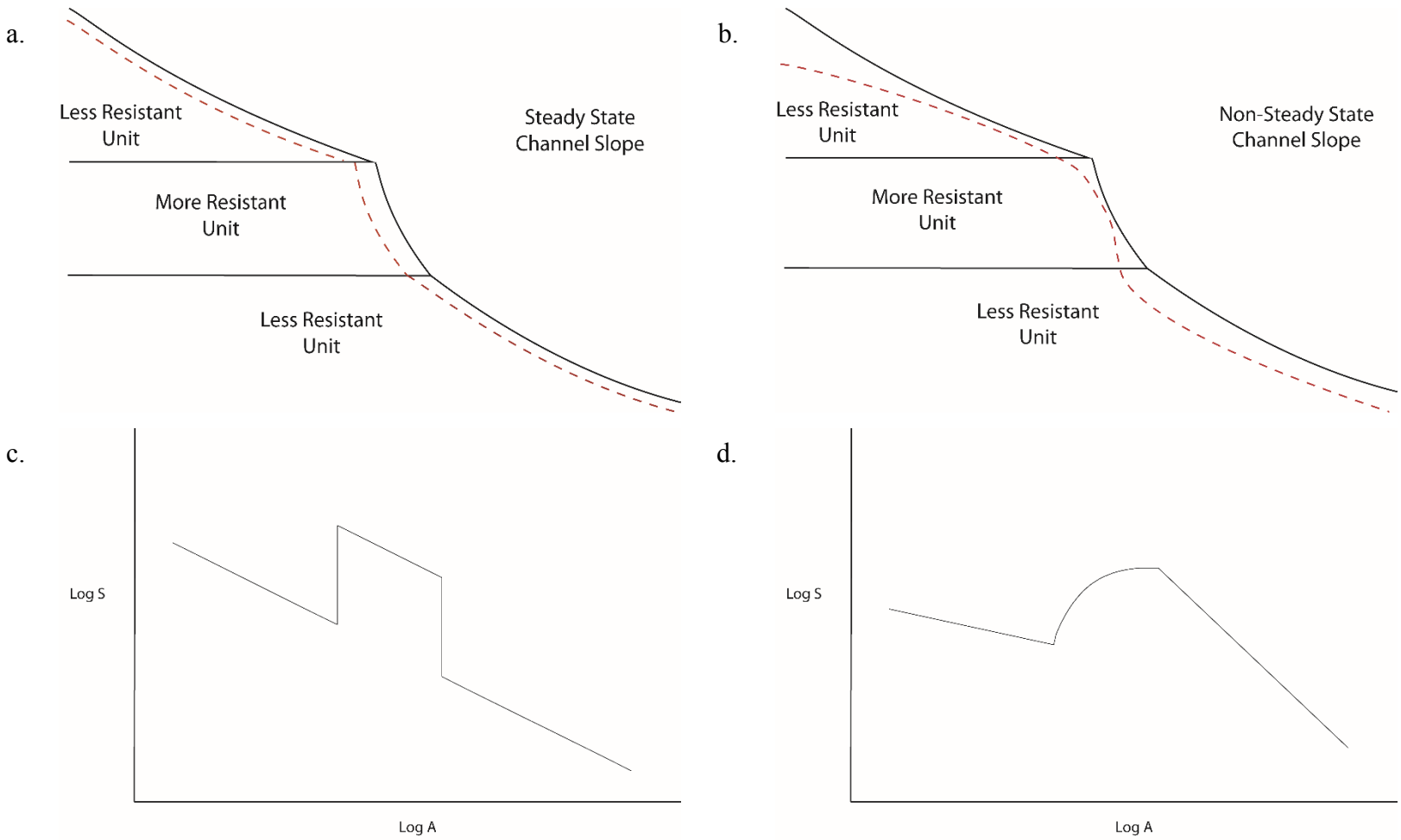

Figure 3. Longitudinal profile showing expected steepness/concavity of a steady state channel (a) and non-steady state channel (b) before and after erosion (red dashed line). Slope-Area plots showing how both steady state (c) and non-steady state (d) relationships would plot in log-log space. The slope of the line is concavity and the y-intercept is the steepness (k_{sn}).

STUDY AREA

The Guadalupe Mountains of western Texas and southern New Mexico represent a Permian reef complex and carbonate platform composed of primarily limestone and dolomite (King, 1948; Boyd, 1958). Elevation and relief increase to the south. The mountains are bounded by a fault-line escarpment to the west and by an exhumed reef escarpment and gypsum plains to the east (Hill, 1987). The study area covers an area of approximately 1630 km^2 (Figure 4). The highest point is located to the south at Guadalupe Peak with an elevation of approximately 2,667 m and the lowest point within the study area is about 1000 m and is in the lower relief northeastern section near Carlsbad Caverns, NM. Much of the study area is managed by the National Park Service, including both Carlsbad Caverns National Park and Guadalupe Mountains National Park, or by Lincoln National Forest, which stretches across the northwestern area of the region (Figure 4).

The regional climate is semi-arid, with mild winters and warm summers. During Pleistocene time, climate was wetter and cooler (Hill, 1987). Today, the mean annual temperature is 17.2°C and annual precipitation averages 37.6 cm for Carlsbad Caverns Park and about 44.2 cm for the Guadalupe Mountains to the south, with most of that falling during the summer months (U.S. National Park Service). Though weather conditions can be more variable in the higher relief southern region, overall there is not strong climate gradient present. The dramatic height of El Capitan above the surrounding desert is evidence of past uplift, which occurred in Miocene time (15 -5 Mya), though the region has been tectonically inactive in recent history (Hill, 1998). This lack of recent tectonic activity, along with the weak climate gradient, make the Guadalupe Mountains an ideal field site for isolating effects of rock properties on topography.

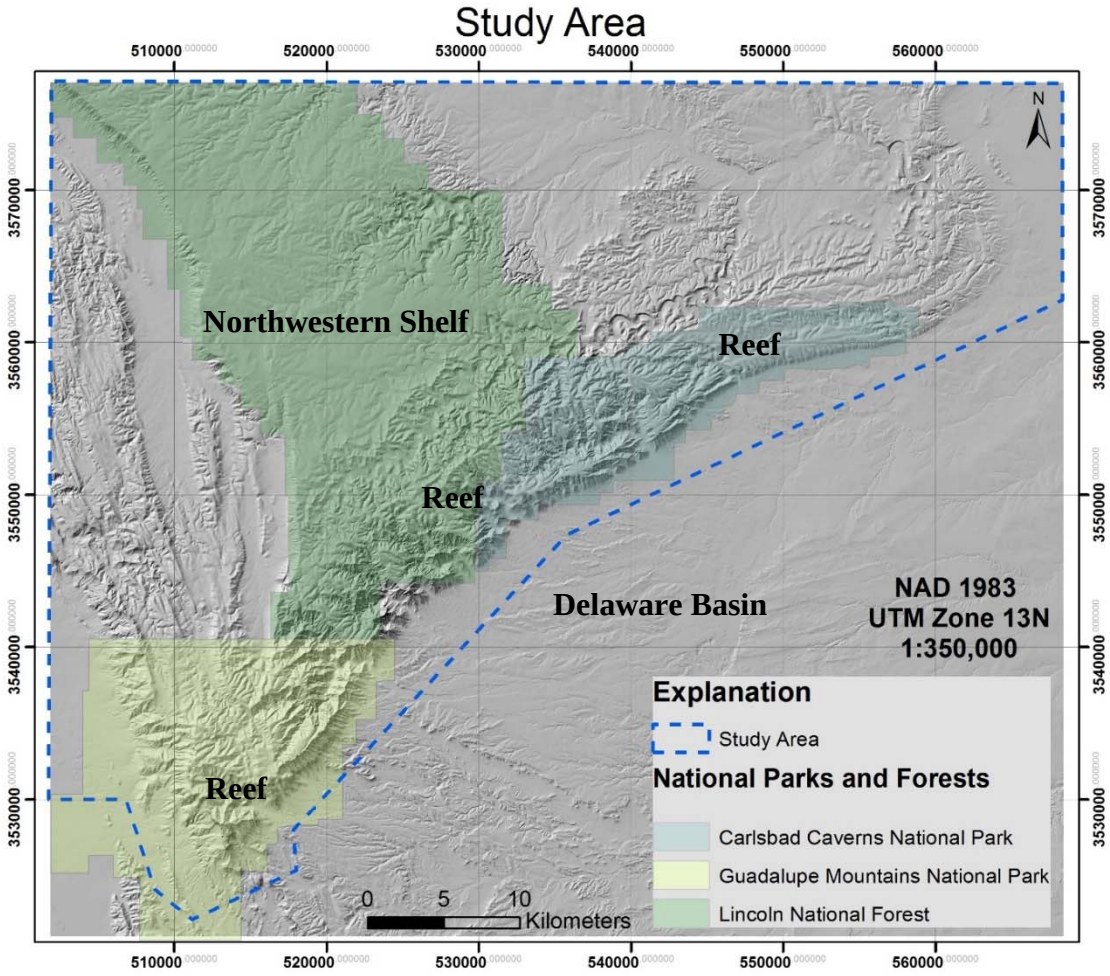

Figure 4. Map illustrating the study area and the various parks that manage it. Variation in topography in region is apparent. The three major depositional environments are also represented: The Delaware Basin, The Reef, and The Northwestern Shelf.

Throughout the Paleozoic era, this region was covered by a shallow sea and during the Permian approximately 10,000 feet of sediment accumulated as sand, shale, and limestone (Richey et al., 1985; Urbanczyk et al., 2001). Though the lithology in the Guadalupe Mountains is dominantly composed of carbonates, many mapped units also contain or primarily consist of sandstone, shale and evaporites, providing enough contrast to study the changes in channel gradient compared to rock type. The stratigraphy for the region and an illustration of the different reef deposits are shown in figure 5. The rocks in the region can generally be divided into three facies: the Delaware Basin, Reef, and the Northwestern shelf (Hill, 1987; Figures 4, 5a). The Delaware Basin deposits consist primarily of sandstones, which are exposed in the south and east, just below the massive carbonate reef deposits. During the Permian, organic reef building began along the rim of the Delaware Basin, ultimately culminating in a great barrier reef (Boyd, 1958). The build-up of these thick reef deposits resulted in a steep-sided, large carbonate platform, which provided a buffer for incoming waves, resulting in a calmer lagoon-type environment on the carbonate shelf, behind the reef (Figures 4, 5b). These deposits, representing much of the northwestern shelf deposits, are broad, thin-bedded limestones and mixed clastic deposits (Hayes, 1964). However, further to the northwest lies another type of reef deposit (Figure 5b). An abrupt change can be seen between the massive reef deposit to the south and the more thin-bedded shelf deposits to the northwest, which represent a ramp-style reef (Harris, 2005). It is important to note the differences in rock units from the northwest to southeast as the depositional setting will influence heterogeneity in the rock across the region (Figure 5a). The mapped lithologic units used for this study are shown in figure 6 and described in Table 1.

a.

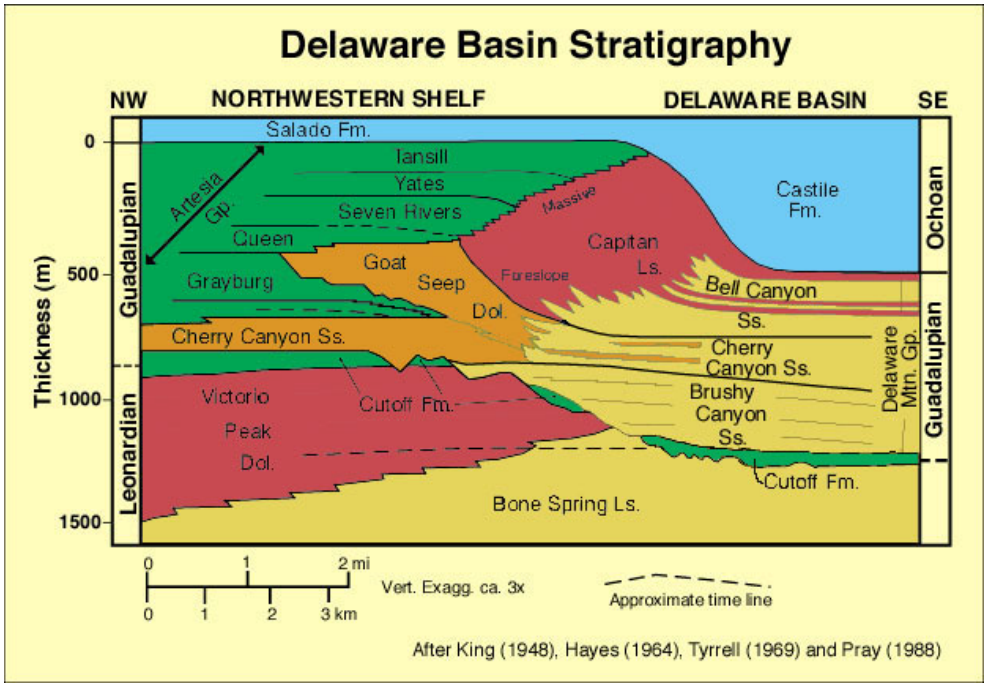

b.

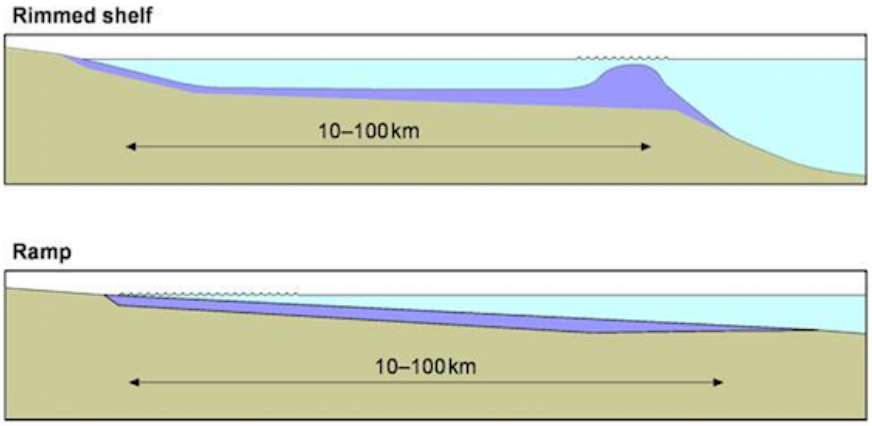

Figure 5. (a) Stratigraphy of the Delaware Basin, showing the basin to shelf transition (Modified from Scholle, 2002). Basin deposits are in yellow (including Pdc, Pds, and Pdb), Reef deposits are in blue (including Pc, Pcm, and Pg), and Shelf deposits are in pink (including Pt, Pya, Pcb, Pq, and Pgb). The lower units in gray include Pbv, Psh, and Pbl. The San Andres formation (Psal, Psau, and Psa) is not included in this figure. Please refer to Table 1 for more information on corresponding rock units. (b) Schematic showing the different types of reef formation in the region (Modified from Nichols, 2009). The Ramped shelf matches the style along the margin of the northwestern shelf (Figure 4). The rimmed style reef corresponds the reefs highlighted in Figure 4 and in blue in the stratigraphic column above.

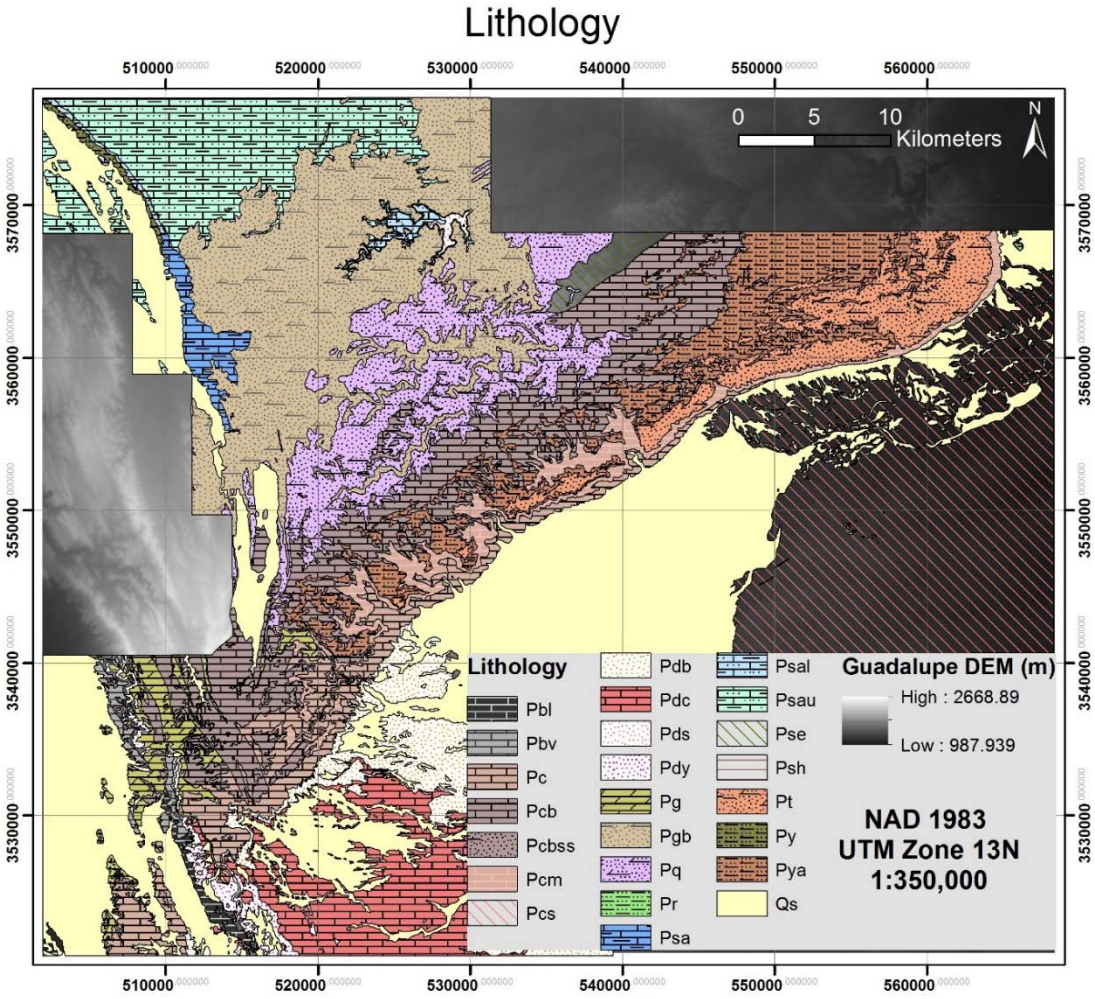

Figure 6. Map of the lithology of the region. Rock unit descriptions are available in Table 1.

Rock unit	Name(s)	Description	Evaporite (+1 per unit)	Shale (+2 per unit)	Sandstone (+3 per unit)	Limestone or Dolomite (+4 per unit)	Massive (+1) and thin or heterogeneity (-1)	Number of rock types (divide)	RDR
Pcs	Castile Formation	Evaporites: Primarily Gypsum and Salt.	2				-1	2	**0.50**
Pt	Tansill Formation	Dolomite with few thin beds of sand/silt. Grades to anhydrite and salt northward.	1		3	4	-1	3	**2.33**
Pya	Yates Formation	Gray and red sand with some dolomite/shale. Weathers to gentle slopes. Three distinct beds of dolomite seperated by persistent beds of quartz sansdstone.		2	6	4	-1	3	**2.75**
Pse	Seven Rivers Formation (evaporite facies)	Evaporite facies: Primarily Gypsum, but with some sandstone, shale, and dolomite.	1	2	3	4	-1	4	**2.25**
Pcb	Carlsbad Limestone + Seven Rivers Formation (carbonate facies)	Limestone combined with northern carbonate facies, which are thin-bedded limestone and dolomite, transitioning into gypsum and red beds in NE.	1	2		8	-1	4	**2.50**
Pq	Queen Formation	Mostly sand with some dolomite (mostly bottom/middle), as well as anhydrite and salt.	1		3	4	-1	3	**2.33**
Pgb	Grayburg Formation	Dolomite to sandy dolomite with abundant sand and some anhydrite.	1		3	8	-1	4	**2.75**
Psa	San Andres Limestone	Thick-bedded limestone transitioning into crytalline dolomite to the NW. Some minor shales present.		2		8	1	3	**3.67**
Psau	San Andres Limestone, upper member	Limestone with some anhydrite and red beds. Possible thick gypsum beds to the North.	1	2		4	-1	3	**2.00**
Psal	San Andres Limestone, lower cherty member	Basal member consisting of dense zone of dolomite. Includes medium-to-fine-grained sandstones and siltstones to very fine-grained sandstone and pisolitic-fenestral dolograinstones/wackestone.			6	8	-1	4	**3.25**
Py	Yeso Formation	Dolomitic limestones with gypsiferous, gray shales.	1	2		4		3	**2.33**
Qs	Quarternary Sediments	Includes both older and younger alluvial deposits ranging from silt-size to gravel/cobbles and even some massive boulder size blocks of limestone (less common). Cemented in some places.		2					**2.00**

Table 1. Rock unit abbreviations, names, descriptions, and RDR values. Unit descriptions were derived from various sources (King, 1948; Boyd, 1958; Alnaji, 2002; USGS, 2017). Units are arranged in approximate stratigraphic order. Please refer to Appendix A, Figure 27 for the stratigraphic column.

Rock unit	Name(s)	Description	Evaporite (+1 per unit)	Shale (+2 per unit)	Sandstone (+3 per unit)	Limestone or Dolomite (+4 per unit)	Massive (+1) and thin or heterogeneity (-1)	Number of rock types (divide)	RDR
Pcm	Capitan Limestone, massive (reef) member	Massive white limestones. Consists in part of compact light-gray, cream-colored, or white calcitic limestone associated with dolomitic limestones.				4	1		**5.00**
Pc	Capitan Limestone (including breccia(reef-talus) member)	Thick-Bedded or massive white limestones of reef facies. Includes brecciated member. Consists in part of compact light-gray, cream-colored, or white calcitic limestone associated with dolomitic limestones.				4	1		**5.00**
Pcbss	Carlsbad Limestone, sandstone member	Mixture of carbonate and sands.			3	4		2	**3.50**
Pg	Goat Seep Dolomite/LS	Thick-bedded to massive dolomite/limestone; in part sandy. Similar to thick-bedded limestones in the south, but different in age. Dolomite interfingers with the			3	8	1	3	**4.00**
Pds	Sandstone tongue of Cherry Canyon Formation	Moderately resistant, indistinctly bedded, grayish orange, very fine grained, well-sorted quartz sandstone with scattered irregular chert nodules. Abundant fossils.			3		1		**4.00**
Psh	Bone Spring Limestone (cutoff shaly member)	Shale and thin-bedded limestone, eroded away completely in some portions. Limestone beds are separated by thin beds of black papery shale. 1-inch-thick layers of black chert are common.		2		4	-1	2	**2.50**
Pbv	Bone Spring Limestone (Victorio Peak gray member)	Black limestones with some lighter-colered beds. Thick-bedded. Some lower beds have numerous chert nodules, but upper beds (approx 2/3) do not. Upper				4	1		**5.00**
Pbl	Bone Spring Limestone (black limestone beds)	Black limestone beds. Thin-bedded limestone, in part shaly.		2		8	-1	3	**3.00**
Pdb	Bell Canyon Formation	Primarily sandstone, with some thin, dark-gray limestone beds. Consists of very thick sandstones, alternating with less thick limestones, and rather hard		2	3	4	1	3	**3.33**
Pdc	Cherry Canyon Formation (all members)	It consists primarily of limestone with brownish, bituminous shales and some fine-grained sandstones.		2	3	4		3	**3.00**
Pdy	Brushy Canyon Formation	It consists primarily of thick, yellowish sandstones with rather distinct shale partings and is capped by massive yellow or brown ledges of coarser grain sandstone. Conglomerates at base.		2	6		1	3	**3.00**

Table 1 (continued). Unit descriptions were derived from various sources (King, 1948; Boyd, 1958; Alnaji, 2002; USGS, 2017).

METHODS

REGRESSION ANALYSIS

To calculate k_{sn} and concavity, slope-area regression analysis was performed using ArcGIS and MatLab software (Whipple et al., 2007). This software extracts elevations, stream head locations, and flow accumulation data from 10m USGS Digital Elevation Models (DEMs), transforming it into data to be analyzed within MatLab. Charts used in the analysis include longitudinal stream profiles and slope-area data, which were used for the regression analysis (Figure 2). Equations 5 and 6, which are described in detail in the section above, were used to find concavity and steepness indices respectively. The crucial advantage of using this method was the ability to calculate individual steepness and concavity indices for different segments of the channel, quantifying how the profile changes spatially. Indices for each stream were mapped in ArcGIS for spatial comparisons.

SPATIAL AND STATISTICAL ANALYSIS

Lithologic units were adapted from National Park Service GIS data in shapefile format (NPS Geologic Resources Inventory Program, 2006 and 2007). Both the Guadalupe Mountains and Carlsbad Caverns National Parks have published maps. However, some mapped bedrock units are inconsistent in places across the state line between New Mexico and Texas, requiring editing to make the transition of units across this divide continuous. Detailed methods of combining some mapped units for consistency across the area are included as Appendix A. Figure 6 shows the finalized lithologic map, and Table 1 provides unit descriptions. Normalized steepness and concavity indices were compared to mapped lithologic units across the region. In addition to the regressed steepness and concavity values, local relief was also calculated and compared to lithology. Software within ArcMap was used to calculate the spatial intersection of the mapped lithologic units and the metrics

listed above, resulting in tables of unique combinations of lithology paired with k_{sn}, concavity, and relief. The resulting datasets can be divided by lithologic unit to make statistical comparisons, which are discussed below.

RELATIVE DURABILITY RATING (RDR)

In addition to the spatial and statistical comparisons described above, I also compared the topographic metrics to the estimated erodibility of the rock units in this region. It would be difficult and time consuming to measure geomorphically-relevant field erodibility over a large area, especially considering the lithologic heterogeneity of this region, where many of the mapped units grade into one another due to the shelf-reef-basin transition (Figure 5a). Lacking direct measurements of geomorphic rock mass strength and other factors affecting erodibility, a semi-quantitative ranking system was developed to estimate the relative durability rating (RDR) of each rock unit. Though this rating is serving as a proxy for bedrock erodibility, larger values represent more resistant material, giving a relative measure of durability rather than erodibility.

For this ranking system, a first order value of 1-4 was assigned to each rock type included in the description, with 1 representing the weakest rocks and 4 representing the hardest rocks. A value of 1 was given to evaporites, which are weak and prone to dissolution. A value of 2 was assigned to shaley units, which are easily eroded. Sandstones were given a designation of 3 due to the presence of quartz particles. Finally, the least erodible lithologies in this region are interpreted to be limestone and dolomite layers, which were given a value of 4. Some of the layers are described as "massive" indicating very thick deposits. These thick deposits add to the durability of the unit, so a value of +1 is applied. There are also units with layered beds that are described as quite thin, which would make them more erodible, so thin-bedded units were given a value of -1. Many of the descriptions included a large variety of rock types for a single unit, indicating

considerable heterogeneity. To account for this, unit descriptions that detailed a great number of rock types or indicated lateral spatial changes in lithology were also given a value of -1. Rock durability values were summed, including values for massive, thin, or heterogeneous, for each distinct unit. This summed value was then divided by the number of rock types present to get an average relative durability for that unit (Table 1). For example, the Queen Formation (Pq) is described as mostly sandstone with some dolomite, as well as anhydrite and salt (Table 1). To calculate the RDR, a value of 3 is assigned for the sand, a value of 4 is assigned for the dolomite, and a value of 1 is assigned for the anhydrite/salt. A value of -1 was assigned to account for heterogeneity. The sum of these values is 7, which was then divided by the number units present (3) to get the RDR, which is 2.33. Relative durability ratings for all units are listed in Table 1, alongside their descriptions. The spatial distribution of RDR values is shown in figure 7.

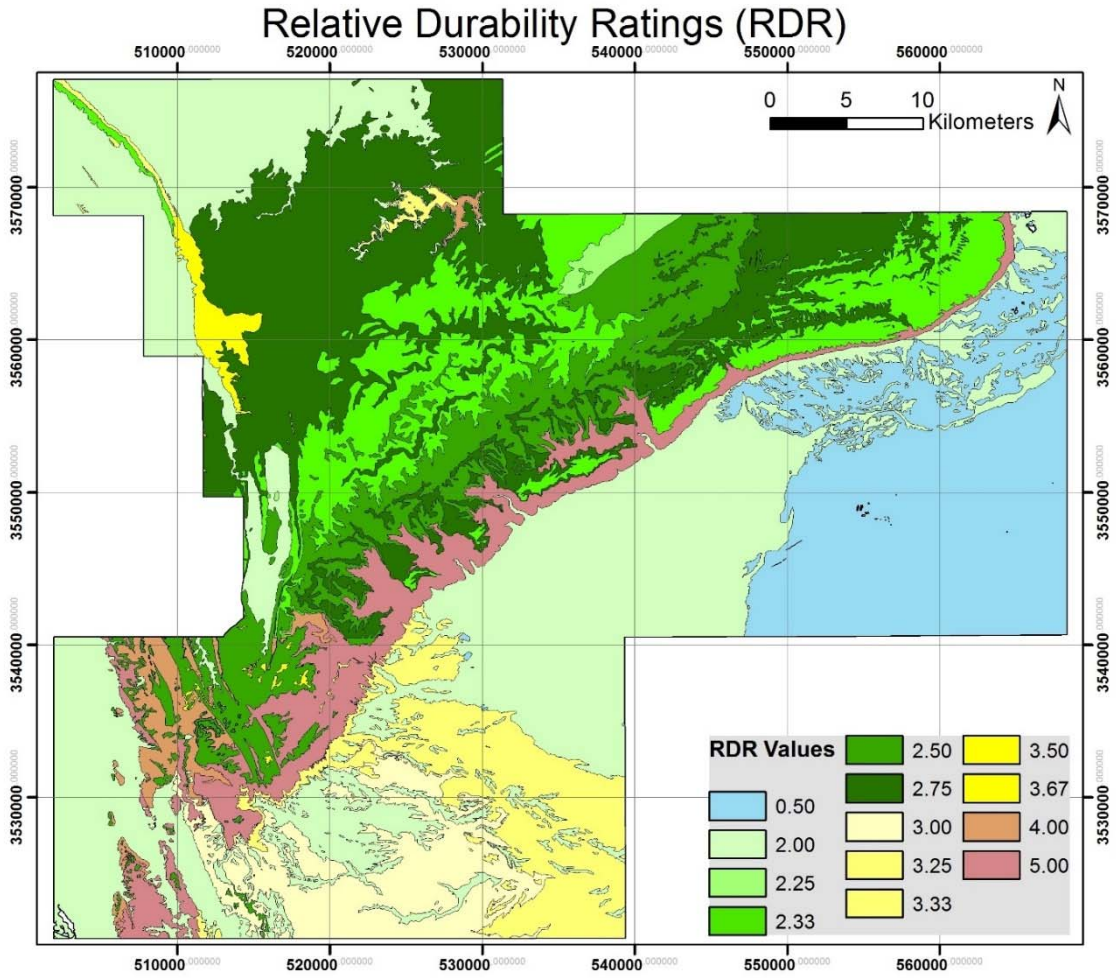

Figure 7. Map of Relative Durability Rating (RDR) for the region. Values also listed in Table 1, along with rock unit names, descriptions, and calculation of RDR values. Figure 5a is colored to match the RDR ratings and provides nice visual arrangement of these units.

RESULTS

Channel topographic metrics, k_{sn} and concavity, are compared to mapped lithologic units. Kruskal Wallis tests are performed to compare the distributions of each metric per mapped lithologic unit. Averaged values of k_{sn} and concavity for each unit are then compared to RDR values in order to determine their predictive potential. This is completed through linear regression analysis and also through a non-parametric correlation using Kendall's τ. Mean k_{sn} and concavity for each unit are also compared to one another. Cluster analyses are presented, showing how groups of statistically high and low k_{sn} and concavity values, independent of lithology, are spatially distributed across the region. Average relief per rock unit is also compared to k_{sn}, concavity, and RDR, providing an additional topographic metric for evaluation.

NORMALIZED STEEPNESS INDICES (K_{SN})

Normalized steepness indices (k_{sn}) were calculated for 1050 total streams within the Guadalupe Mountains region (Figure 8). For each of the channels, reaches with similar slope-area scaling were manually fit to equation 6. The fitting of different segments was done based on the slope-area data alone, without considering locations of lithologic contacts (Figure 2b). The overall mean and standard deviation (+/- 1 σ) for k_{sn} was 8.96 +/- 7.21 (Figure 9a). The distribution of k_{sn} values were also determined for the channel reaches falling within each of the 23 mapped lithologic units (Figure 6; 9b; Table 2). The largest and smallest average k_{sn} belongs to the Victorio Peak member (Pbv; k_{sn} = 21.36) and the Castile formation (Pcs; k_{sn} = 2.52), respectively. The Bell Canyon formation (Pdb; k_{sn} = 11.32) has the largest standard deviation (+/- 1σ) at 10.96 and the evaporite facies of the Seven Rivers Formation (Pse; k_{sn} = 3.38) has the least variability with a standard deviation of only 1.48. It is important to note that lithologic units have varying sample

sizes, dependent upon the extent mapped within the study area. I performed a Kruskal Wallis hypothesis test to determine if the distributions are the same or whether any unit distributions were statistically and significantly different than the others. The Kruskal Wallis test demonstrates that at least one, but possibly several, of the k_{sn} distributions are significantly different, indicating that bedrock lithology does influence channel steepness in the study area. However, this test cannot identify which specific groups are dissimilar, warranting additional investigation.

To determine the predictive quality of these topographic metrics, I compare the mean k_{sn}, which is weighted by channel length, of each rock unit to its relative durability rating (RDR). The linear regression of the mean k_{sn} and RDR for each lithologic unit gives an R^2 value of 0.43 (p-value = 0.0006), indicating a moderate significant correlation (Figure 10). To better understand the relationship between these values, a non-linear rank correlation coefficient was calculated. The distribution of k_{sn} indicates that the data are not normally distributed (Figure 9), so a non-parametric test may be a more useful measure of correlation. Using the non-parametric Kendall's Tau coefficient (τ), I determined the relationship between RDR and mean k_{sn} by comparing the ranked values. Kendall's τ, which measures a correlation between 0.0 and 1.0, was 0.52 (p-value = 7.4675×10^{-4}) for these variables, suggesting a statistically significant higher degree of correlation than the linear fit.

Unit	Ksn Sample Size	Weighted Mean Ksn	Ksn Standard Deviation (+/- 1 SD)	Ksn Standard Error (+/- 1 SE)	Concavity Sample Size	Weighted Mean Concavity	Concavity Standard Deviation (+/- 1 SD)	Concavity Standard Error (+/- 1 SE)	Relief (1500m)
Pbl	41	15.09	8.55	1.34	41	1.47	2.25	0.35	641.4
Pbv	51	21.36	10.44	1.46	51	0.97	1.34	0.19	847.4
Pc	369	14.37	7.94	0.41	373	0.74	2.17	0.11	609.2
Pcb	781	6.89	5.07	0.18	784	0.19	1.15	0.04	344.5
Pcbss	46	8.65	4.38	0.65	45	0.32	0.79	0.12	489.6
Pcm	303	12.12	8.53	0.49	306	0.58	2.64	0.15	486.6
Pcs	95	2.52	1.50	0.15	94	0.61	1.13	0.12	75.8
Pdb	103	11.32	10.97	1.08	103	1.72	3.21	0.32	339.1
Pdc	62	12.18	5.96	0.76	62	0.76	3.96	0.50	354.9
Pds	51	15.41	8.63	1.21	53	1.49	1.88	0.26	635.6
Pdy	52	13.62	9.91	1.37	52	0.60	2.40	0.33	658.6
Pg	141	11.58	7.63	0.64	142	0.34	1.24	0.10	578.6
Pgb	708	4.50	3.58	0.13	718	0.08	0.94	0.03	179.1
Pq	378	4.71	3.50	0.18	382	0.37	0.85	0.04	217.1
Psa	86	10.33	7.01	0.76	86	0.57	1.59	0.17	364.9
Psal	74	11.33	6.15	0.71	74	0.00	10.00	1.16	360.6
Psau	312	4.51	5.55	0.31	313	0.15	0.98	0.06	174.2
Pse	42	3.38	1.48	0.23	43	0.33	0.28	0.04	175.6
Psh	36	19.41	7.61	1.27	36	0.82	0.87	0.15	782.1
Pt	248	4.71	4.70	0.30	253	-0.07	3.92	0.25	209.0
Py	35	11.09	5.44	0.92	35	1.82	2.40	0.41	514.7
Pya	472	5.07	5.93	0.27	475	0.17	2.97	0.14	276.4
Qs	550	7.08	5.42	0.23	553	1.27	1.54	0.07	224.5

Table 2. Mean k_{sn} and concavity values for each rock type. Sample sizes, standard deviations, and standard errors are also reported. The mean relief (given in meters and evaluated using a 1500-m radius circular window) for each rock type is also included.

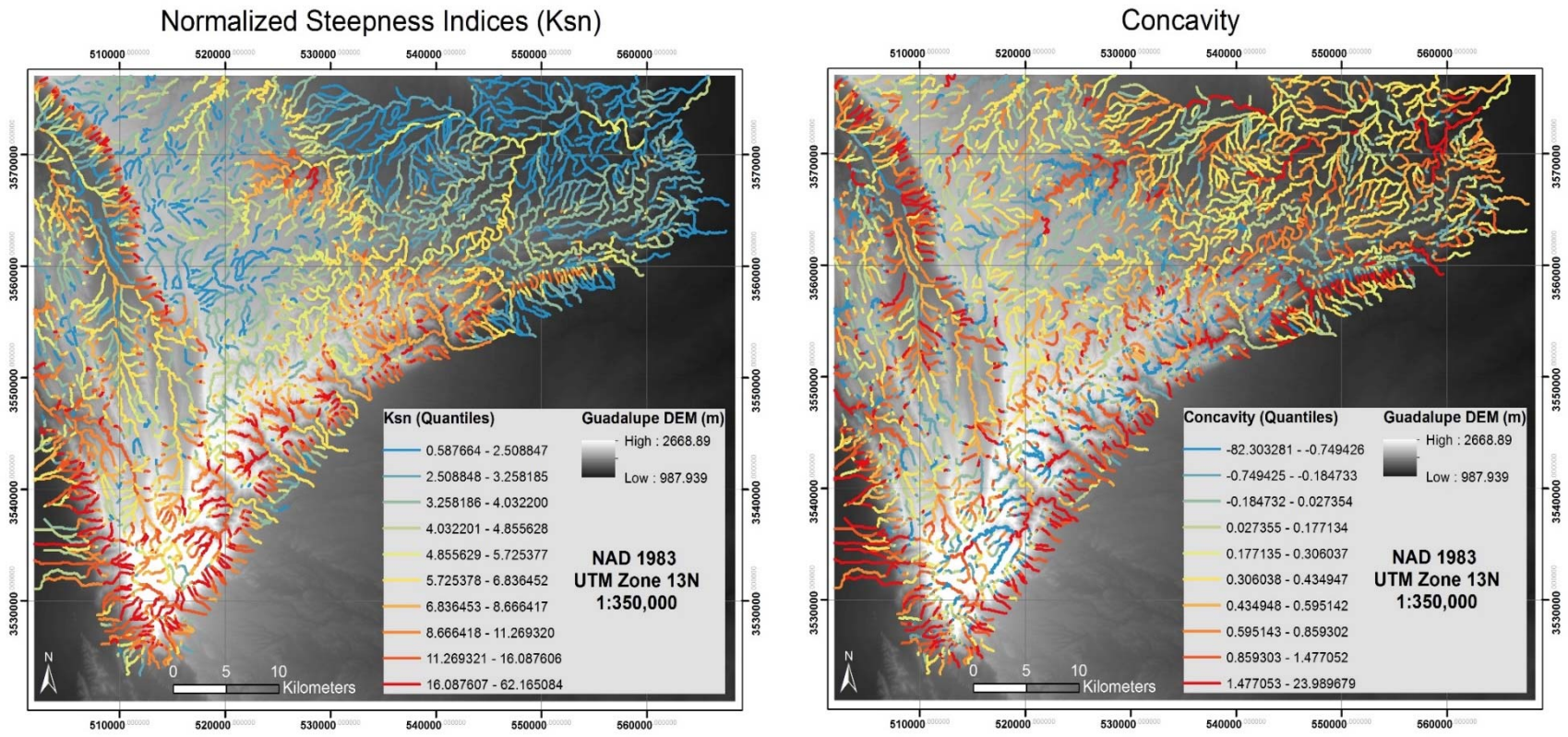

Figure 8. Spatial distribution of steepness (k_{sn}) and concavity across the region for 1050 streams.

a.

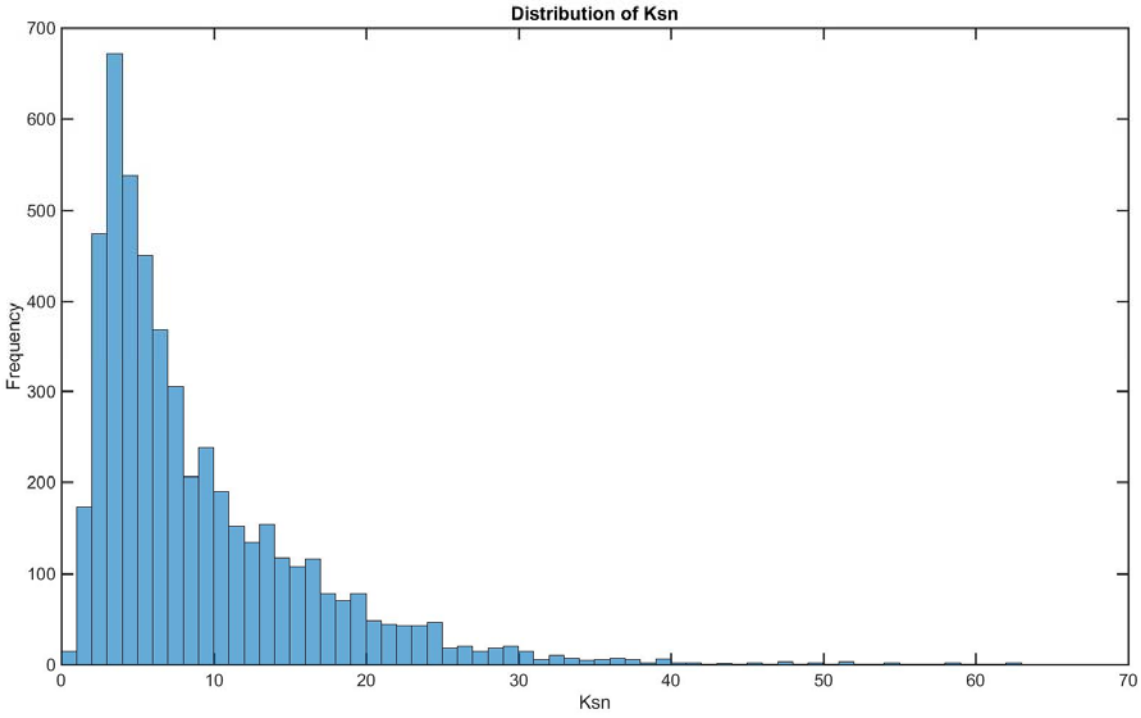

b.

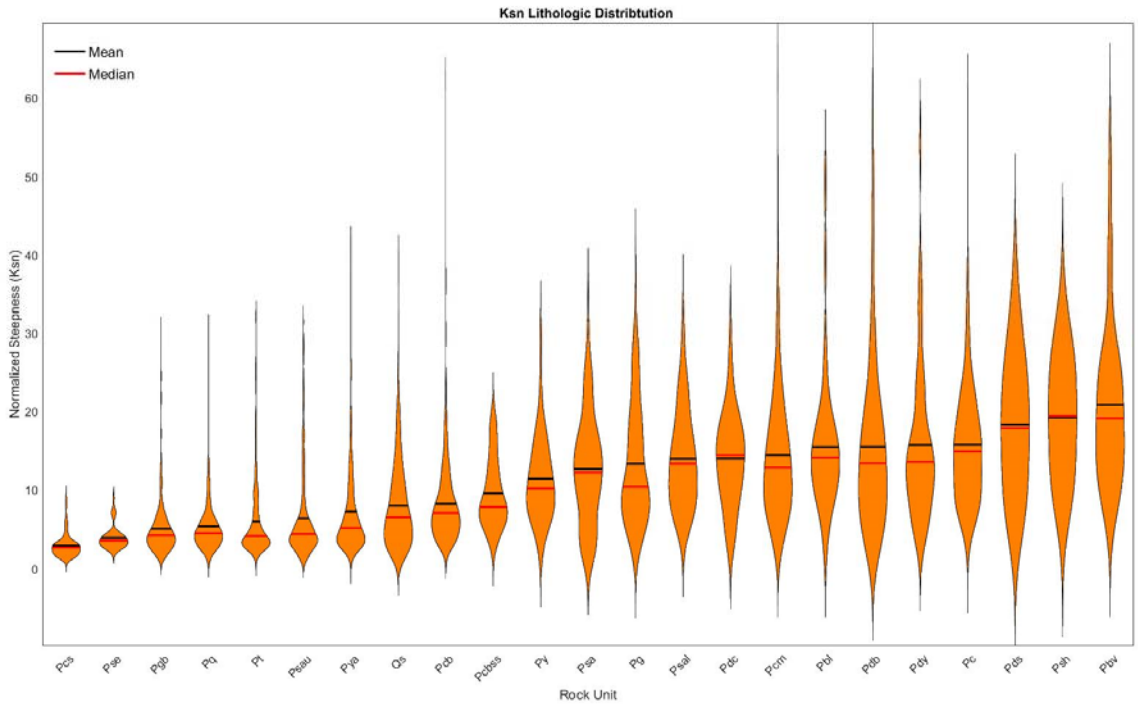

Figure 9. (a) Total k_{sn} distribution. (b) The k_{sn} distribution per rock unit. Means are in ascending order. Violin plots created using code developed by Hoffman (2015).

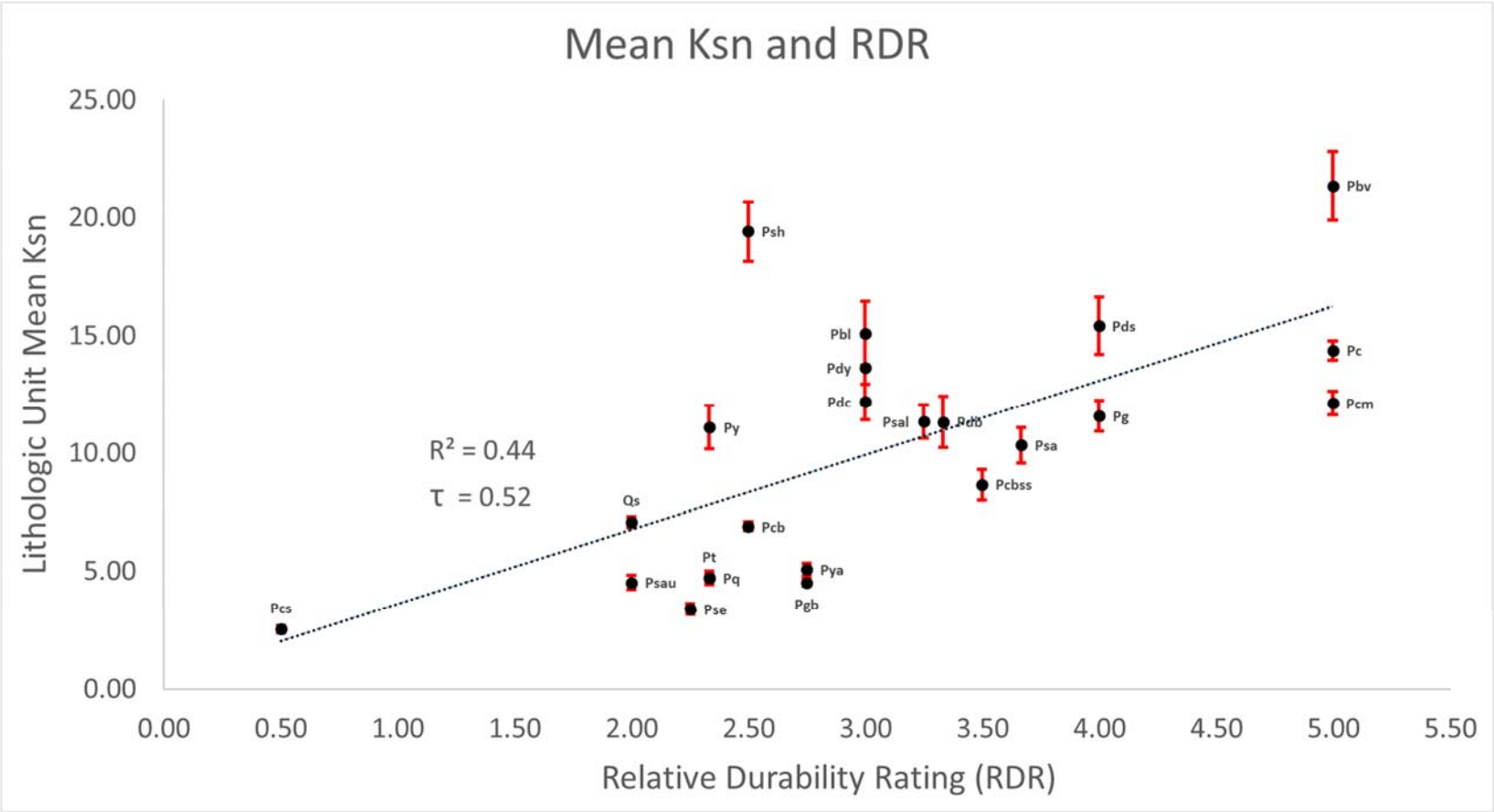

Figure 10. Correlation of mean k_{sn} and Relative Durability Rating (RDR). R^2 and Kendall's Tau coefficient included on chart.

CONCAVITY

Like k_{sn}, concavity values for the region can be characterized by a single value for some shorter channels, but many were fitted with multiple values in order to track spatial changes (Figure 8). The overall mean and standard deviation (+/- 1 σ) for concavity values was 0.34 +/- 2.14. The total distribution, as well as the distribution of concavity for each rock unit, are displayed in Figure 11. Weighted mean concavity values, along with standard deviations and sample sizes, for each rock unit are displayed alongside k_{sn} values in Table 2. Concavity values, like k_{sn}, were weighted by channel length. The most negative average concavity value, which indicates this rock type was slightly convex, was within the Tansill formation (Pt; θ = -0.073) and the most positive value of concavity fell within the Bell Canyon sandstone (Pdb; θ = 1.72), respectively. The lower San Andres (Psal; θ = 0.001) unit has the largest standard deviation of 10.00 and the Queen formation (Pq; θ = 0.37) has the least variability with a standard deviation of only 0.85. I performed a Kruskal Wallis test for concavity results and like the k_{sn} test, they show that at least one, but possibly several, of the distributions are significantly different. To determine the predictive potential of the concavity measurements, I compared the mean concavity for each rock unit to RDR. The linear regression for this relationship is displayed in Figure 12. This linear correlation gives an R^2 value of 0.016, indicating a poor relationship. I also calculated the non-parametric Kendall's τ coefficient, which showed a slightly stronger correlation with a coefficient of 0.13, yet the p-value was large (p = 0.40) indicating the results are not statistically significant. The linear regression of k_{sn} and concavity yield an R^2 value of 0.25 (p-value = 0.015) and a τ of 0.43 (p-value = 0.0035), which are statistically significant, indicating some degree of correlation, but not a particularly strong one (Figure 13).

a.

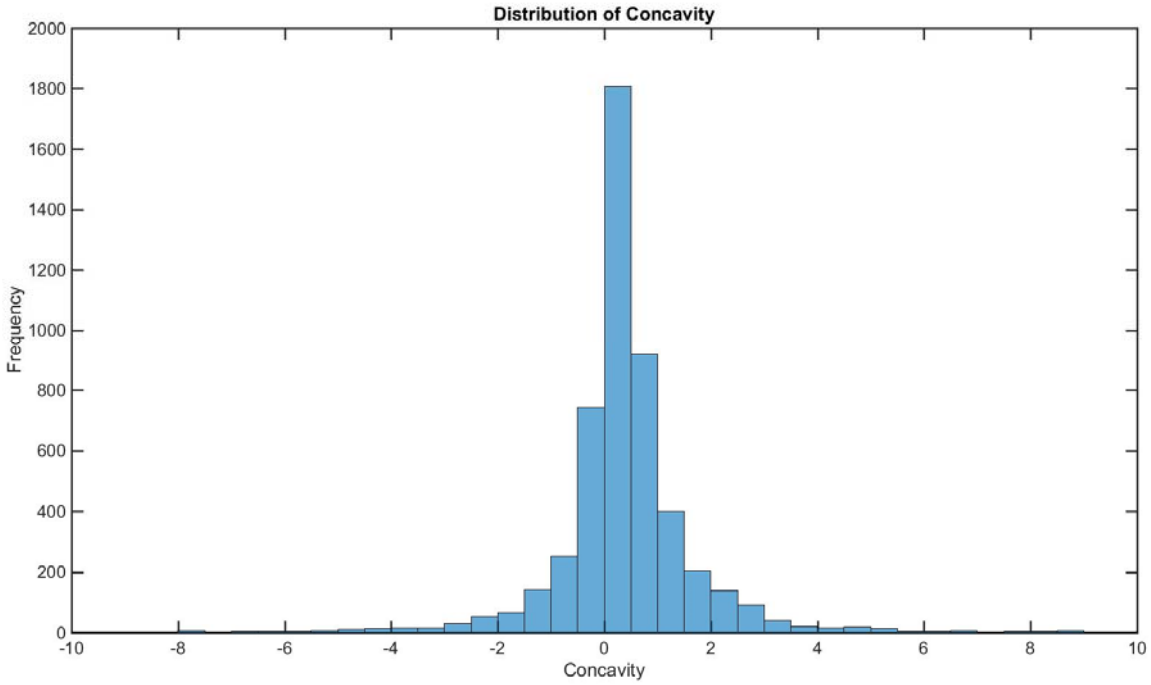

b.

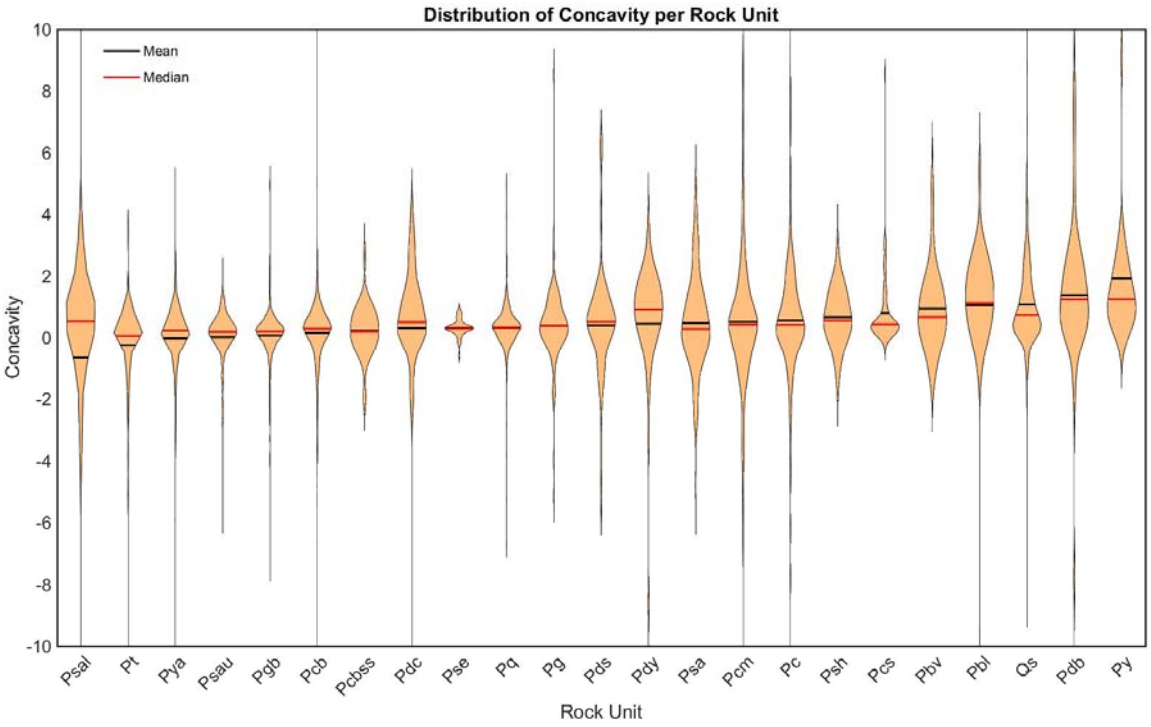

Figure 11. (a) Overall concavity Distribution. (b) Concavity distribution per rock unit. Means are in ascending order. Y-axis is set at 10 and -10, though there are few outliers beyond this point. Violin plots created using code by Hoffman (2015).

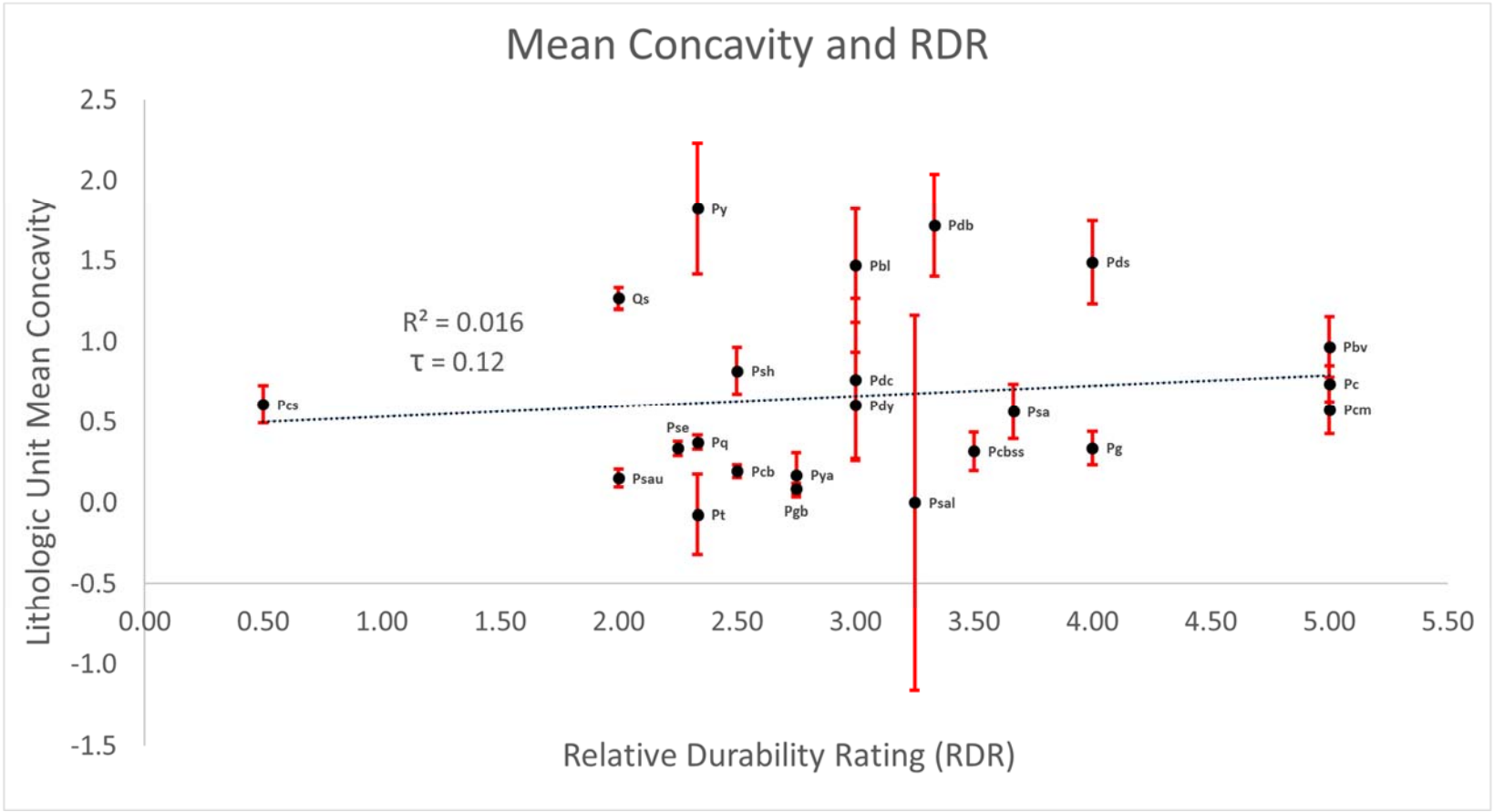

Figure 12. Correlation of mean concavity and Relative Durability Rating (RDR). R^2 and Kendall's Tau coefficient included.

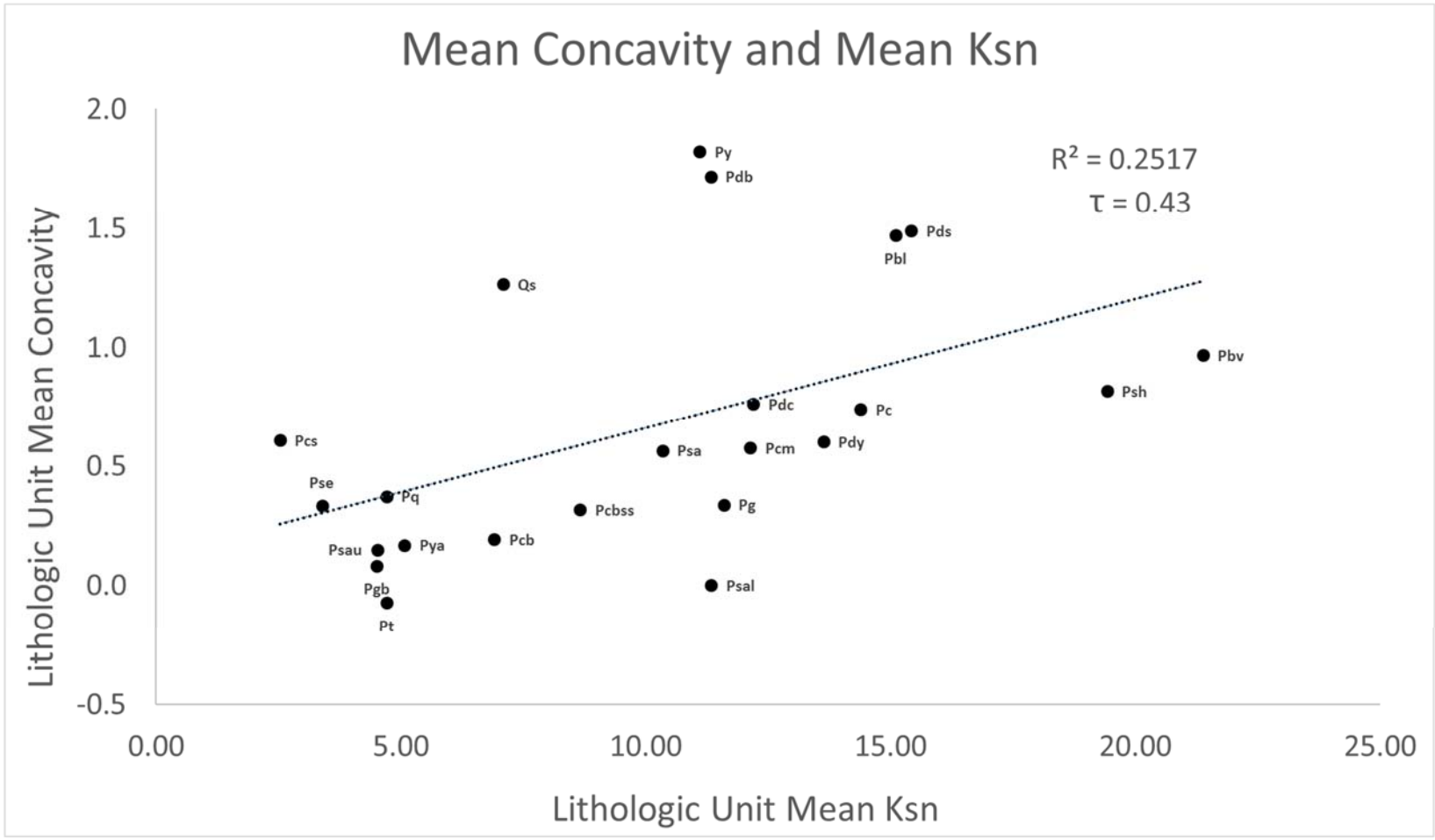

Figure 13. Correlation of mean concavity and mean k_{sn}. R^2 and Kendall's Tau coefficient included.

CLUSTER ANALYSES

Cluster statistics are used to gain a better understanding of how k_{sn} and concavity values may be spatially related or grouped. Calculated clustering is independent of lithologic contact locations and calculations were completed using ArcGIS. Spatial cluster analysis was performed using inverse distance weighting, which assumes that nearby neighboring features have a larger influence on the computation for a target feature than features that are further away. The clustering analysis is based on Anselin's Local Moran's I statistics, which identifies local spatial clustering of high and low values. The analysis produces a spatial distribution of cluster types, which indicate clusters of high-high (HH) and low-low (LL) values, as well as high-low (HL) and low-high (LH) values. For example, for an HH value it simply means that the specific value for a given channel is high and is also surrounded by other channels with similarly high values. Statistically insignificant values are also indicated (INS). The spatial distribution of the results for both k_{sn} and concavity are displayed in Figure 14. The clustering statistics demonstrate that many of the spatial patterns in k_{sn} are statistically significant. However, patterns of concavity may be less meaningful.

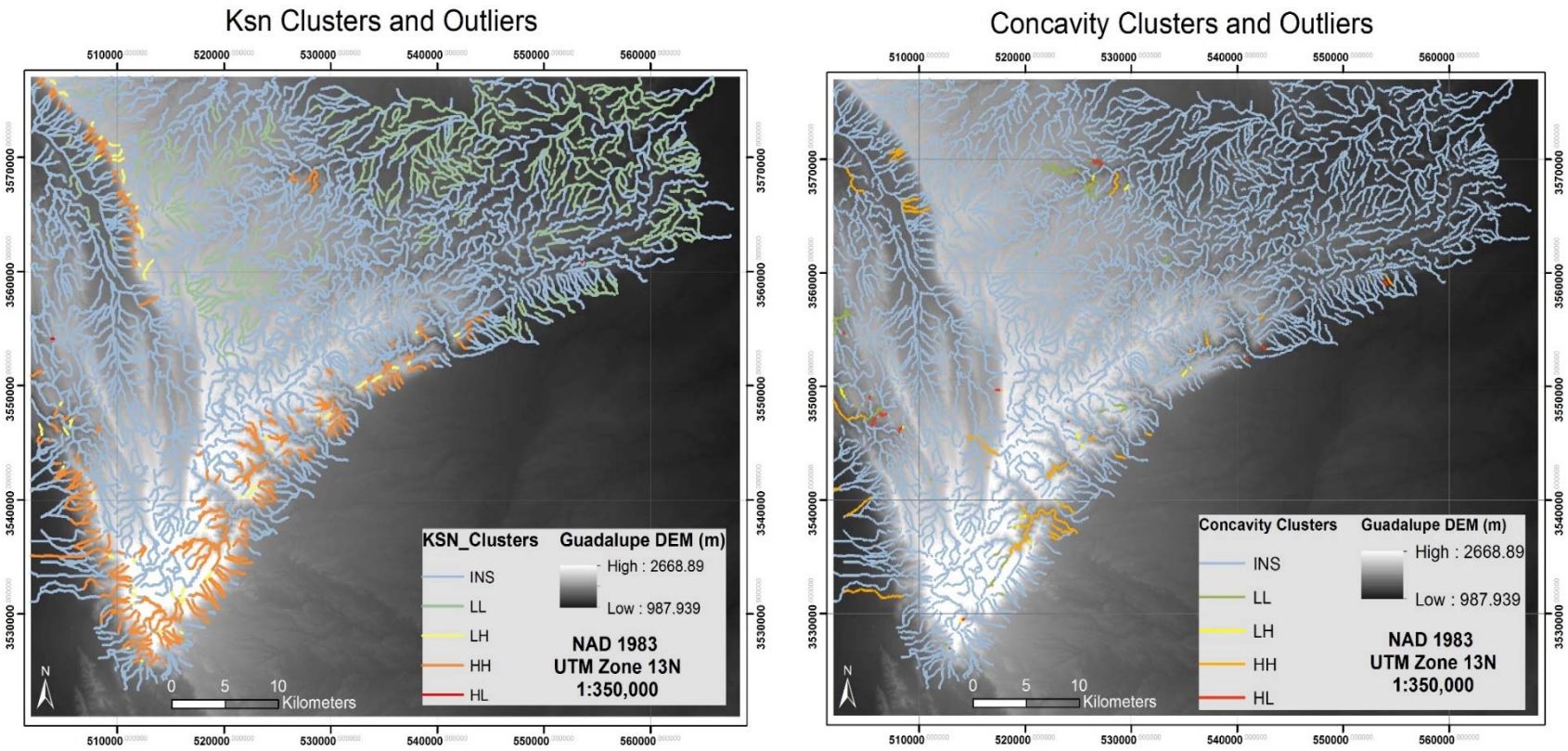

Figure 14. Cluster analyses show high and low values for k_{sn} and concavity. Values plotted as INS are insignificant.

COMPARISON TO RELIEF

A map of relief for the region is shown is Figure 15. Relief was calculated using a 1500-meter circular window in which the minimum elevation was subtracted from the maximum elevation. This distance was chosen in order to fully characterize the drainage divides in the region, where there is an average ridge-to-ridge distance of approximately 1500 meters. The relief of each unit was compared to RDR (Figure 16). The regression of the two gives an R^2 of 0.43 (p-value = 0.0006) and a τ of 0.54 (p-value = 5.0515×10^{-4}), indicating similar success for predicting RDR as k_{sn}. A comparison of mean k_{sn} and relief is shown in Figure 17. The mean relief for each lithologic unit was calculated, excluding data outside of the main study area (Figure 4). Importantly, note that the relief was not only calculated along channels (as with k_{sn}), but over the entire area of each lithologic unit. The linear regression in Figure 17 shows that the relief of each rock unit correlates well with mean k_{sn}, giving an R^2 0.89 (τ = 0.8; p-value = 1.36×10^{-11}). The linear correlation of concavity and mean relief was poor, with an R^2 value of only 0.18.

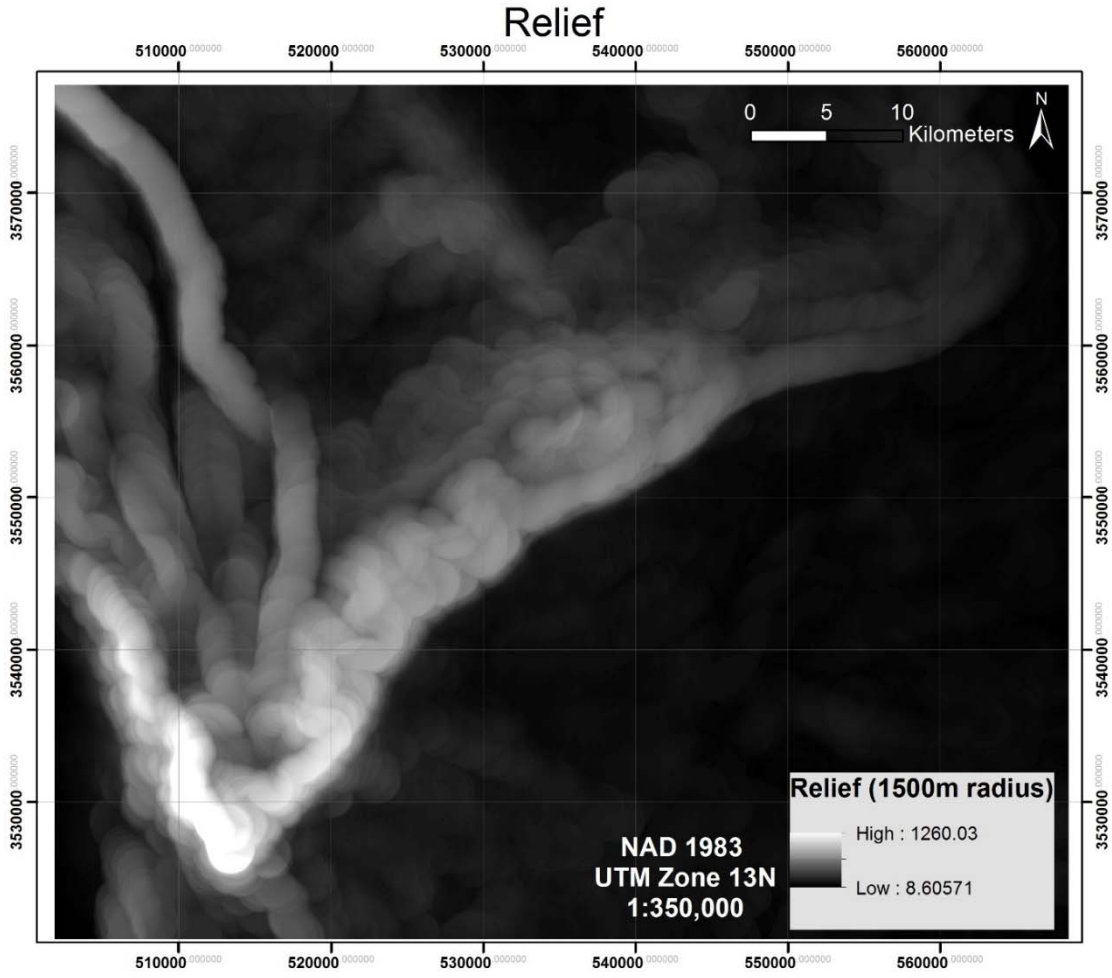

Figure 15. Map of relief, calculated using circular windows of 1500m radius.

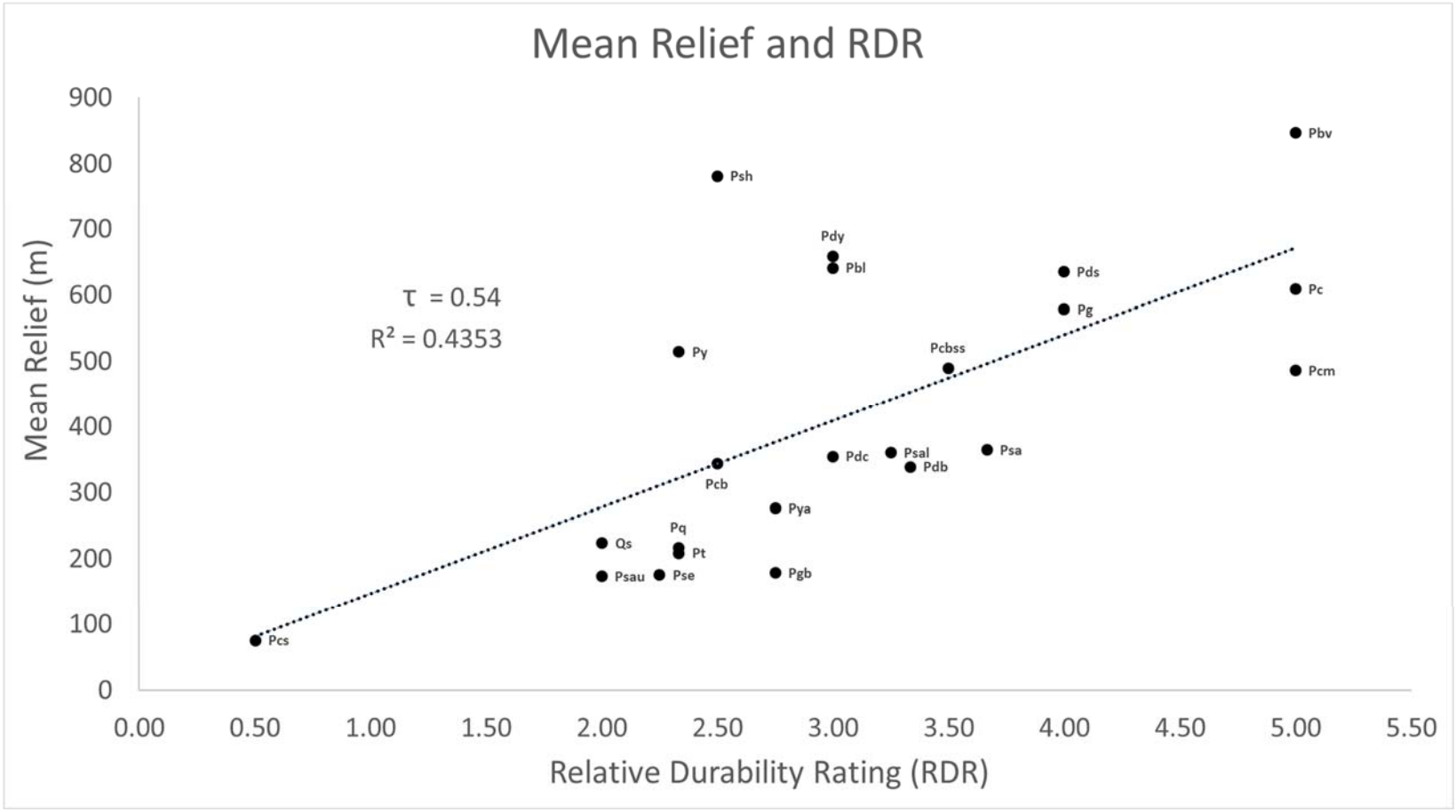

Figure 16. Correlation of mean relief and Relative Durability Rating (RDR). R^2 and Kendall's Tau coefficient included.

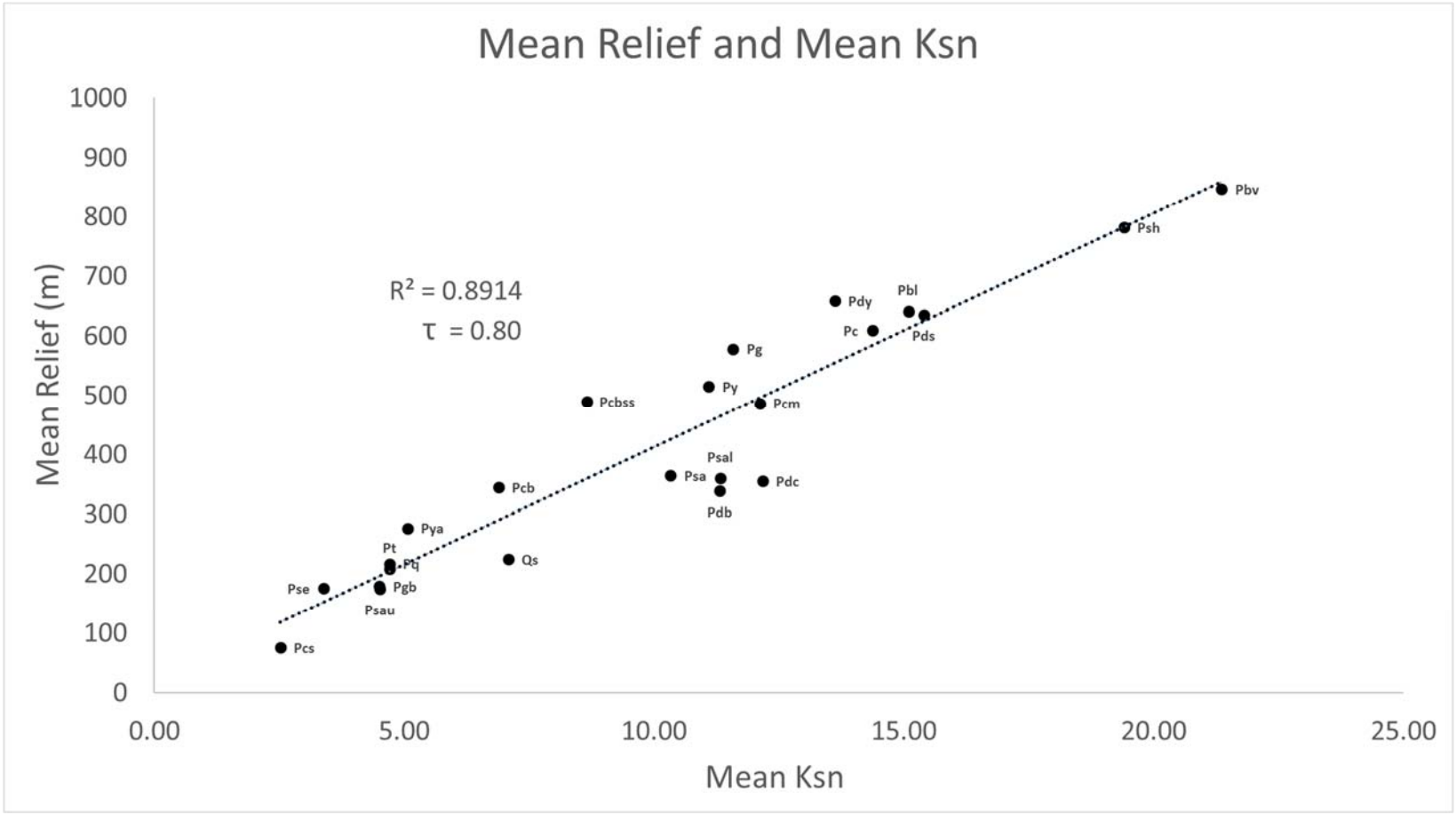

Figure 17. Correlation of mean relief and mean k_{sn}. R^2 and Kendall's Tau coefficient included

DISCUSSION

The stream power erosion law is widely used as a straightforward method for modeling landscape evolution and studying various factors that control landscape form. However, the influence of bedrock properties and other factors that affect erodibility, while evident in landscape form, remains difficult to model accurately. The goal of this study was to determine the relationship between bedrock properties, namely rock durability/erodibility, and topographic metrics such as steepness and concavity, which can be easily extracted from remotely sensed elevation data. In this section, I interpret the significant but relatively weak correlation between RDR and k_{sn} to be influenced by the resistant reef deposits along the different locations of the carbonate platform margin. Additionally, I discuss how these resistant units, and the relative stacking of units of different durabilities, can affect channel form. Spatial relationships of k_{sn} and concavity show that lithologic control exerted by resistant reef deposits heavily influences the shape of the channels in this region.

NORMALIZED STEEPNESS INDICES (K_{SN})

When steepness is differentiated by rock type (Table 2; Figure 9b), we see that standard deviations remain quite high, but that differences among the k_{sn} of the units are obvious. In general, we expect that stronger lithologic units will exhibit higher steepness (Duvall et al., 2004; Jansen et al., 2010; Pike et al., 2010; Goode et al., 2010); however, the degree of lithologic control is not clear. The linear correlation of the two shows a moderate link between the measurements, which was expected, but certain rock units fall far outside of the relationship predicted by the linear fit (Figure 10). This indicates that lithologic strength is not the only factor affecting the steepness of the channel. The location of many of these atypical units within the stratigraphic framework suggest some degree of

lithologic control, which relates to the resistant reef deposits in the region, but does not directly correlate to the erodibility of a given unit. The mapped quantiles of k_{sn}, as well as the cluster analyses, show three areas of high k_{sn} values (Figures 8, 14), which correspond to these locations: The Southern Reef Rim (Zone 1), The North Central Reef Rim (Zone 2), and The Algerita Escarpment and Last Chance Canyon, which are located at the Northwest Shelf and Margin (Zone 3) (Figure 18). These regions correspond to the two types of reef deposits, which formed on the platform margins (Figures 4, 6b).

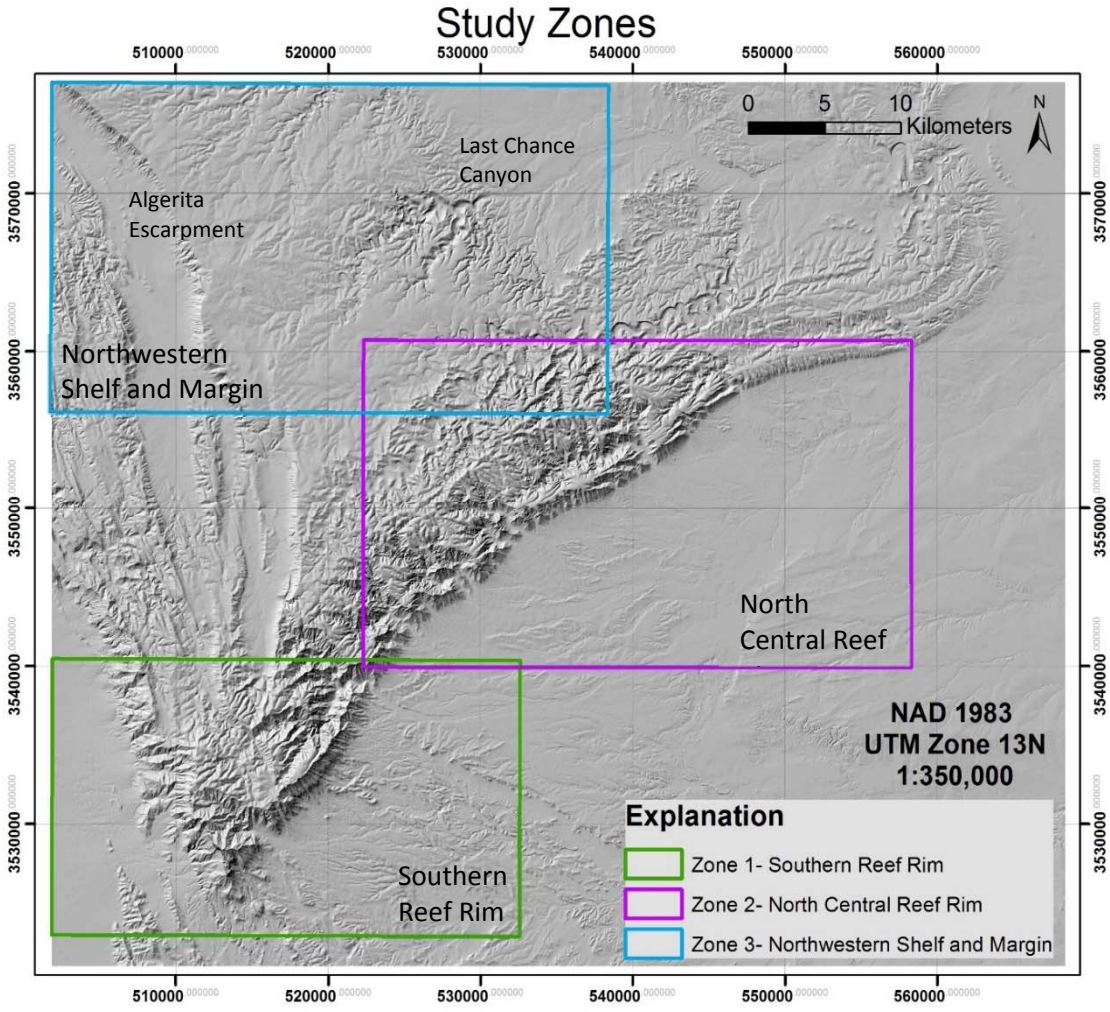

Figure 18. Focused study zones highlighting areas where stratigraphic relationships between resistant and more erodible units will be examined in detail. Key areas within the Northwestern Shelf and along the margin, namely The Algerita Escarpment and The Last Chance Canyon, are identified.

The Rimmed Reef Platform Margin

The reef rim is the largest section of high k_{sn} values and consists of units including the Capitan Limestone (Pc; RDR = 5.0), the massive deposits of the Capitan (Pcm; RDR 5.0), and the Goat Seep Dolomite (Pg; RDR = 4.0). These resistant units are providing a source of lithologic control on weaker (lower RDR) units that are found both stratigraphically above and below. The weaker units along this reef rim display different geomorphic responses depending on their location in the stratigraphic column in comparison to the strong reef units. The weaker units to the south, which underlie the thick limestone reef rim deposits, display a higher than expected k_{sn} (Figure 10). In contrast, the weaker units to the north, which sit atop the reef rim, display lower than expected k_{sn} values (Figure 10).

Zone 1 - Southern Reef Rim

Many of the beds showing over-steepened values are located to the south, within the Guadalupe Mountains National Park (Figure 4, 10 and 18). The Cutoff shaley member (Psh), part of the Bone Spring Formation, stands out as a weaker rock in this region with a high k_{sn}. The member, which consists of primarily shale, with some thin beds of black limestone and chert, was predicted to be less durable due to the high shale content (RDR = 2.5). The regression line in Figure 10 would predict a corresponding steepness of 8.34. However, this unit has the second highest mean k_{sn} of all units, at 19.41 (Table 2). I interpret this high k_{sn} is a consequence of the resistant Pg unit above, which is protecting the less durable shale unit from erosive processes. Moving further south, the Pbl, Pdy, and Pdc units are all identified as having similar durability (RDR = 3.0), but all fall well above the regression line in Figure 10. These units only outcrop in the southern region and are stratigraphically related, with Pdc on the top, followed by Pdy, and Pbl outcropping on the bottom (Figure 19a). El Capitan peak corresponds to an especially thick deposit of resistant

Pc limestone (RDR=5.0) directly above these units (Figure 19b). Like the Psh member to the west, the high steepness indices of these units could be explained by coarser sediments shed from the Capitan unit.

In this same area, the Victorio Peak member (Pbv), which is also part of the Bone Spring Formation, displays the highest k_{sn} in the entire study area. Though the Pbv member was identified as one of the more durable rocks (RDR = 5.0), the mean steepness is 21.36, yet the predicted k_{sn} is only 16.23 (Table 2; Figure 10). The Pbv member lies at the bottom of the stratigraphic sequence and the higher than expected k_{sn} could be explained by mantling of coarse sediments from upstream units.

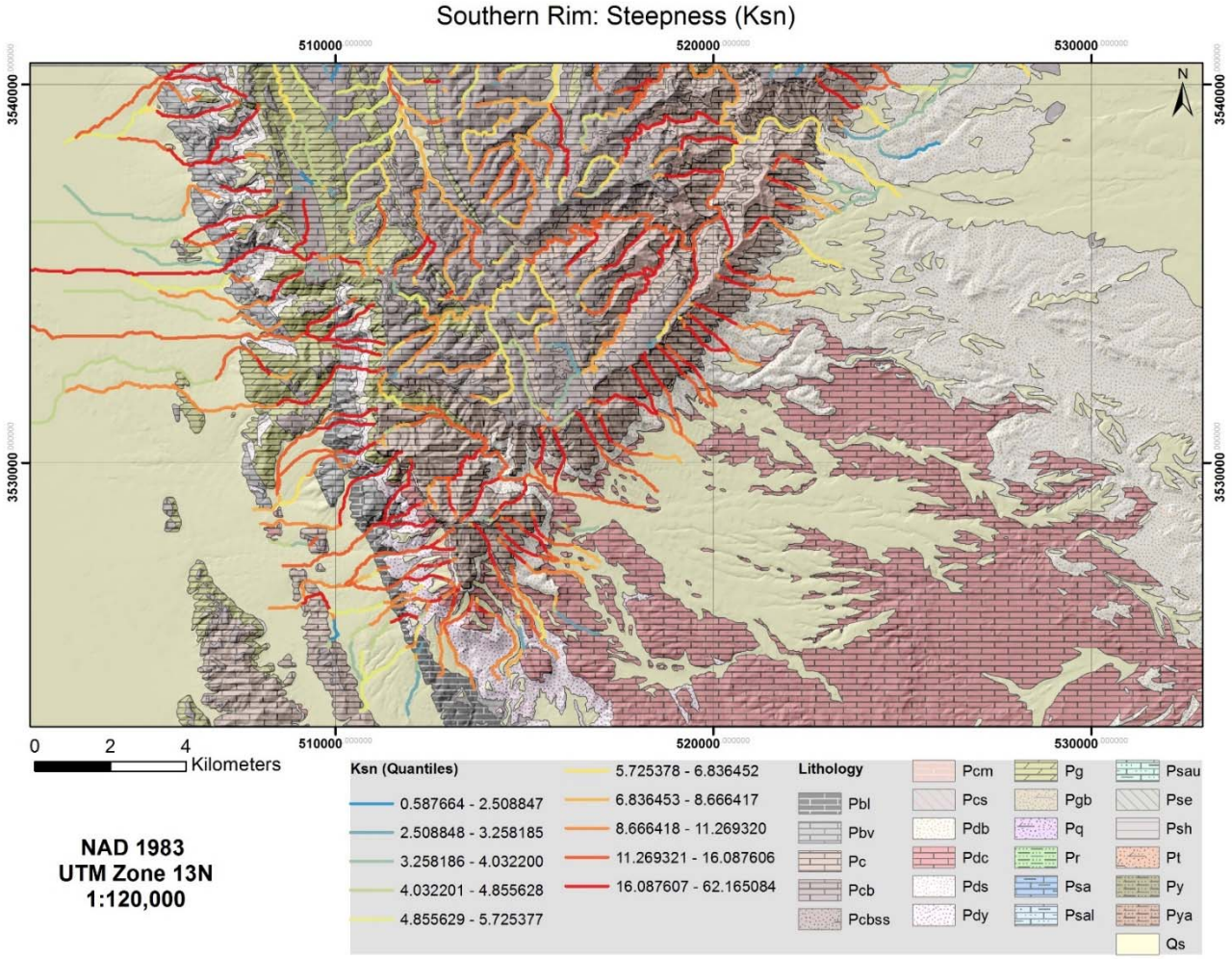

Figure 19 (a). Map of k_{sn} and Lithology at the Southern Reef Rim.

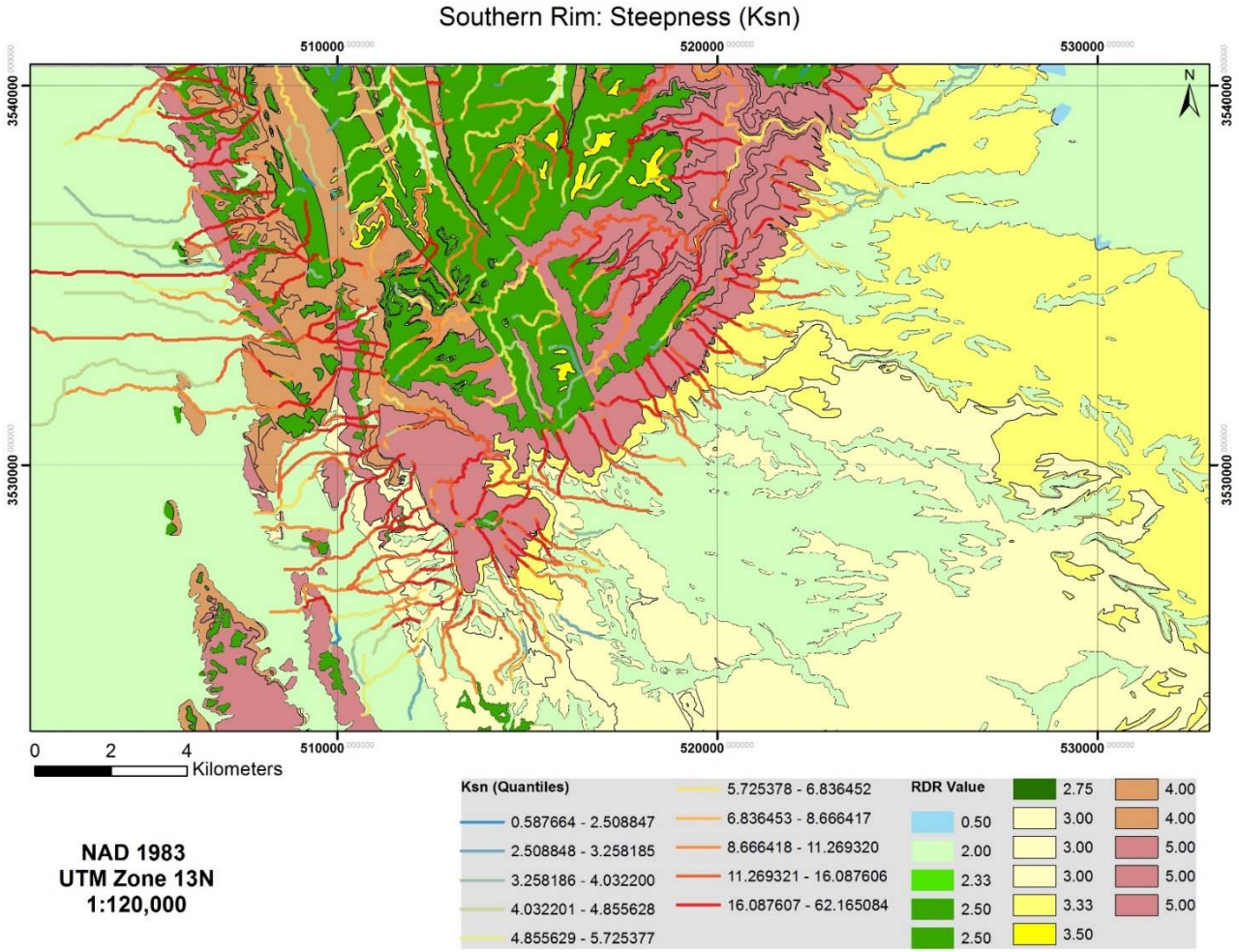

Figure 19 (b). Map of k_{sn} and RDR at the Southern Reef Rim.

Zone 2- North Central Reef Rim

In the region just north of the TX-NM line up to Carlsbad Caverns National Park, many units display lower than expected k_{sn} (Figure 10; 20). The Tansill formation (Pt) is the top-most rock exposed in this region and lies atop the Yates formation (Pya). The Pt formation consists of dolomite with thin beds of sand and silt (RDR=2.33). The Pya formation is primarily sandstone with some dolomite and shale (RDR=2.75), and is said to weather to gentle slopes (Figure 20b) (Boyd, 1958; Alnaji, 2002). Both units display low k_{sn} values and I suspect that this is due to the stronger limestone deposits (Pc and Pcm) which underlie them (Figure 20a). The Pcb (RDR = 2.5) unit to the west has a significantly lower RDR value than the Pc and Pcm units and represents a transition into the carbonate shelf, where the calm waters (protected by the reef) resulted in thinner, broader limestone deposits (Harris, 2005). This less resistant unit does not provide the same lithologic control or effect the stronger reef units do. The Pcb unit also has a relatively low k_{sn} (Figure 10), but can likely be attributed to the depositional environment. This unit represents the Carlsbad limestone and was combined with carbonate facies of the Seven Rivers formation because alignment on the map and their similar lithologic descriptions (Figure 6; Table 1). However, there could be considerable lithologic heterogeneities due to the transition in depositional environment from south to north.

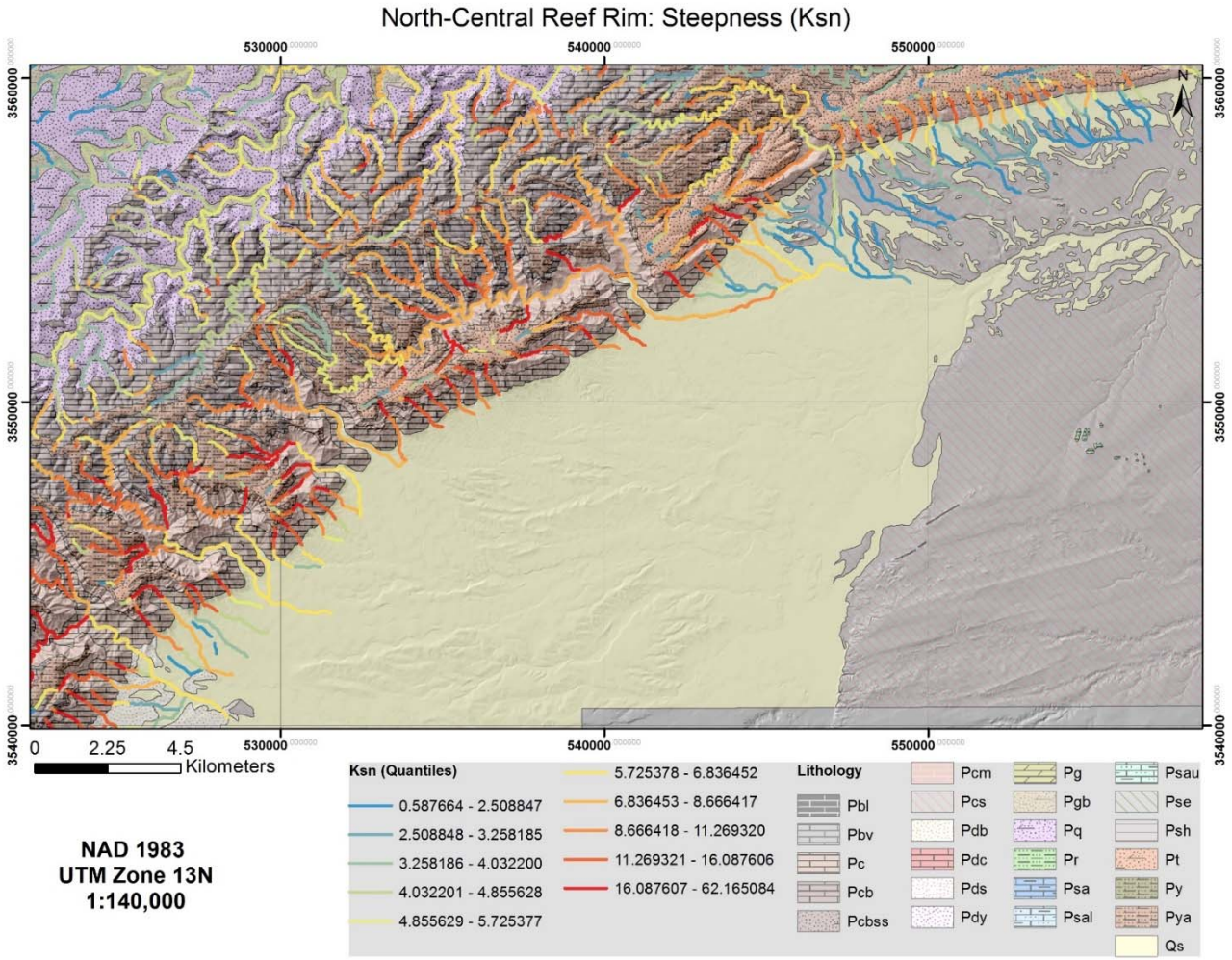

Figure 20 (a). Map of k_{sn} and Lithology at the North-Central Reef Rim.

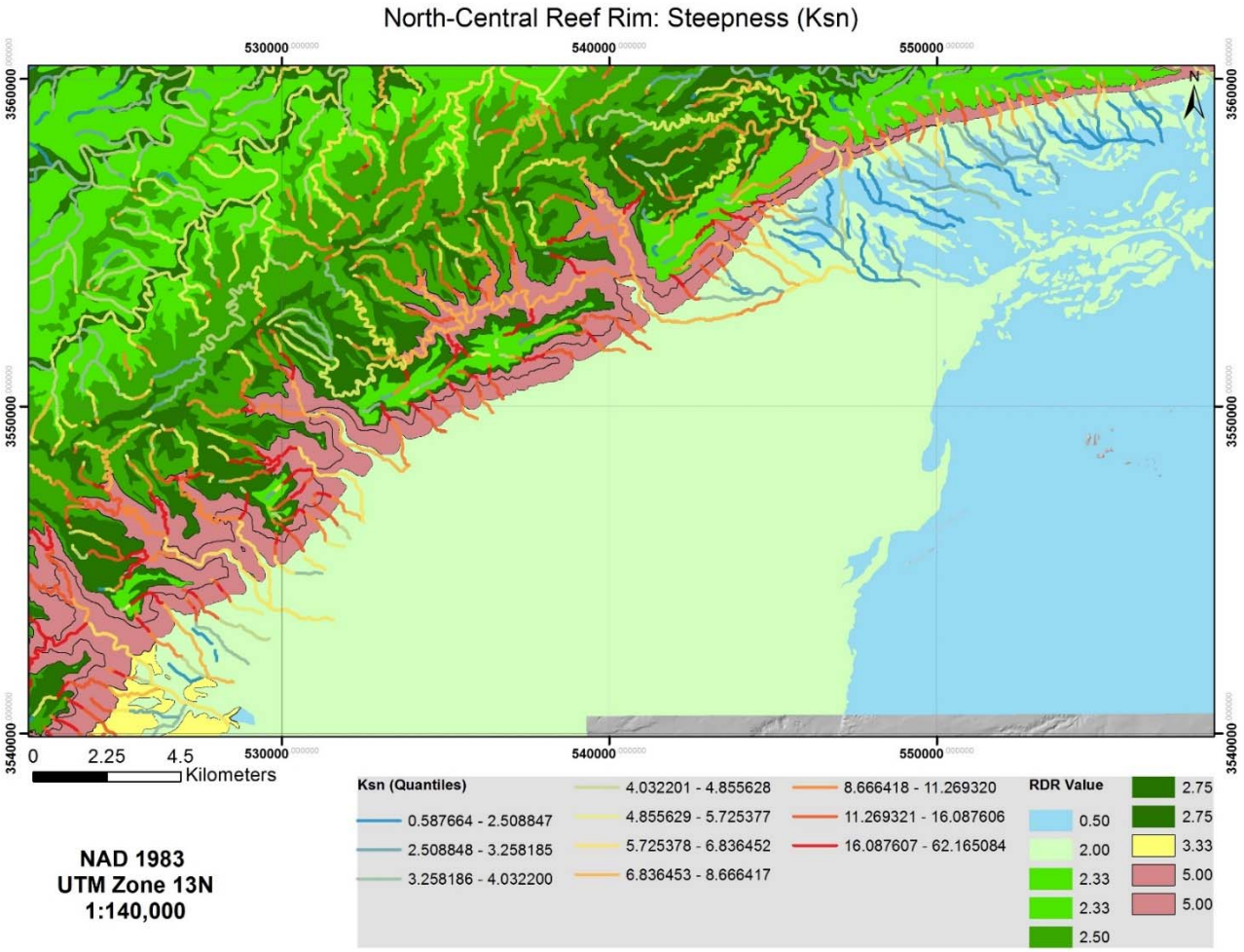

Figure 20 (b). Map of k_{sn} and RDR at the North-Central Reef Rim.

The Northwestern Shelf and Ramped Reef Platform Margin

To the northwest, the shelf deposits are dominant and include the thin-bedded Carlsbad Limestone (Seven Rivers Formation), Grayburg, Queen, and Yeso formations (Figure 21a). The main reef deposit in this region is the San Andres formation, though there are three different mapped sections of the formation and each exhibit different durability ratings, and therefore may influence morphology somewhat differently (Figure 21b). Many of the deposits in the south grade into these units, signifying the transitional environment across the carbonate platform and adding complexity when trying to differentiate between units. However, uniform erodibility across a given mapped unit is assumed for this study. The San Andres limestone represents an example of a ramp-style platform margin, as opposed to the rimmed-style platform to the south and east (Harris 2005). Within this region, two areas of high k_{sn} are present: The Algerita Escarpment and The Last Chance Canyon (Figure 18).

Zone 3- The Algerita Escarpment and The Last Chance Canyon

The Algerita Escarpment is a high relief area in the far northwest and The Last Chance Canyon is a small pocket of increased steepness located in central northern region (Figure 8; 14; 18). The stratigraphy exposed along the Algerita escarpment includes the San Andres formation (Psa), which splits into an upper (Psau) and lower member (Psal) to the northwest where they are underlain by the Yeso formation (Py) (Figure 21a). The Py unit was steeper than expected based on RDR (Figure 10). This formation is a dolomitic limestone with gypsiferous gray shales with the upper 600 ft. outcropped along the escarpment (Hayes, 1964). Though the upper San Andres limestone (Psau, RDR = 2.0) is not a particularly strong unit, the lower San Andres (Psal) has a moderate RDR at 3.25 (Figure 21b). Given it is rated stronger than the Yeso and also contains a fair amount chert (not accounted for in the RDR number), I interpret that this unit acts as a more resistant

cap rock, protecting the weaker Yeso formation below from downcutting near the contact between these units, while also potentially supplying coarse sediment that could mantle the bed.

To the south, the Yeso formation pinches out and the escarpment stratigraphy is represented by the Grayburg (Pgb) formation overlying the San Andres (Psa). The Pgb (RDR = 2.75) is unit is weaker than the Psa (RDR = 3.67) unit, and though k_{sn} values appear high for Psa, it does not plot above the regression line in Figure 10. The Grayburg formation, however, does exhibit low k_{sn} (Figure 10), so the stronger Psa unit could be providing the resistant base need to support this softer formation.

The lithology of the Last Chance Canyon is very similar to that of The Algerita Escarpment, except the bottom-exposed unit is the sandstone tongue of the Cherry Canyon formation (Pds), instead of the Yeso formation (Figure 21a). The Pds formation plots above the regression line (Figure 10), indicating a relatively steep unit. This steepness is apparent when looking at the mapped k_{sn} values (Figure 8; 14). The Pds unit is present in the southern region as well and is said to grade laterally into the upper San Andres (Hayes, 1964). The only area in the northwestern shelf where this unit is exposed, is within the Last Chance Canyon, where the unit is approximately 264 feet thick and consists of "…moderately resistant indistinctly bedded grayish-orange very fine grained well-sorted quartz sandstone with scattered irregular chert nodules and silicified megafossils." (Hayes, 1964). The moderate resistance of this bed (RDR = 4.0), produces an expectedly high k_{sn}, and it is interesting to see the small cluster of high k_{sn} given the surrounding topography and lithology (Figure 14; Figure 21). The low k_{sn} Grayburg formation (Pgb), is atop the upper and lower San Andres (Psau and Psal), with the Pds unit on the very bottom. I interpret that the combination of the resistance provided by the Psal and Pds unit, are again

acting a supporting base for this softer formation, ultimately resulting in low gradient channels.

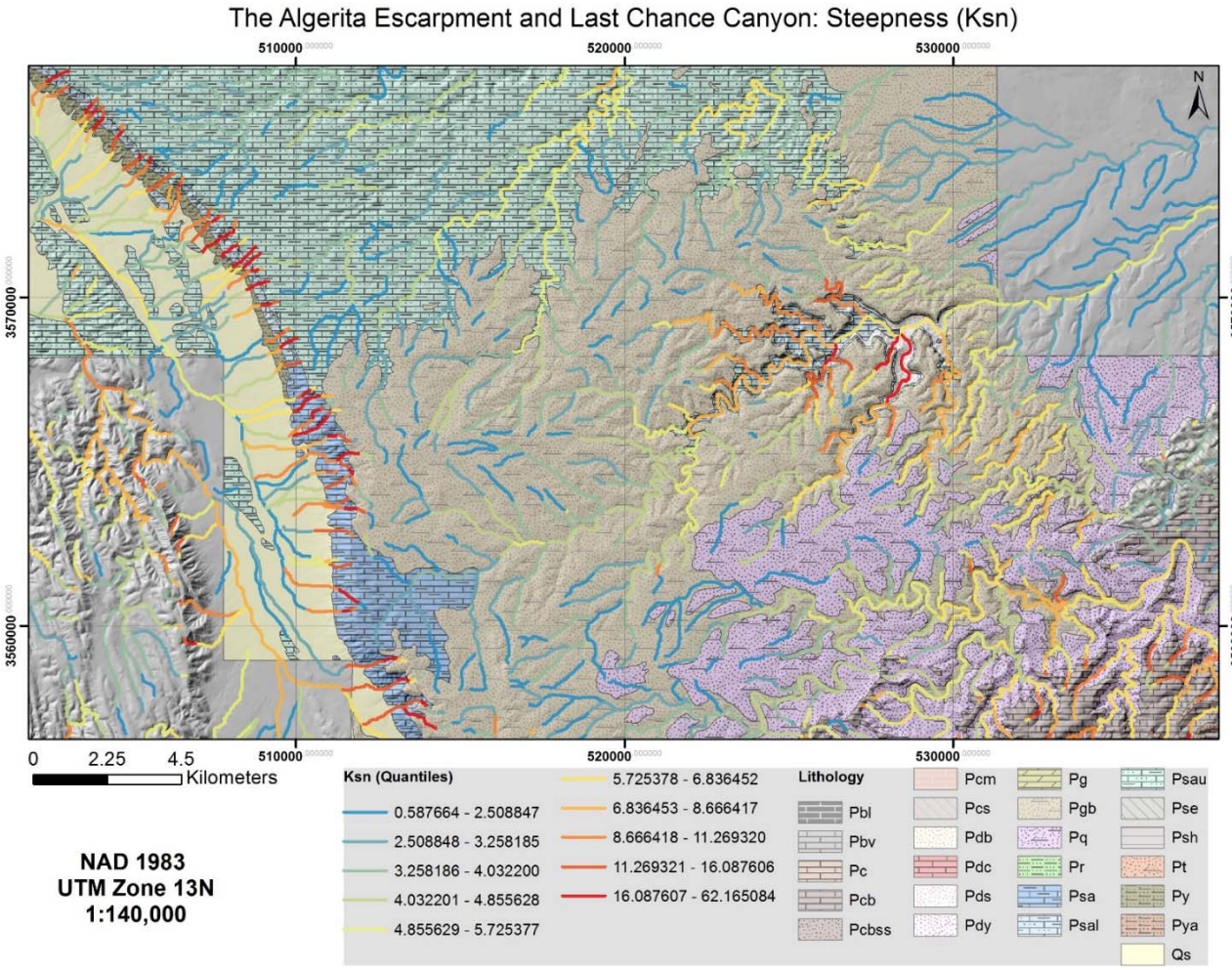

Figure 21 (a). Map of k_{sn} and Lithology at the Algerita Escarpment and the Last Chance Canyon.

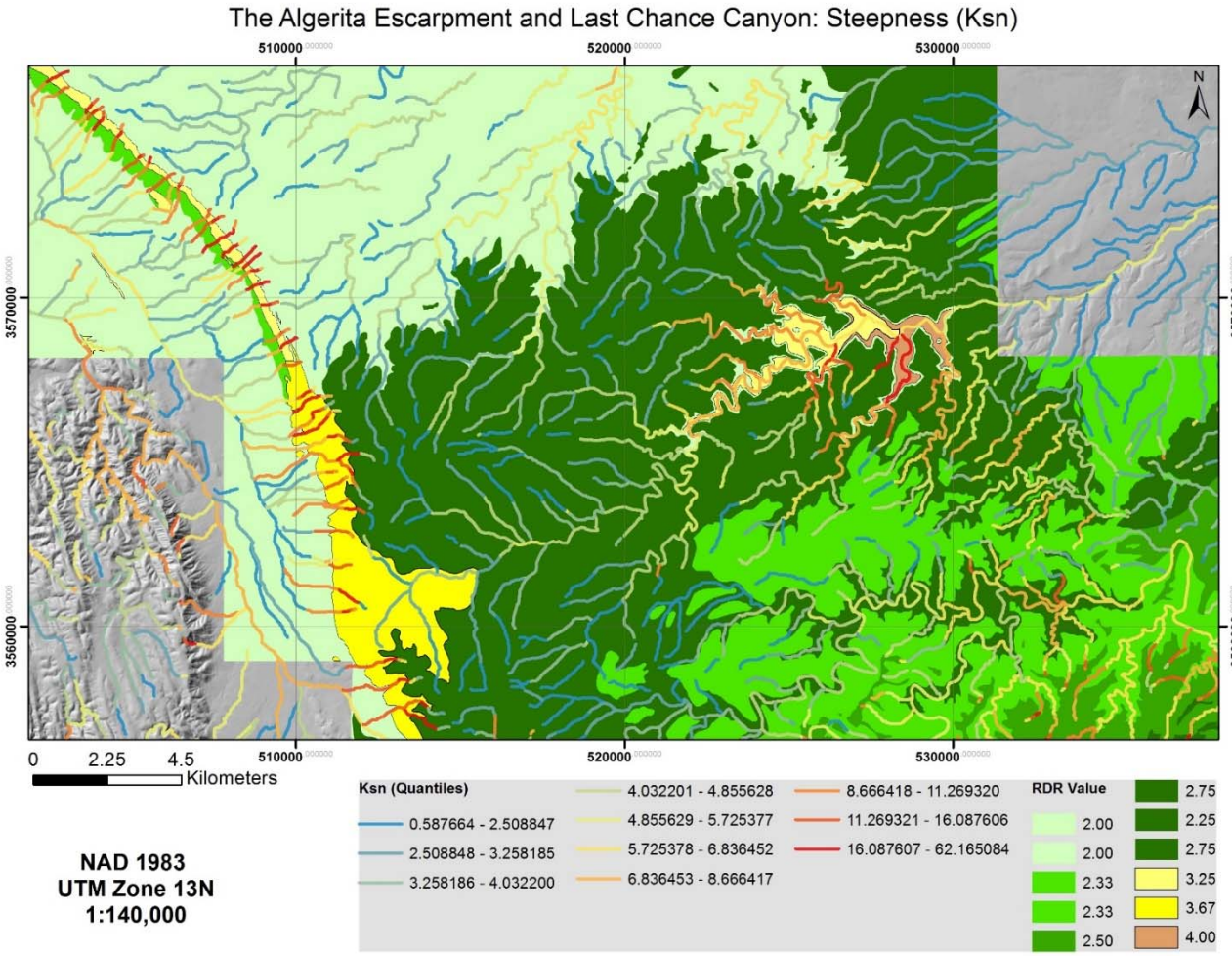

Figure 21 (b). Map of k_{sn} and RDR at the Algerita Escarpment and the Last Chance Canyon.

In both the southern and northern regions of the Guadalupe Mountains, the more resistant reef deposits exert a clear control on the k_{sn} of under- and over-lying units (Figure 3b). In the case of higher k_{sn} underlying the resistant units, I interpret the thick limestone and dolomite beds are acting as cap rock, simultaneously protecting the weaker beds from erosion and potentially providing a source of coarse sediment mantling the units below, which could result in over-steepening. The resistant units "pin" the units lying below, providing protection from the elements and limiting the lateral retreat of the more erodible rocks. This can result in the steepening of the unit, especially just below this contact point (Figure 3b). Additionally, as the more resistant unit weathers, the larger sediments could provide another form of protection via mantling of the bed. This theory works especially well for steep units with little exposed area, such as Psh and Pbv, as the resistant unit can over-steepen the entire unit through both mechanisms described.

For the less resistant units on top that display lower than expected k_{sn}, the resistant beds play a different role in this case, providing a strong base unit which provides support and sets the base level for lowering. The resistant beds, in a similar fashion to the beds below, "pin" the upper beds in place, slowing the lateral retreat significantly (Figure 3b). However, in contrast to the units below the reefs, the units above are still exposed to weathering, resulting in thinner, weathered beds, which display lower gradients. As the weaker units weather laterally, this pinning effect of the resistant units can be compared to a base level. The stark contrast in erodibility of the stronger unit provides the lowest elevation the weak units can erode to, therefore setting the relief structure artificially low at these higher elevations, resulting in flatter beds (Figure 3b).

CONCAVITY

Much like the k_{sn} values discussed above, the average concavity value for the entire study area is also somewhat low, but still falls within the expected range for bedrock regions, which is typically between 0.3 to 1.2 (Whipple, 2004). The overall standard deviation is very high and represents the high variability of river profile shapes across the region, which could potentially be an effect of varying rock type. When concavity is grouped by rock type and compared to RDR, the standard deviations remain high, indicating large variation in profile form within individual units. This effect could still be a result of interactions between units of different durability, but the relationship is not as straightforward as k_{sn}. Convex reaches represent deviations from the expected concave-up form and indicate some sort of perturbation (Pederson and Tressler, 2012). When the concavity values for each rock unit are compared to the RDR, the linear correlation of the two variables is not statistically significant ($p=0.56$), and there is a lot of scatter among the data (Figure 12). Unlike the mapped k_{sn} quantiles, it is difficult to discern distinct regions or spatial patterns of high or low concavity (Figure 8). Cluster analyses confirm this (Figure 14). However, many of the units far away from the regression line in figure 12 are neighboring rock units within different parts of the stratigraphic column. I surmise that the interactions of these beds are exerting control on the concavity, so I will frame the discussion by examining specific portions of the stratigraphy in various locations within the region.

Zone 1- Southern Reef Rim

To parallel the discussion of k_{sn}, I will begin with units associated with the southern portion of the rimmed reef platform margin (Figure 5; 18). Units in in this area with higher concavity values include the black shaley limestone beds (Pbl), which also had anomalously high k_{sn}, the Bell Canyon formation (Pdb), and the Cherry Canyon formation

(Pds) (Figure 12). These units tend to outcrop at the bottom of the stratigraphic column beneath the more resistant reef deposits of Pg, Pc, and Pcm (Figure 22a). In this case, of weaker units under stronger units, I suggest the increased concavity in the weaker units could be due to increased coarse sediment supply from the stronger units above. Given this interpretation, we would also expect a moderately steep slope and this appears to be the case for these units with k_{sn} values of 15.09, 11.32, and 15.41 for Pbl, Pdb, and Pds, respectively (Table 2). Other units in this region (Psh and Pbv) also have high values of k_{sn}, but have lower concavity values, which fall closer to the linear trend (Figure 12). This could be due to their position within the stratigraphic column and the relatively small area of exposed bedrock for these units. These units do not lie under the very resistant Capitan Limestone, but rather the Goat Seep Dolomite (Figure 22 a and b). Perhaps this layer does not weather in the same manner, affecting how the sediment supply shapes the units below. Additionally, these outcrops are relatively small, so it can be difficult to get a good read of changes in longitudinal channel shape across such a short distance.

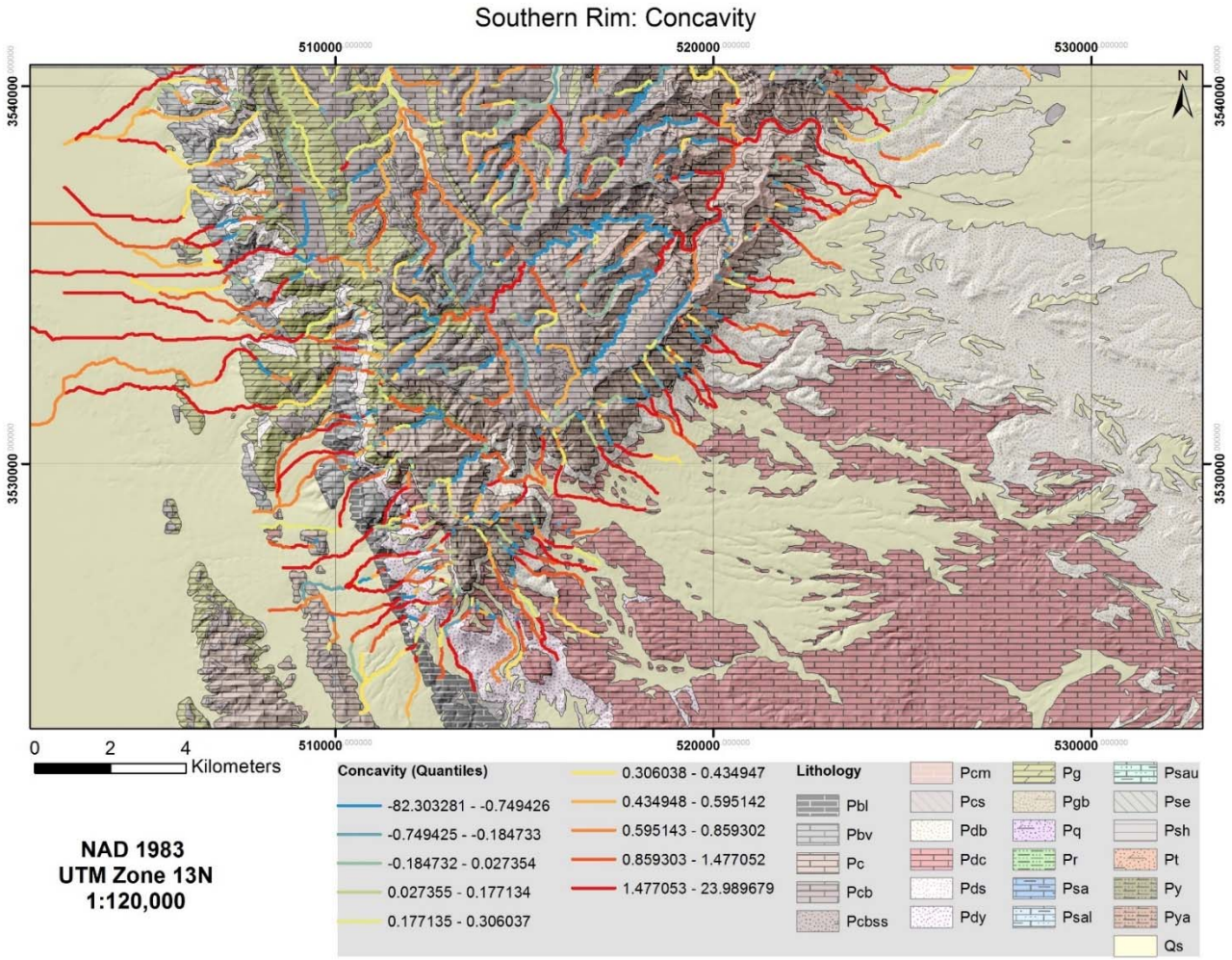

Figure 22 (a). Map of concavity and Lithology at the Southern Reef Rim.

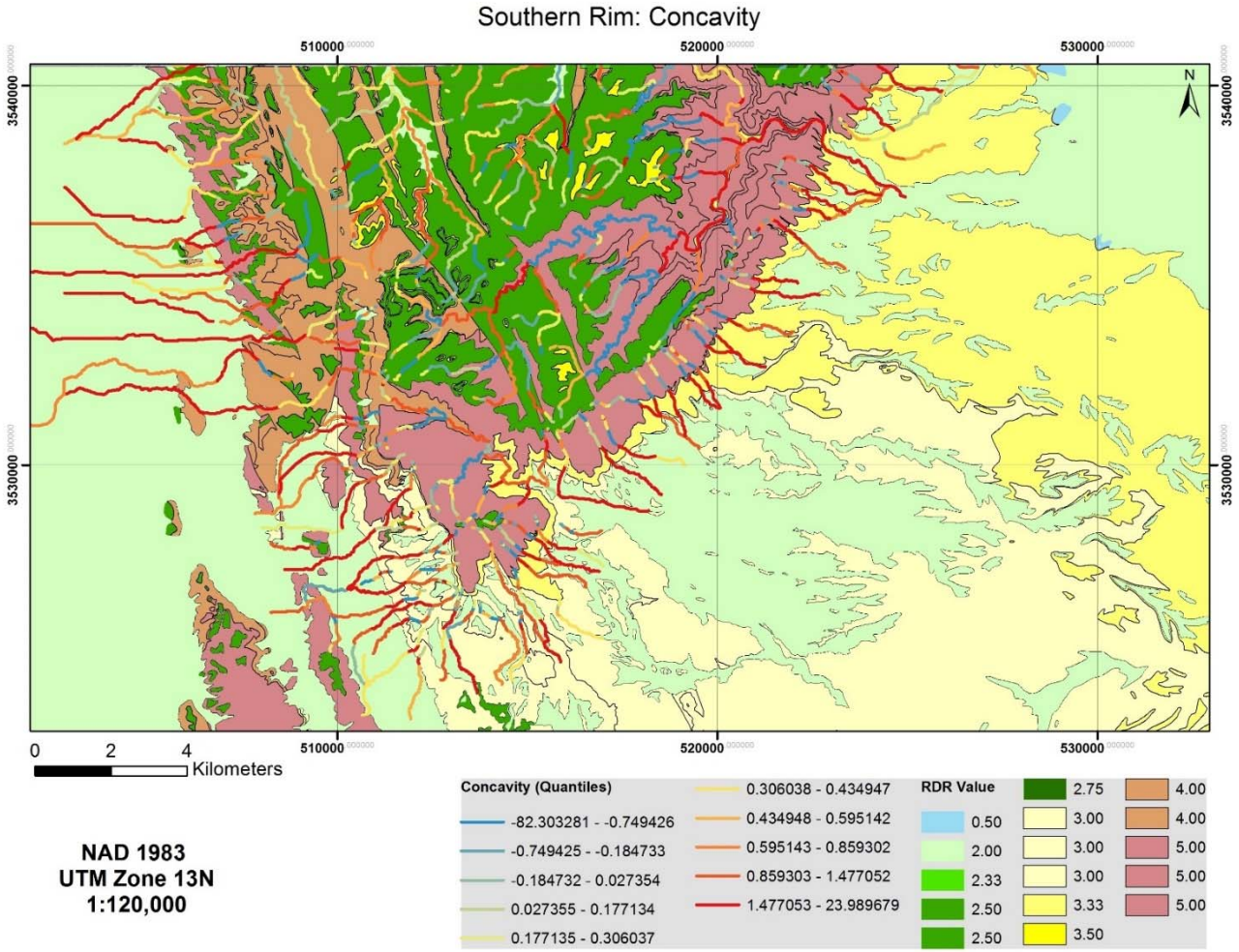

Figure 22 (b). Map of concavity and RDR at the Southern Reef Rim.

Zone 2- North Central Reef Rim

In the north-central reef rim, a different relationship can be observed. Units Pt and Pya, as previously discussed, are both upper units of medium resistance. When examined more closely, both units exhibit going from lower concavity, or increased convexity, at their stream heads to higher concavity. This is especially evident for the Tansill unit in Carlsbad Caverns National Park, showing convex reaches (highly negative values of concavity) at the top of the reef escarpment (Figure 23 a and b). In the area along this reef rim, these weaker upper units are held up by the thick, resistant reef deposits (Pc and Pcm), which limits downcutting of the units above. The resistant units lying directly below sometimes share a portion of the convex reach, but then transition to a higher concavity below this, indicating the change the in lithology from a less durable to a more resistant lithology, which also shows higher k_{sn}.

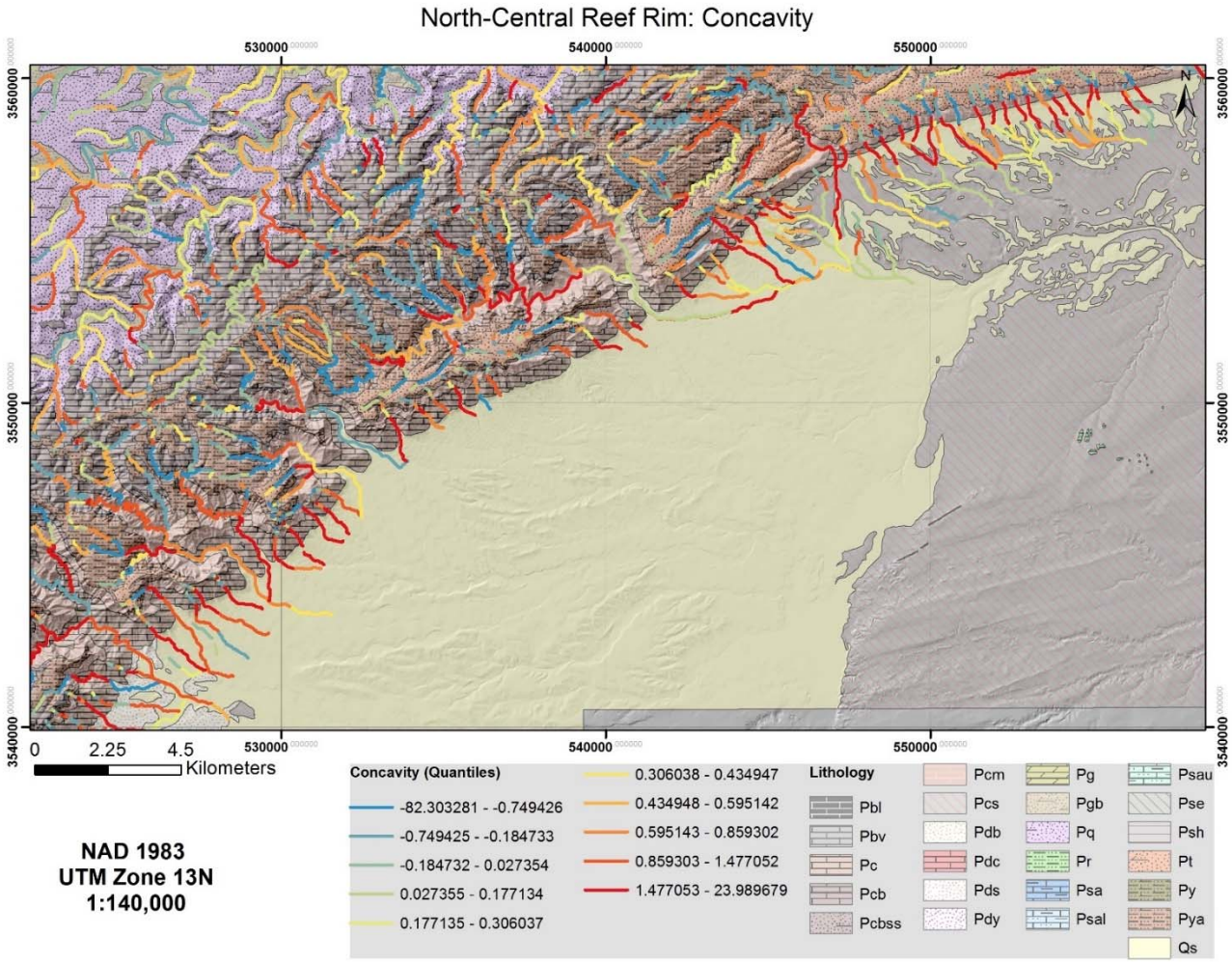

Figure 23 (a). Map of concavity and Lithology at the North-Central Reef Rim.

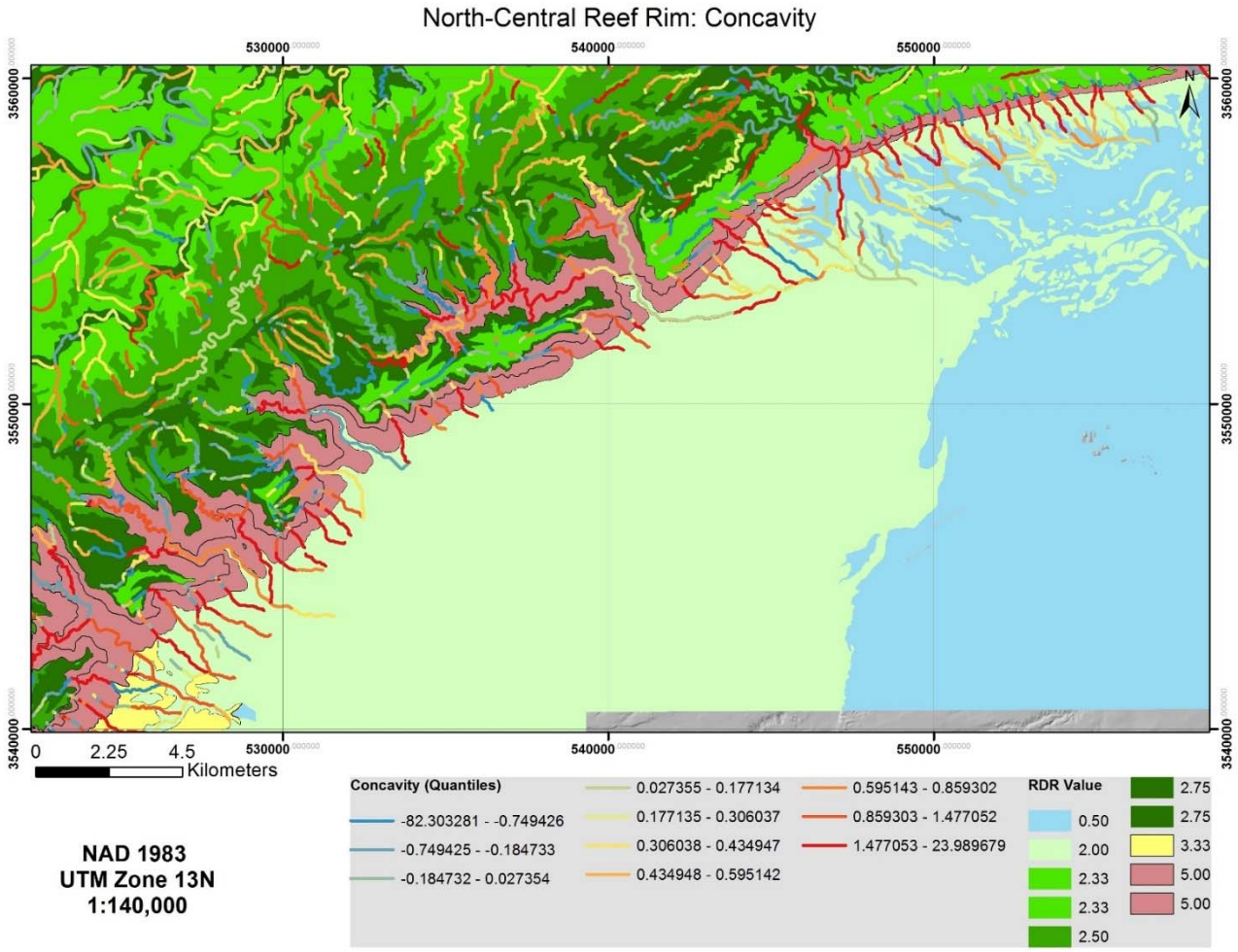

Figure 23 (b). Map of concavity and RDR at the North-Central Reef Rim.

Zone 3- Northwestern Shelf and Margin

In the northwestern area, regional concavities remain highly variable, but the Algerita Escarpment and Last Chance Canyon do appear to exhibit higher concavities comparatively (Figure 8; 14). Like the units associated with the reef rim, units appearing at the bottom of the stratigraphic column tend to display the highest concavity (Figure 24 a and b). The Yeso formation (Py), which also displayed higher than expect k_{sn}, exhibits high concavity also consistent with the interpretation that coarse sediment supply from the Psal unit (RDR = 3.5) is increasing incision and over-steepening at least a portion of this unit. The Psau and Psal units, which lie atop the Yeso, both exhibit lower concavities, much like the upper units in southern region (Figure 24b). In the Last Chance Canyon area, the Cherry Canyon Sandstone (Pds) and the lower San Andres (Psal) display high concavities. In this case, softer rocks (Pgb and Psau) are transitioning into the more resistant units, much like the examples on the north central reef rim (Figure 24b). A similar morphology is displayed here, marking a stark transition from convexity to concavity with increasing durability.

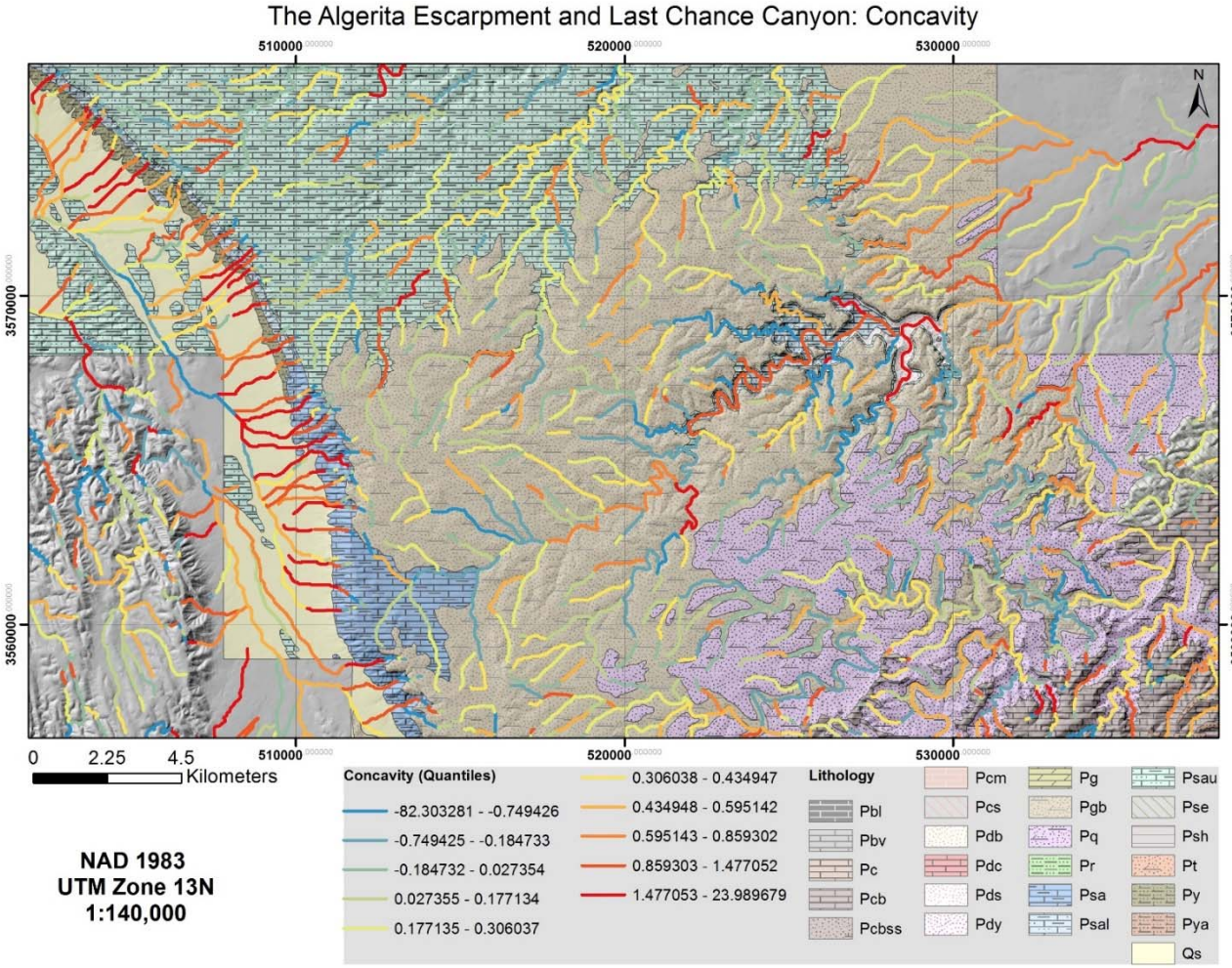

Figure 24 (a). Map of concavity and Lithology at the Algerita Escarpment and the Last Chance Canyon

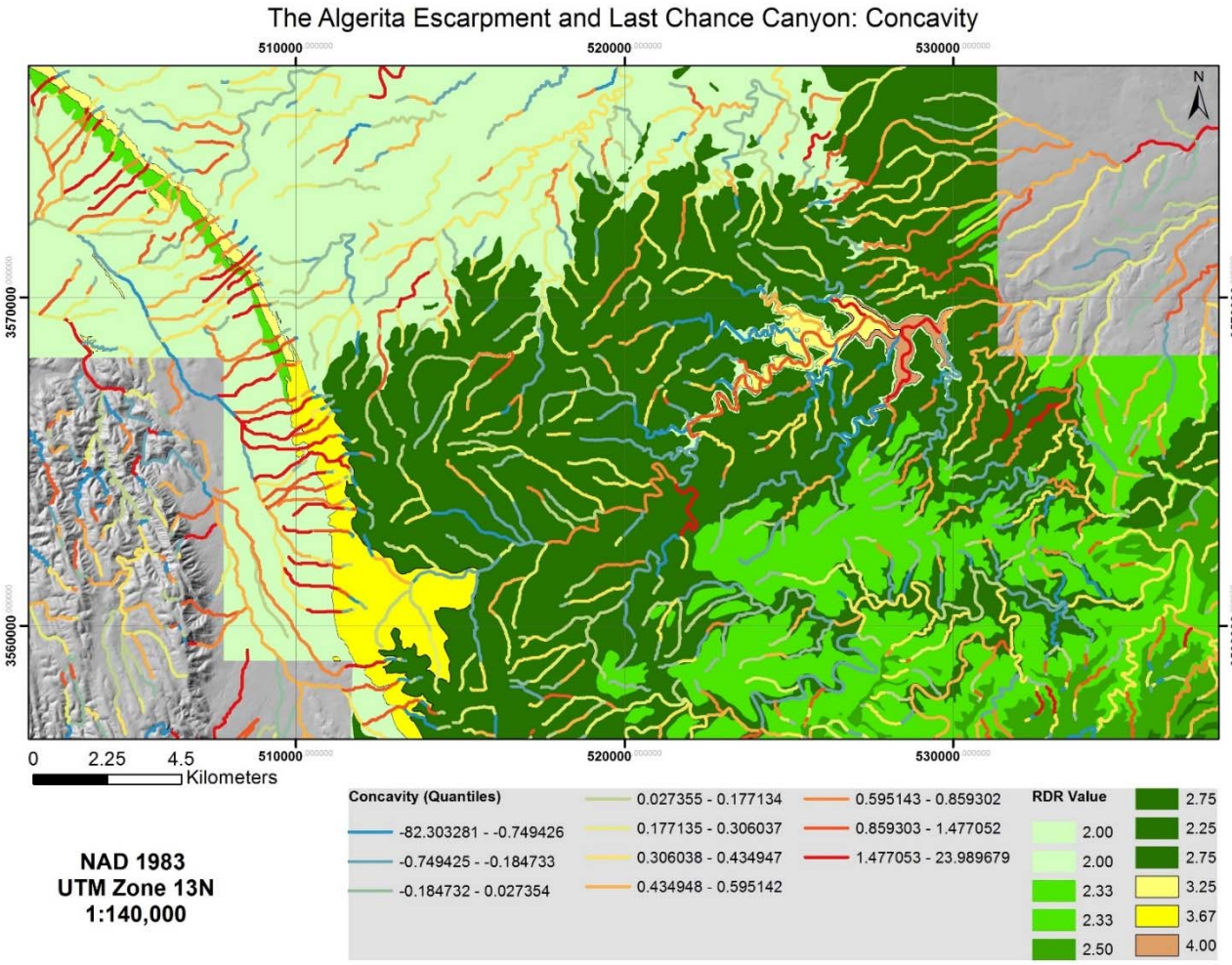

Figure 24 (b). Map of concavity and RDR at the Algerita Escarpment and the Last Chance Canyon.

There appear to be two processes affecting the concavity of rock types in this region, which depend partly on stratigraphic order and partly on RDR. The first process involves more durable units on top of more erodible units. In this case, the more durable unit supplies coarse sediment, which erodes the lower unit to a higher degree at and just below the contact (Figure 3b). The lower unit then tends to flatten out away from this contact, resulting in a classic concave-up form. This could occur if coarse sediment size and abundance were to decrease substantially downstream. Sediment size could decrease due to sediment particle abrasion in the upstream reaches where channel steepening occurs. However, it could also be an effect of size-dependent transport, where larger sediments mantle lower portions of the bed. Geometries created by "pinning" from the resistant units above could also play a role (Figure 3b).

The second process occurs when more erodible units are on top of more resistant units, resulting in convex reaches and low k_{sn} on top before transitioning into an area with high k_{sn} and concavity. The upper less resistant units are limited by the resistant unit beneath, setting the base level for erosional processes (Figure 3b). However, the unit is still exposed weathering, resulting in relatively low relief beds. The stark elevation change at the edge of the contact can result in preferential weathering resulting in more convexity due to the transition from flat, low relief to a knickpoint (Figure 3b). An important aspect to note however, is that regardless of durability ordering within the column, whether the durable units are on top not, the more concave values always occur in the lower units. This relationship is likely why the RDR values and concavity do not show a strong correlation (Figure 12). When the resistant reef units, Pc/Pcm or Psa/Psal, are on top, they exhibit lower concavities, yet they exhibit higher concavity when on the bottom. This could be due to concentrated weathering at the top of these units, which could occur if the weaker units above have retreated back from the contact point, exposing the top of the resistant

unit, which could result in rounding from the increased weathering. This makes it appears as if the concavity of a given rock unit is relatively independent of strength. The insensitivity of concavity to bedrock properties was predicted by Whipple and Tucker (1999) through non-dimensional analysis of the stream power law. In this region, concavity depends more on its location within the exposed stratigraphic units, especially in relation to the strongest units within the region. This indicates, much like k_{sn}, that the most resistant reef units still exert some control for this metric.

RELIEF

Average local relief was calculated for each lithologic unit and the linear regression of relief and RDR values give a fair correlation (R^2 =0.43; τ = 0.53), very similar to the correlation of RDR and k_{sn}. Given that the correlation between relief and k_{sn} is also strong (R^2=0.89; τ = 0.8, Figure 17), this is not completely unexpected. The high correlation of mean k_{sn} and relief is also expected, considering elevation changes are required to have a steep slope. However, relief is much easier to determine than k_{sn}, and could provide an even quicker way to infer the erodibility of rock units. Work by Schmidt and Montgomery (1995) showed that relief was not limited by incision alone and could potentially serve as an indicator of landscape-scale material strength. Units with the highest mean k_{sn} values mostly outcrop in south, where the morphology is characterized by steep cliffs and therefore high relief. Other areas of high relief are along the reef rim, the Algerita Escarpment, and the Last Chance Canyon, which correspond to areas of high k_{sn}, as indicated by the correlation above.

LIMITATIONS AND FUTURE WORK

Lithologic map resolution was adequate for this the scale of this study, but the lack of continuous units along the state line was a complicating factor. Some units were combined for continuity across state lines, which could impact the assumption of equal

erodibility across individual units. For example, the Carlsbad Limestone and the carbonate facies of the Seven Rivers Formation were combined into a single unit, Pcb, given their spatial relationship at the state line. However, there could be considerable lithologic differences given that this unit traverses the entire region. Additionally, bedrock was originally classified into mapped units in order to understand the stratigraphy and depositional environments, not rock properties. The issue of heterogeneity within the distinct rock units is also of some concern. Due to the nature of the depositional environment, many of the broader shelf deposits have significant heterogeneity, making interpretations more difficult in the transitional zones.

For this study, beds were assumed to be primarily horizontal. However, a more detailed investigation into dips, of the beds could provide additional evidence for some of the results. Model results from Forte et al. (2016) show that even small changes in dip angles can have a large effect on erosion rates and landscape evolution. Strike and dip data are available within the National Park GIS files and future work will include a comparison of dip to k_{sn} and concavity results. Faults and other structural features were not a focus of this study, but could be a potential factor, especially in the western escarpment of the southern Guadalupe Mountains where several NW-SE trending faults are present. Another possible source of error, would be the potential variation in RDR values. For example, the Yeso formation, received a low strength value due to the gypsum and shale present, yet the dolomitic limestone may be the major influence (Table 1). A more detailed survey of past studies and rock composition could help to refine the RDR values and give better estimates to rock erodibility/durability.

Field work verifying rock strength and fracture spacing could also provide more direct comparisons to bedrock properties. However, given the spatial scale of this project, and the variability in the rock across the region, that is not necessarily feasible. However,

specific units and locations that represent deviations from the predicted relationship in figure 10 could studied more intensively, allowing a more detailed and focused study of the mechanisms and interpretations presented in this thesis. For example, outcrops in these areas could be characterized by the semi-quantitative Selby Rock Mass Strength system (Selby, 1980), which could provide more specific details of bedrock properties. Additionally, channels that exhibit high k_{sn} or concavity be examined more closely, by evaluating the amount of bedrock exposure versus alluvial cover in the channels. Sediment size within channels could also be surveyed to assess the extent of coarse sediment abrasion and mantling of large resistant boulders.

APPLICATIONS

This method has a variety of potential applications. This method could be used to evaluate remote field sites or perform preliminary analyses prior to field studies. This could be especially helpful for studying the topography and rock properties of planetary bodies. We cannot yet conduct field studies on other planets, so we rely on remotely sensed data to complete research on planetary surfaces. This would work especially well on Mars considering the absence of modern climate and tectonic influences. Though multi-spectral scanners are used to remotely collect information from planetary surfaces, it can only provide chemical information of the rock types present. However, high-resolution topographic information is available for some locations, which could be used with this technique to predict other rock properties, such as erodibility/durability, which are imbedded in the topography. This information could provide additional information about these landscapes and lead to a greater understanding of how they are formed.

CONCLUSIONS

This study compares topographic metrics, normalized channel steepness (k_{sn}), concavity, and relief, to the estimated relative durability ratings (RDRs) of mapped lithologic units, which serve as a proxy for bedrock properties such as durability or erodibility, showing that the correlation of k_{sn} with RDR values demonstrate some degree of predictive power for that metric (R^2 =0.43; τ = 0.52). The variability among these results can be explained by the influence of lithologic control exerted by more durable limestone and dolomite reef deposits in the Guadalupe Mountains region. I interpret that these reef deposits affect morphology in two ways: First, by serving as a cap rock and protecting units which underlie them, resulting in steep slopes and high k_{sn} values for most of the lower units. Secondly, by providing a resistant base and supporting weaker units which lie on top, resulting in low k_{sn}.

In contrast, the correlation of concavity and RDR values gave a poor relationship (R^2 =0.016; τ = 0.13), signifying poor predictive properties for that metric and possibly indicating that concavity is independent of rock erodibility. Despite this poor correlation, the influence of the resistant reef units can still be seen, typically resulting in higher concavity for units below the reefs and lower concavity, or higher convexity, for weak units atop the resistant units. Resistant units displayed both low and high concavity values, complicating the relationship between this metric and rock erodibility, and further indicating that concavity may not be sensitive to strength in a simple or consistent manner.

The results of this study show a quantifiable relationship between bedrock erodibility and channel steepness, offering insights into the stream power law that have yet to be fully explored in other studies. Model results and empirical data from previous

studies have demonstrated that more resistant units typically have higher steepnesses (Duvall et al., 2004; Jansen et al., 2010; Pike et al., 2010; Goode et al., 2010, Bursztyn et al., 2015, Forte et al., 2016; Perne et al., 2016). These results confirm this, showing clear control of bedrock lithology on steepness, while also offering lithologic and stratigraphic interpretations for results that do not follow this convention, suggesting that the ordering of stronger and weaker units also matter. Though the relationship of RDR and concavity is not as straightforward, this thesis explores the possible sources of lithologic control affecting channel shape. These relationships provide valuable insight into lithologic control and concepts explored here could be applied to other settings or within landscape evolution modeling.

APPENDICES

The purpose of these appendices are to provide additional figures and supplementary information on the study area, the spatial and statistical analyses, and detailed methodology within ArcGIS and MatLab.

APPENDIX A: ADDITIONAL FIGURES

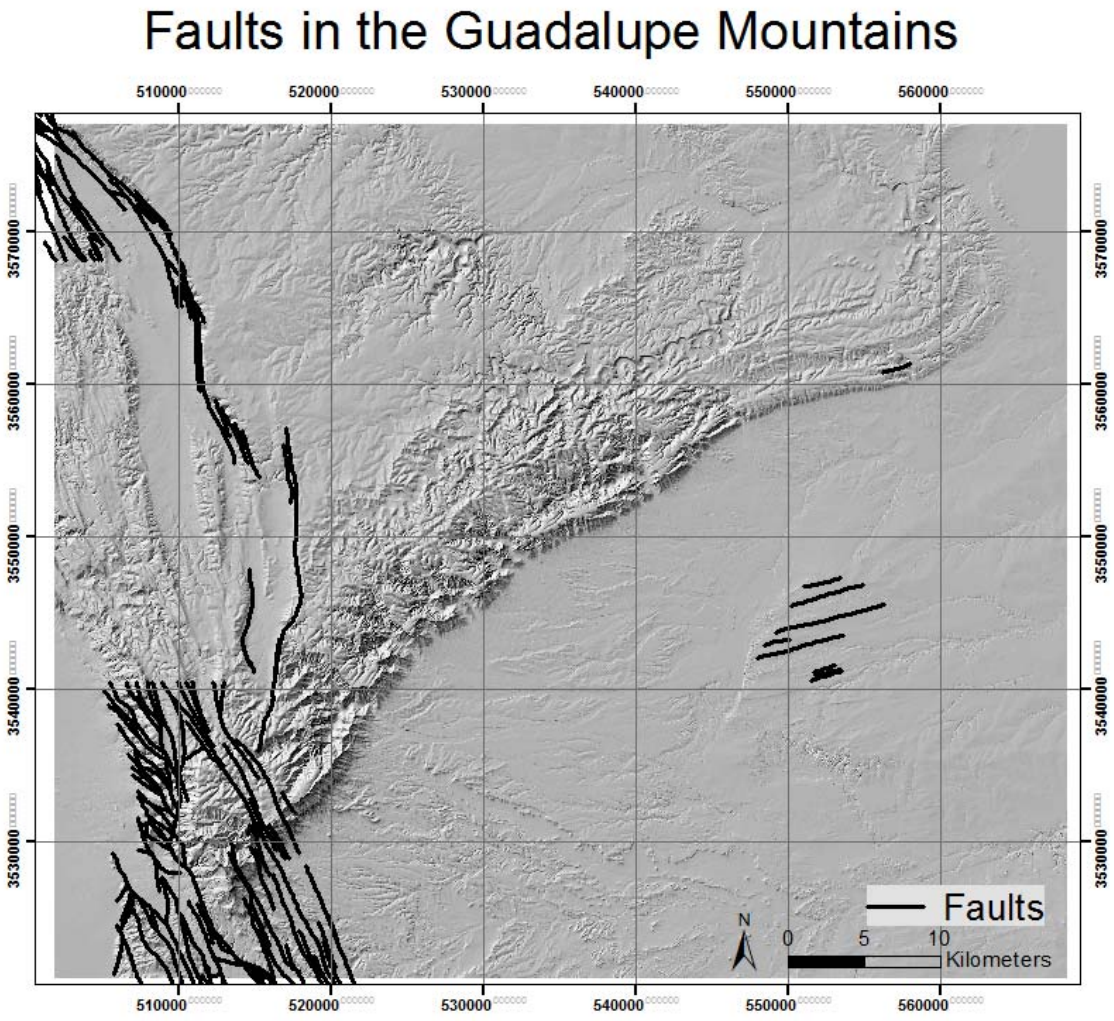

Figure 25. Map of faults in the region. The effect of faulting and other structural components were not examined in this study.

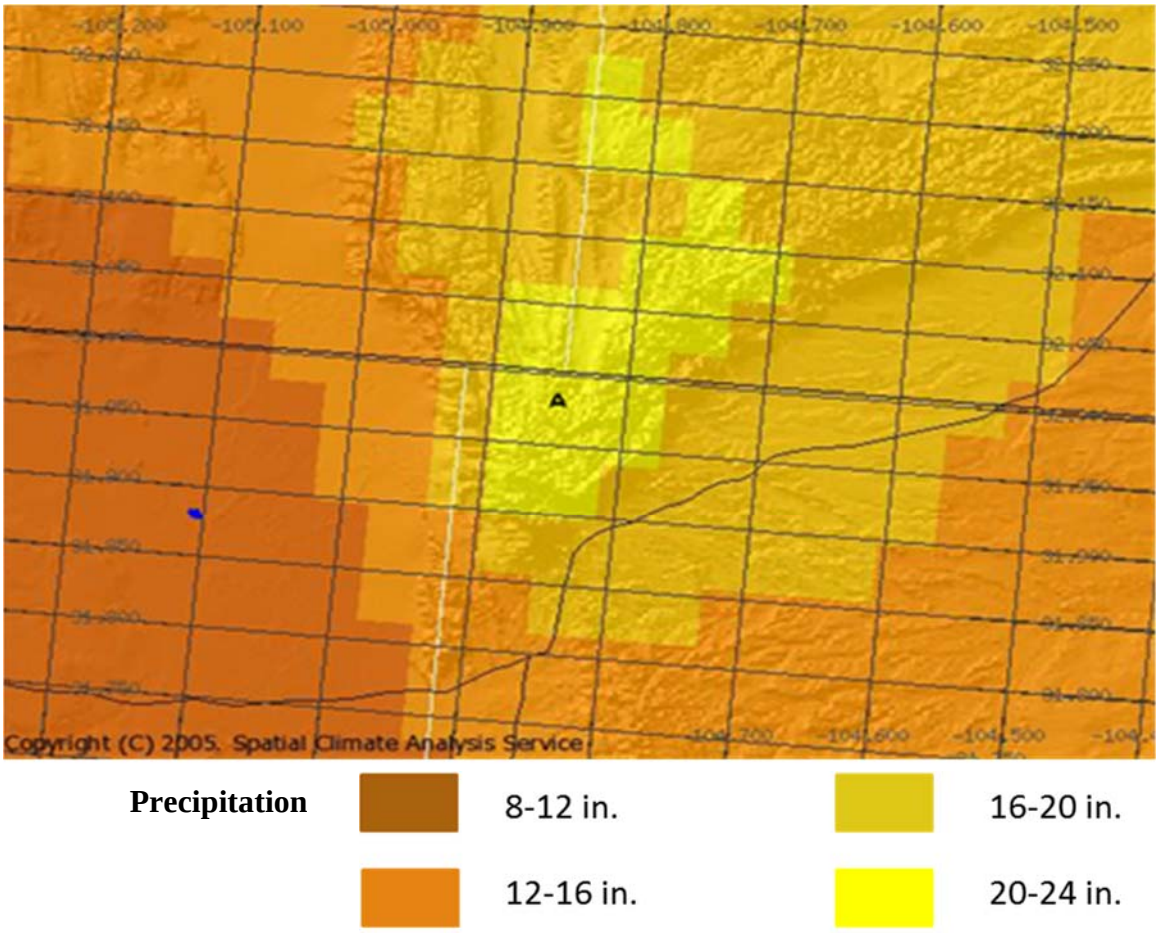

Figure 26. Precipitation map demonstrating the relatively mild climate gradient in the Guadalupe Mountains. Modified from Natural Resources Conservation Service National Water and Climate Center (2005).

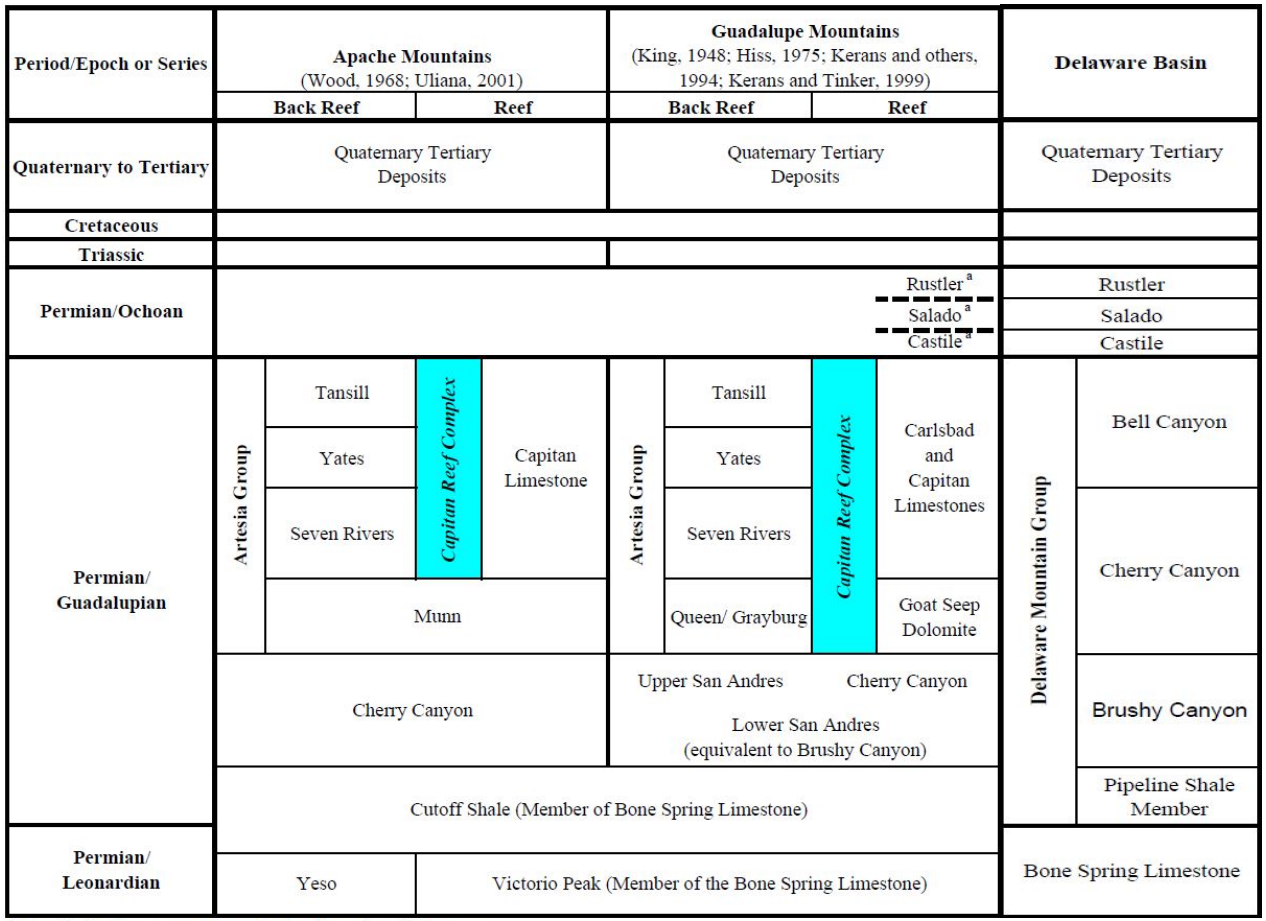

Note: Cell sizes are not to scale for formation thickness

Sources: Modified after King, 1930, 1948; Wood, 1968; Hiss, 1975; Uliana, 2001; Hill, 1999; Kerans and others, 1994; Kerans and Tinker, 1999

[a] Formations overlie Capitan Reef Complex between the Guadalupe and Glass Mountains

Figure 27. Stratigraphic column displaying units found in the region. Modified from Standen et al. (2009).

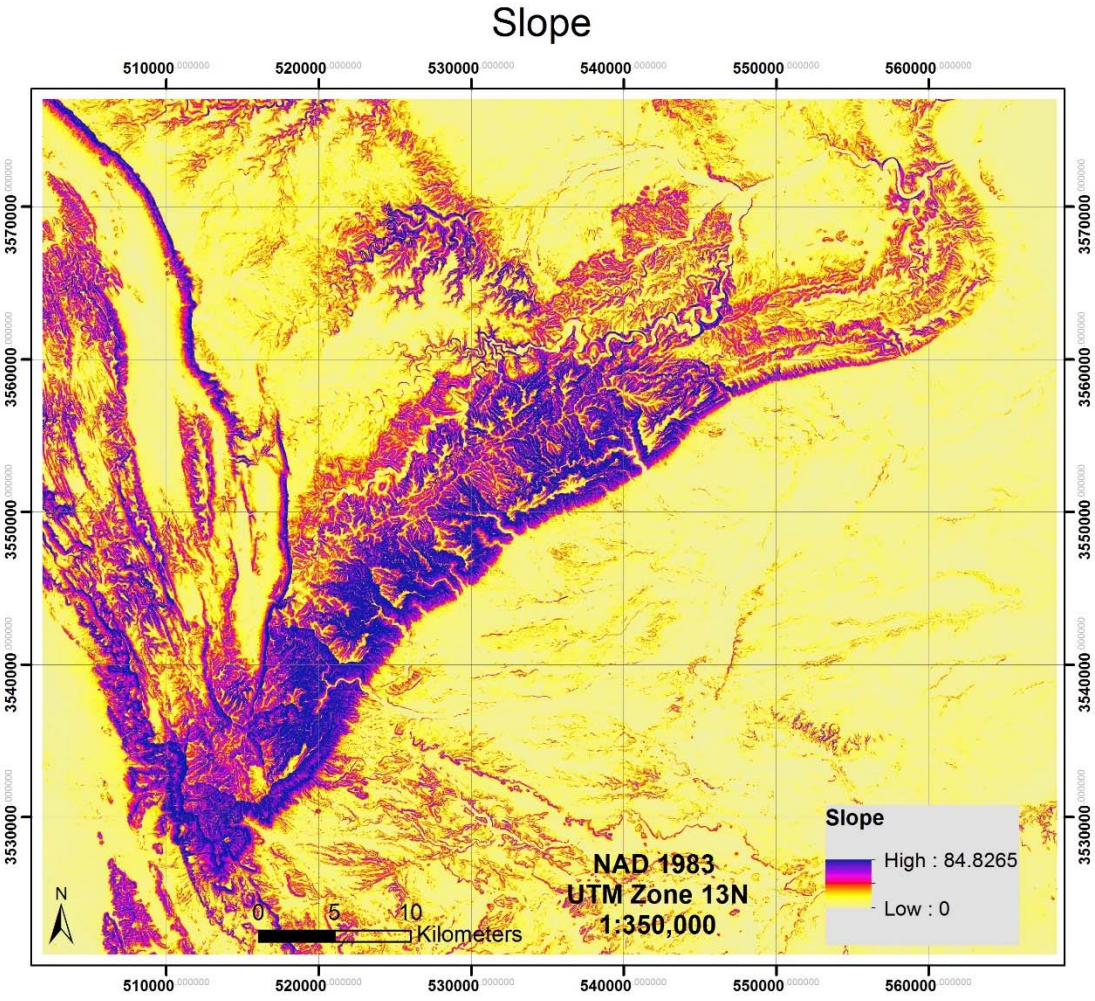

Figure 28. Map displaying slope in the region.

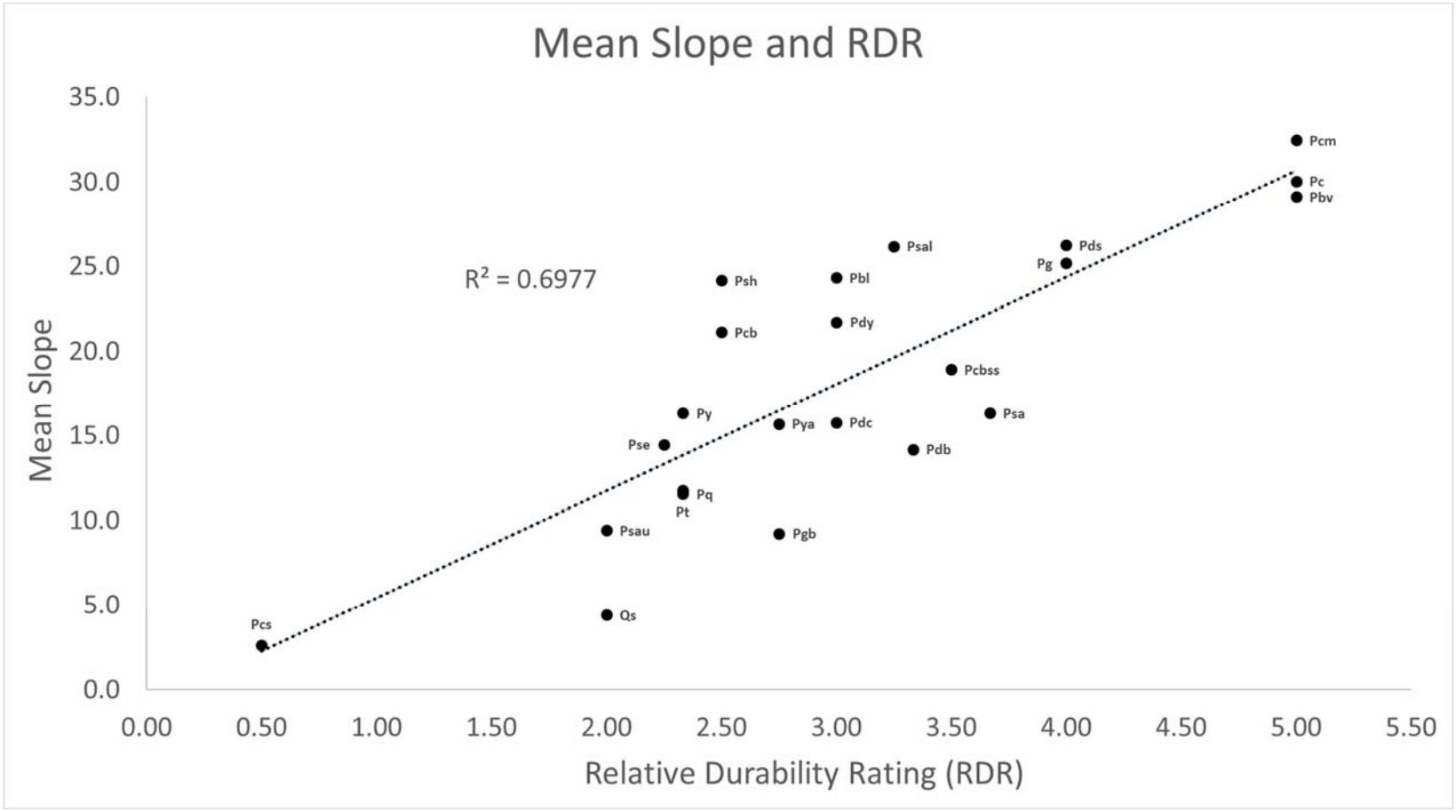

Figure 29. Correlation of mean slope and Relative Durability Rating (RDR). R^2 included on chart.

APPENDIX B: DETAILED METHODOLOGY

Data Collection

Elevation Data

USGS 10m Digital Elevation Models (DEMs) were downloaded from the National Elevation Dataset (http://ned.usgs.gov/). The "USGS NED n33w105 1/3 arc-second 2013 1 x 1 degree ArcGrid" covers the northern extent or the New Mexico portion of the study area and the "USGS NED n32w105 1/3 arc-second 2013 1 x 1 degree ArcGrid" covers the southern extent or the Texas portion of the region (Figure 30). The DEMs are in 1/3 arc-second resolution and were published in 2013, but last updated April 1, 2016. According to the metadata, the raster datasets are distributed in geographic coordinates in units of decimal degrees, and in conformance with the North American Datum of 1983 (NAD 83). All elevation values are in meters and, over the continental United States, are referenced to the North American Vertical Datum of 1988 (NAVD 88).

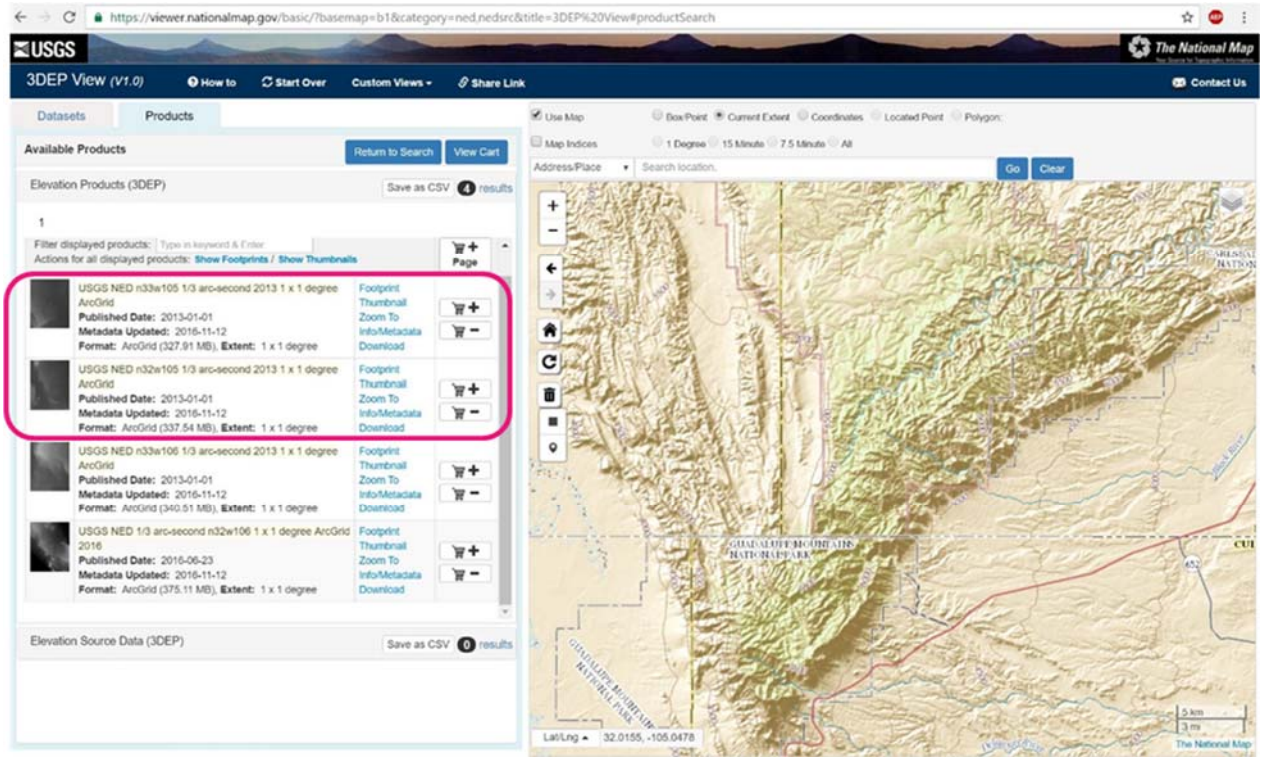

Figure 30. National Elevation Dataset website showing study site and available USGS 10m Digital Elevation Models (DEMs).

Geology Data

Digital GIS layers detailing the geology of the region are available at the National Park Data Store (https://irma.nps.gov/DataStore/). Separate layers were downloaded for Guadalupe Mountains National Park and Carlsbad Caverns National Park. Both digital geologic maps were developed by Stephanie O'Meara (Colorado State University) as a component of the Geologic Resources Evaluation (GRE) program, a National Park Service (NPS) Inventory and Monitoring (I&M) funded program that is administered by the NPS Geologic Resources Division (GRD). The Carlsbad Caverns geology map was published December, 8 2006 and the Guadalupe Mountains geology map was published January 29, 2007. The GIS data for both parks is available as coverage and table export (.E00) files, and as a shapefile (.SHP) and DBASEIV (.DBF) table files. The GIS data projection is NAD83, UTM Zone 13N.

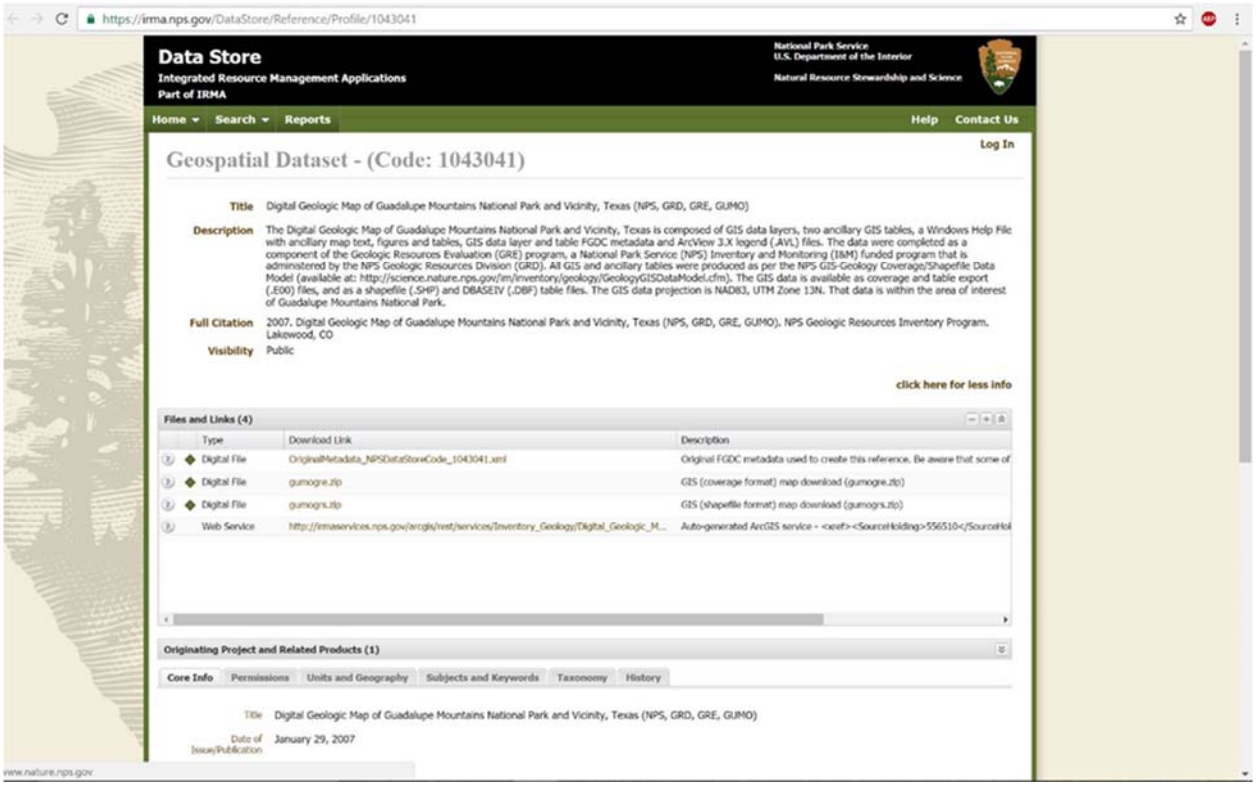

Figure 31. National Park Service Data Store website showing geospatial datasets available for download for the Guadalupe Mountains National Park (code GUMO). Data available for Carlsbad Caverns National Park can be found using code CAVE.

The National Park Service Describes the Datasets below:

The data layers (feature classes) that comprise the Digital Geologic Map of Carlsbad Caverns National Park and Vicinity, New Mexico include: CAVEGLG (geologic units and contacts), CAVEFLT (geologic faults), CAVEATD (geologic attitude observation points), CAVELN (geologic contour and form lines), CAVEMIN (mine and mine related point features), and CAVESEC (cross section lines). There are three additional ancillary map components, the Geologic Unit Information (CAVEGLG1) Table, the Source Map Information (CAVEMAP) Table, and the Map Help File (CAVEGLG.HLP).

The data layers (feature classes) that comprise the Digital Geologic Map of Guadalupe Mountains National Park and Vicinity, Texas include: GUMOGLG (geologic units and contacts), GUMOFLT (geologic faults), GUMOATD (geologic attitude observation points), GUMOGLN (linear geologic units), GUMOGPT (point geologic units), GUMOSUR/GUMOSURA (surficial geologic units and contacts), GUMOMIN (mine and mine related point features), and GUMOSEC (cross section lines). There are three additional ancillary map components, the Geologic Unit Information (GUMOGLG1) Table, the Source Map Information (GUMOMAP) Table and the Map Help File (GUMOGLG.HLP).

Stream Profiler Tool

To calculate steepness indices, a stream profiler tool, developed in 2006 by Dr. Kelin Whipple and associates at MIT, was downloaded at http://web.mit.edu/gis/www/profiler_code/. This tool is designed to work in both ArcMap and MatLab and includes an ArcMap tool bar that can be added by customizing toolbar extensions, as well as several MatLab codes for processing and calculating steepness. Detailed instructions for installing and using the tool are available (Whipple, 2007). The key advantage of using this tool is the ability to manually fit steepness indices for different segments of the longitudinal stream profile. This information can then be re-imported into ArcMap as shapefile.

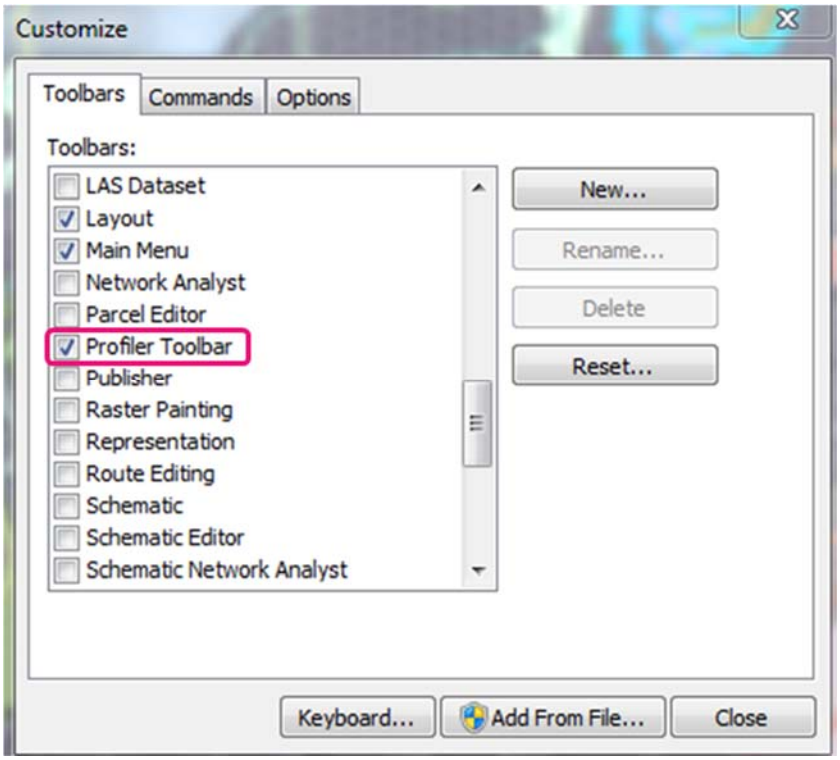

Figure 32. Profiler toolbar installed in ArcMap using Customize > Toolbars > Customize…, which brings up the window shown above (top). Check the box next to Profiler Toolbar and close window. Once installed, the toolbar will appear as above (bottom) showing options to Set Parameters, Select Points, Import Streams, etc.

Data Pre-Processing

DEM Preparation

To prepare the DEMs for stream profile analysis, several steps must first be completed and are also detailed within the stream profiler tool guide (Whipple, 2007).

1. The 10m USGS DEMs are need to be in UTM coordinates for accurate analysis within MatLab. The original DEMs are in geographic coordinates in units of decimal degrees, and in conformance with the North American Datum of 1983 (NAD 83). To change this, we must go to Data Management Tools > Projections and Transformations > Raster > Project Raster and enter the following options:

    a. The Output Coordinate system selected: NAD_1983_UTM_Zone_13N.

    b. Resampling Technique (optional): BILINEAR

    c. Output Cell Size (optional): 10 (Chosen to match 10m DEM cell size)

    Optional selections were chosen based on recommendations listed in the stream profiler guide (Whipple, 2007).

2. Once projected, the two DEMs will need to be merged together to ensure continuous analysis, especially for streams that cross the state line boundary. To achieve this, we go to Data Management Tools > Raster > Mosaic to New Raster, input our projected rasters, and enter the following options:

    a. Pixel Type (optional): 31_BIT_FLOAT (Must match input raster data)

    b. Number of Bands: 1

    c. Mosaic Operator (optional): Blend

    d. Mosaic Colormap Mode (optional): Match

3. The remaining DEM preparation steps can be computationally time consuming, so it is best to go ahead and clip the DEM to the area of interest to reduce this processing time. To clip the area of interest, a feature class clip polygon was created using the Editor toolbar. Once the polygon was created, the rasters were clipped using Spatial Analyst Tools > Extraction > Extract by Mask and specifying the polygon as the "Feature Mask Data."

4. Fill pits in the DEM. This step is completed to allow flow to escape depressions when completing the flow direction array (next step). This is competed by using Spatial Analyst Tools > Hydrology > Fill.

5. Create the Flow Direction Array. Use Spatial Analyst Tools > Hydrology > Flow Direction. Be sure to specify the filled DEM from the previous step as the input DEM.

6. Create the Flow Accumulation Array. Use Spatial Analyst Tools > Hydrology > Flow Accumulation. Be sure to specify the flow direction array DEM from the previous step as the input DEM.

    a. Leave the Input weight raster (optional) blank

    b. IMPORTANT: Output data type must be specified as "INTEGER"

7. Export Integer Flow Accumulation and unfilled DEM to ASCII files. These .txt outputs will be used in MatLab to extract channel profiles for analysis. Use Conversion Tools > From Raster > Raster to ASCII. NOTE: Be careful to follow naming conventions and keep files organized in their respective directories.

8. Use MATLAB to convert the exported .txt files into .mat data files. This is completed within MatLab using the "arcdemtxt2matlab.m" code.

    After the DEM is prepared using the steps above, we can begin manually selecting streams within ArcMap for analysis.

ArcGIS Processing

OBJECTIVE 1: CREATING REGIONAL STEEPNESS (k_{sn}) SHAPEFILE

1. Define Parameters for DEM Analysis

    a. Make sure the unfilled DEM is loaded and visible in ArcMap

    b. Select the "Set Parameters" button on the Stream Profiler Toolbar and specify parameters in the window (As seen in Figure 33 below):

        i. "Working Folder"

        Set to appropriate directories where ArcMap files can be stored.

        ii. Select unfilled DEM from the dropdown list

        iii. Choose project name

        This will save your settings in a file "projectname_parameters.txt" so you retain a record and can easily reload these settings with the "Import Saved Parameters" button at the top of the form

        iv. Choose and Set Theta Ref

        Typically, between 0.4 and 0.6, but was determined to be 0.34 for this region through preliminary analyses.

        v. Spike Remover

        Takes out any data spikes in your profile. Recommended for DEMs that had many pits to fill.

        vi. Step Remover

        Removes artifacts from USGS 10m DEMs, and allows no additional smoothing.

        vii. Smoothing Window

        The length of a moving average window over which MatLab will smooth raw profile data (in meters). Not needed if using Step Remover.

        viii. Contour Sampling Interval

        Interval is the vertical distance MatLab will use to calculate raw slopes (NOTE: 12.192m is equivalent to the 40ft contour interval most DEMs were created from).

ix. Auto_k_{sn} Window

The width of a moving window that MatLab uses to calculate normalized steepness indices along the entire length of a profile.

x. Search Distance

The distance MatLab will search downstream from your selected channel head (in pixels) to make sure it's actually in the channel. The routine used to locate actual stream heads (and to eliminate the need to very carefully pick points selected in step 2 below) is as follows: (1) from your selected point the channel extractor runs downhill a number of pixels set by "Search Distance"; (2) the channel extractor then turns around and follows the channel all the way to the divide; (3) it then turns around again, moving downstream and begins data extraction (distance, elevation, drainage area) when it reaches the "Minimum Accumulation" (again in pixels) specified below. This way by picking anywhere near the channel of interest you can always extract exactly the same channel, and you can always start as near the divide as you like without needing to zoom way in when choosing your channel head position.

xi. Minimum Accumulation

Helps MatLab define where the actual channel head is: it is the number of pixels that contribute to the uppermost pixel in your channel

After selecting parameters, be sure to save to file. Check that a new text file has been created called "run_parameters.txt"

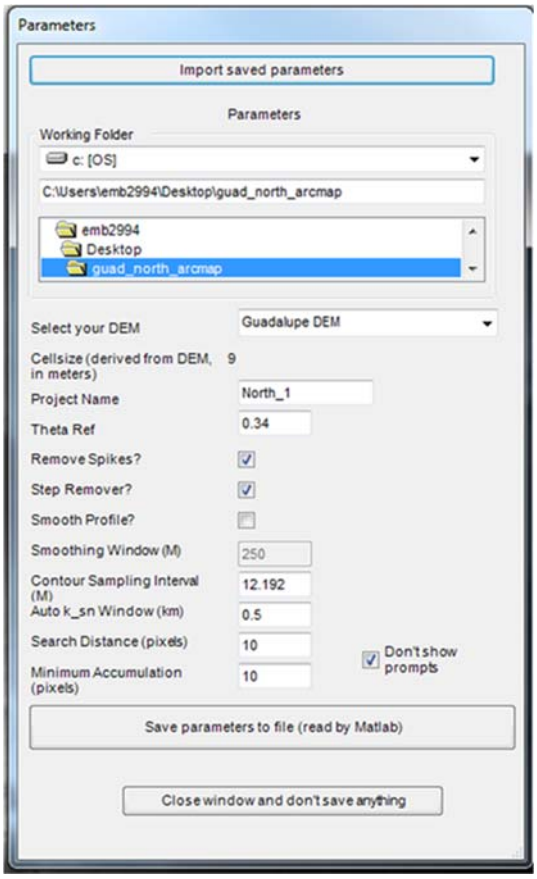

Figure 33. "Set Parameters" window. The settings displayed above were used for these analyses.

2. Selecting Streams in ArcMap

a. Before manually selecting streams it can be useful to add or manipulate layers to better visualize the stream network and topography and guide stream head selection. Suggestions are as follows:

i. Reclassify the Flow Accumulation. (Figure 34)

ii. Create a shaded Relief Map (Figure 34)

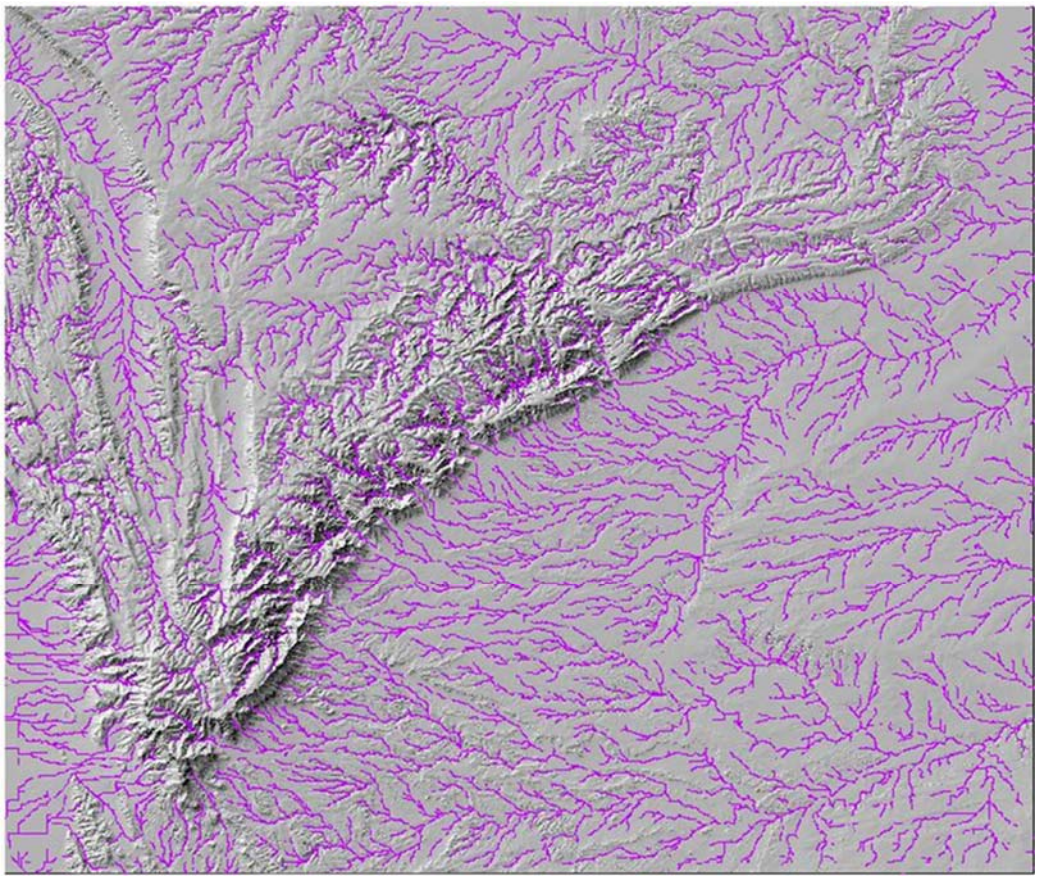

Figure 34. Reclassified Flow Accumulation and Hillshade for the study area to guide manual stream selection (1:350,000). Flow Accumulation was reclassified using 1-5000 in order to produce the stream density above.

b. Pick streams using Profiler toolbar. Select the toolbar button "Select Points" (See Figure 4). This will bring up crosshairs that can be used to locate which stream you would like to extract. This tool remains active until another ArcMap tool or another button on the Profiler Toolbar is selected.

i. Use the cross-hairs to click near a channel head on your DEM.

ii. Name and save point selection to text file by clicking "Submit Name." The text file with saved locations will be called "location_ij.txt" Data format is [row column easting northing stream name].

3. MatLab Processing

After all streams are selected, the stream profile extraction and analysis in MatLab can begin. The main code used for this analysis is "profile51.m" and calls on several other stream profiler codes to produce results. The MatLab codes generate two plots and step you through a series of analyses, where the most crucial step includes selecting a plot from which to pick regression limits, allowing for several fitted values of k_{sn} to be calculated and saved. This process is described in detail in the Theoretical Background section.

4. Return to ArcMap/Shapefile Creation

Now back in ArcMap, we need to download the k_{sn} data collected in MatLab in order to visualize it in ArcGIS and plot the data over the map.

a. Use the Stream Profile Toolbar and select "Import Streams" to import k_{sn} data as stream vector shapefiles. Each of the streams will be imported separately and downstream portions will have many overlapping lines.

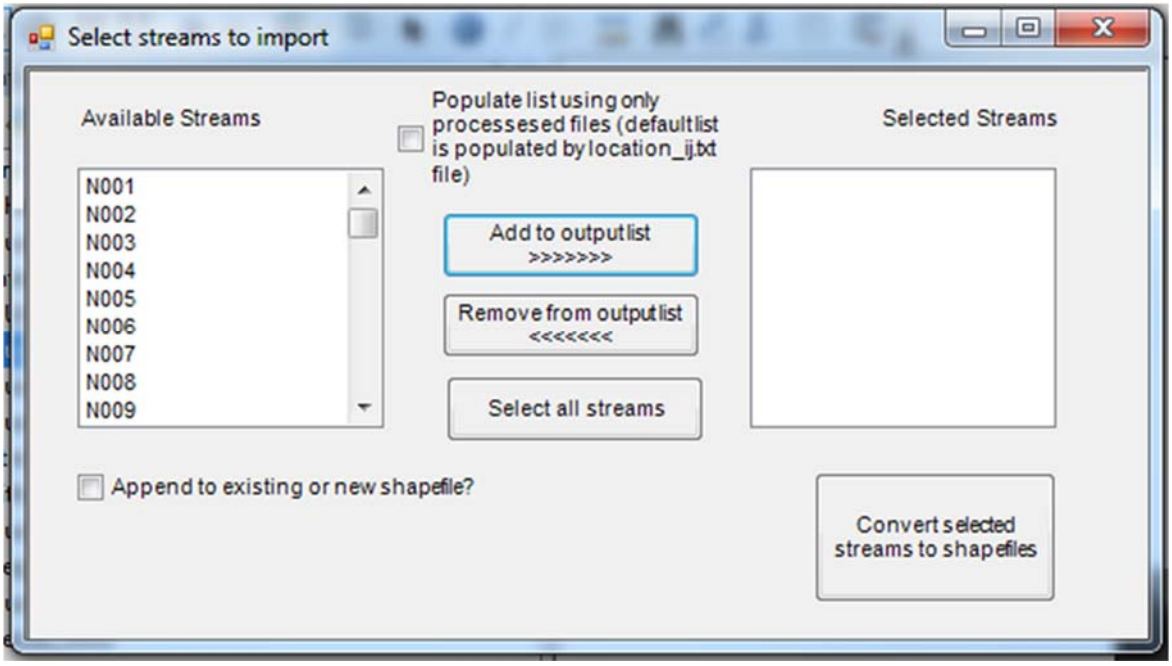

Figure 35. Window used to import streams and convert to shapefiles after MatLab processing.

b. Use Data Management > General > Merge to combine all stream shapefiles into a single regional shapefile. This should be completed in batches depending on the number of stream shapefiles to be merged together.

c. To better visualize results, it is recommended to change the Symbology to represent categories of steepness. To do this, right click on the shapefile layer and go to the Symbology Tab > Quantities > Graduated Colors. For Value field, select "k_{sn}." The classification method can be changed depending on the objective. Results of this analysis were symbolized using 10 Natural Breaks (Jenks) and then the "prediction" color ramp was applied.

REFERENCES

Alnaji, N.S. 2002. Two carbonate shelf margins with hydrocarbon potential compared: Upper Jurassic Formations of Arabian Basin and Guadalupian Formations of Permian Basin of Texas and New Mexico (Submitted in Partial Fulfillment of the Requirements for the Degree of Master of Sciences in the Department of Geological Sciences University of South Carolina). Retrieved from:http://www.sepmstrata.org/page.aspx?&pageid=126&2

Berlin, M.M. and Anderson, R.S., 2009. Steepened channels upstream of knickpoints: Controls on relict landscape response. Journal of Geophysical Research: Earth Surface, 114(F3).

Boyd, D.W., 1958. Permian sedimentary facies, central Guadalupe Mountains, New Mexico. State Bureau of Mines and Mineral Resources, New Mexico Institute of Mining & Technology.

Bursztyn, N., Pederson, J.L., Tressler, C., Mackley, R.D. and Mitchell, K.J., 2015. Rock strength along a fluvial transect of the Colorado Plateau–quantifying a fundamental control on geomorphology. Earth and Planetary Science Letters, 429, pp.90-100.

Chadwick O.A., Roering J.J., Heimsath A.M., Levick S.R., Asner G.P., Khomo L. 2013. Shaping post-orogenic landscapes by climate and chemical weathering. Geology. Vol. 41 (11): 1171-1174.

Clarke, Brian A., and Douglas W. Burbank. "Quantifying bedrock-fracture patterns within the shallow subsurface: Implications for rock mass strength, bedrock landslides, and erodibility." Journal of Geophysical Research: Earth Surface 116.F4 (2011).

Crosby, B.T. and Whipple, K.X., 2006. Knickpoint initiation and distribution within fluvial networks: 236 waterfalls in the Waipaoa River, North Island, New Zealand. Geomorphology, 82(1), pp.16-38.

DiBiase R., Heimsath, A.M., Whipple KX. 2012. Hillslope response to tectonic forcing in threshold landscapes. Earth Surf. Process. Landforms. 37: 855–865.

Duvall, A., Kirby, E. and Burbank, D., 2004. Tectonic and lithologic controls on bedrock channel profiles and processes in coastal California. Journal of Geophysical Research: Earth Surface, 109(F3).

Flint, J.J., 1974. Stream gradient as a function of order, magnitude, and discharge. Water Resources Research, 10(5), pp.969-973.

Forte A.M., Yanites B.J., and Whipple K.X. 2016. Complexities of landscape evolution during incision through layered stratigraphy with contrasts in rock strength. Earth Surface Processes and Landforms.

Gilbert, G.K., 1877. Report on the Geology of the Henry Mountains. US Government Printing Office.

Goode, J.R. and Wohl, E., 2010. Substrate controls on the longitudinal profile of bedrock channels: Implications for reach-scale roughness. Journal of Geophysical Research: Earth Surface, 115(F3).

Hack, J.T., 1975. Dynamic equilibrium and landscape evolution. Theories of landform development, 1, pp.87-102.

Han, J., Gasparini, N.M. and Johnson, J.P., 2015. Measuring the imprint of orographic rainfall gradients on the morphology of steady-state numerical fluvial landscapes. Earth Surface Processes and Landforms, 40(10), pp.1334-1350.

Hayes, P.T., 1964. Geology of the Guadalupe Mountains, New Mexico (No. 446). US Geological Survey.

Hill, C.A., 1987. Geology of Carlsbad cavern and other caves in the Guadalupe Mountains, New Mexico and Texas (Vol. 117). New Mexico Bureau of Mines & Mineral Resources.

Hill C.A. 1998.Geology of the Guadalupe Mountains: An Overview of New Ideas. Pages 219-227 in The Guadalupe Mountains Symposium, 1998. Armstrong and Keller Lynn, editors. National Park Service, Guadalupe Mountains National Park, Texas.

Hilley, G.E. and Arrowsmith, J.R., 2008. Geomorphic response to uplift along the Dragon's Back pressure ridge, Carrizo Plain, California. Geology, 36(5), pp.367-370.

Hoffmann, H. 2015. violin.m - Simple violin plot using matlab default kernel density estimation. INRES (University of Bonn), Katzenburgweg 5, 53115 Germany. hhoffmann@uni-bonn.de.

Howard, A.D., 1994. A detachment-limited model of drainage basin evolution. Water resources research, 30(7), pp.2261-2285.

Howard, A.D. and Kerby, G., 1983. Channel changes in badlands. Geological Society of America Bulletin, 94(6), pp.739-752.

Hurst M.D., Mudd, S.M., Yoo K., Attal M., Walcott R. 2013. Influence of lithology on hillslope morphology and response to tectonic forcing in the northern Sierra Nevada of California. Journal of Geophysical Research. Vol.118 (2): 832–851.

Jansen, J.D., Codilean, A.T., Bishop, P. and Hoey, T.B., 2010. Scale dependence of lithological control on topography: bedrock channel geometry and catchment morphometry in western Scotland. The Journal of geology, 118(3), pp.223-246.

Johnstone S.A. and Hilley G.E. 2014. Lithologic control on the form of soil-mantled hillslopes. Geology. Vol. 43(1): 1–5.

King, P.B., 1948. Geology of the southern Guadalupe Mountains, Texas (Vol. 215). US Government Printing Office.

Kirby, E. and Whipple, K.X., 2012. Expression of active tectonics in erosional landscapes. Journal of Structural Geology, 44, pp.54-75.

Kirby, E., Whipple, K.X., Tang, W. and Chen, Z., 2003. Distribution of active rock uplift along the eastern margin of the Tibetan Plateau: Inferences from bedrock channel longitudinal profiles. Journal of Geophysical Research: Solid Earth, 108(B4).

Lague, D., 2014. The stream power river incision model: evidence, theory and beyond. Earth Surface Processes and Landforms, 39(1), pp.38-61.

Moon S., Chamberlain C.P., Blisniuk K., Levine N., Rood D., and Hilley G. 2011. Climatic control of denudation in the deglaciated landscape of the Washington Cascades. Nature Geoscience. Vol. 4: 469-473.

Murphy B.P., Johnson J.P.L., Gasparini, N.M., and Sklar, L.S. 2016. Chemical weathering as a mechanism for the climatic control of bedrock river incision. Nature. Vol. 532: 223-227.

Natural Resources Conservation Service National Water and Climate Center. 2005. Climate Narrative for Guadalupe Mountains National Park, Texas. www.wcc.nrcs.usda.gov/legacy/ftp/.../climate/soil.../tx/Guadalupe_mts_natl_park.doc

Nichols, G., 2009. Sedimentology and stratigraphy. John Wiley & Sons. pp. 227

NPS Geologic Resources Inventory Program. 2006. Digital Geologic Map of Carlsbad Caverns National Park and Vicinity, New Mexico (NPS, GRD, GRE, CAVE). Lakewood, CO.

NPS Geologic Resources Inventory Program. 2007. Digital Geologic Map of Guadalupe Mountains National Park and Vicinity, Texas (NPS, GRD, GRE, GUMO). Lakewood, CO.

Pederson, J.L. and Tressler, C., 2012. Colorado River long-profile metrics, knickzones and their meaning. Earth and Planetary Science Letters, 345, pp.171-179.

Perne, M., Covington, M.D., Thaler, E.A. and Myre, J.M., 2017. Steady state, erosional continuity, and the topography of landscapes developed in layered rocks. Earth Surface Dynamics, 5(1), p.85.

Perron J.T. 2011. Numerical Methods for nonlinear hillslope transport laws. Journal of Geophysical Research. Vol. 116.

Perron, J.T. and Royden, L., 2013. An integral approach to bedrock river profile analysis. Earth Surface Processes and Landforms, 38(6), pp.570-576.

Pike, A.S., Scatena, F.N. and Wohl, E.E., 2010. Lithological and fluvial controls on the geomorphology of tropical montane stream channels in Puerto Rico. Earth Surface Processes and Landforms, 35(12), pp.1402-1417.

Richey, S.F., Wells, J.G., Stephens, K.T. 1985. Geohydrology of the Delaware Basin and Vicinity, Texas and New Mexico. USGS Survey. Water-Resources Investigations Report 84-4077.

Roy, S.G., Tucker, G.E., Koons, P.O., Smith, S.M. and Upton, P., 2016. A fault runs through it: Modeling the influence of rock strength and grain-size distribution in a fault-damaged landscape. Journal of Geophysical Research: Earth Surface, 121(10), pp.1911-1930.

Rush J. and Kerans C. 2010. Stratigraphic response across a structurally dynamic shelf: The latest Guadalupian composite sequence at Walnut Canyon in New Mexico, U.S.A. Journal of Sedimentary research. Vol. 80: 808-828.

Schmidt, K.M. and Montgomery, D.R., 1995. Limits to relief. Science, 270(5236), p.617.

Scholle P.A. 1980 and 1992. Generalized geologic map of the Guadalupe Mounts and surrounding areas. Compiled from numerous published sources, including Barnes (1968), Boyd (1958), Kelley (1971), King (1948), and Motts (1962). http://geoinfo.nmt.edu/staff/scholle/graphics/permdiagr/guadgeolmap.html

Selby, M.J. 1980. A rock mass strength classification for geomorphic purposes: with tests from Antarctica and New Zealand. Z. Geomorphology. Vol. 24: 31–51.

Sklar, L. and Dietrich, W.E., 1998. River longitudinal profiles and bedrock incision models: Stream power and the influence of sediment supply (pp. 237-260). American Geophysical Union.

Small, E.E., Blom, T., Hancock, G.S., Hynek, B.M. and Wobus, C.W., 2015. Variability of rock erodibility in bedrock-floored stream channels based on abrasion mill experiments. Journal of Geophysical Research: Earth Surface, 120(8), pp.1455-1469.

Snyder, N.P., Whipple, K.X., Tucker, G.E. and Merritts, D.J., 2000. Landscape response to tectonic forcing: Digital elevation model analysis of stream profiles in the Mendocino triple junction region, northern California. Geological Society of America Bulletin, 112(8), pp.1250-1263.

Standen, A., Finch, S., Williams, R., Lee-Brand, B., Kirby, P. September 2009. Capitan Reef Complex Structure and Stratigraphy. Texas Water Development Board Report. Contract Number 0804830794.

Stock, J.D. and Montgomery, D.R., 1999. Geologic constraints on bedrock river incision using the stream power law. Journal of Geophysical Research. B, 104, pp.4983-4993.

Urbancyzk K., Rohr, D., and White, J. C. 2001. Geologic History of West Texas. Texas Water Development Board. Report 356.

U.S. National Park Service. Weather. Accessed April 20 2017. https://www.nps.gov/cave/learn/nature/weather.htm https://www.nps.gov/gumo/planyourvisit/weather.htm .

Whipple, K.X. 2004. Bedrock Rivers and the Geomorphology of Active Orogens. Annual Review of Earth and Planetary Sciences. 2004. 32:151–85

Whipple K.X. and Tucker G.E. 1999. Dynamics of the stream-power river incision model: Implications for height limits of mountain ranges, landscape response timescales, and research needs. Journal of Geophysical Research. Vol. 104 (B8): 17661–17674.

Whipple, K.X., Wobus, C., Crosby, B, Kirby, E., and Sheehan, D. 2007. New Tools for Quantitative Geomorphology: Extraction and Interpretation of Stream Profiles from Digital Topographic Data. GSA Annual Meeting: October 28, 2007 Boulder, CO. Sponsored by: NSF Geomorphology and Land Use Dynamics.

Wobus, C., Crosby, B., & Whipple, K. 2006. Hanging valleys in fluvial systems: Controls on occurrence and implications for landscape evolution. Journal of Geophysical Research, 111.

Vita

Emily Bradshaw Marino grew up in the Raleigh-Durham area in the piedmont of North Carolina. She attended the University of North Carolina in Asheville, where she enjoyed the pristine nature and geology of the surrounding Blue Ridge Mountains. She graduated cum laude, with distinction in December of 2011, earning a B.S. in Earth and Environmental Science. Shortly after graduation, she began her career as a Research Scientist with the Unimin Corporation, working on geochemical applications in high purity quartz. She was accepted into the graduate program at the Jackson School of Geosciences at the University of Texas at Austin in 2015. Before moving to Austin, she married her high school sweetheart and the love of her life, Anthony Marino. During her time at the Jackson School, she has served as a teaching assistant for Introductory Geology and Geomorphology courses. Emily will present will this work at a joint AGU-JpGU conference in Tokyo in May of 2017. After graduation, Emily looks forward to continuing her career as a geoscientist.

Permanent email: ebmarino@utexas.edu

This thesis was typed by Emily Bradshaw Marino.